RHEOLOGY OF AGING SUSPENSIONS

Thesis by E.H. Purnomo

Cover design by E. H. Purnomo and D. van den Ende

The work described in this thesis was supported financially by the Foundation for Fundamental Research on Matter (FOM) and was part of the research program of the Institute for Mechanics, Processes and Control - Twente and the J.M. Burgerscentrum.

RHEOLOGY OF AGING SUSPENSIONS

PROEFSCHRIFT

ter verkrijging van
de graad van doctor aan de Universiteit Twente,
op gezag van de rector magnificus,
prof.dr. W.H.M. Zijm,
volgens besluit van het College van Promoties
in het openbaar te verdedigen
op donderdag 3 juli 2008 om 13.15 uur

door

Eko Hari Purnomo

geboren op 12 april 1976
te Cilacap, Indonesia.

Dit proefschrift is goedgekeurd
door de promotores

prof. dr. F. Mugele
prof. dr. J. Mellema

en de assistent-promotor

dr. H.T.M. van den Ende

Contents

Chapter 1

Introduction

1.1 General background

For many of us, we start the day by squeezing tooth paste onto a toothbrush, applying gel to our hair or spreading chocolate paste onto our bread. These materials belong to a group of materials namely soft glassy materials (SGMs). The characteristic property of these soft glassy materials is that they have an amorphous microscopic structure just like a liquid but macroscopically they behave like a solid at low stresses [1]. Above a certain stress, called yield stress, they will flow. It costs little energy to spread the chocolate paste but it does not flow from your sandwich.

In a case of colloidal hard sphere suspensions, the glassy state exists at volume fraction $\phi \simeq 0.58 - 0.64$. The polydispersity of the particles prevents the system from crystallization [1]. These suspensions can be brought from the liquid state into the glassy state by decreasing the temperature quickly. The system is quenched into an amorphous glass leaving no time to rearrange into a crystalline structure [2]. The relaxation processes of the system in the glassy state can be 10 orders of magnitude slower than in the liquid state [2].

We will study the properties of SGMs via their rheology. For the interpretation we use the soft glassy rheology (SGR) modelling. Therefore the characteristic of both the rheology in general and the model will be discussed in the next two sections before we discuss the state of the art and the outline of the thesis in the remaining of this introductory chapter.

1.2 Rheology

Rheology is the study of the deformation and flow of matter. The term rheology originates from the Greek: "rheos". It has several meanings such as river,

flowing, and streaming [3]. Even though rheology literally means science of flow, it covers not only the flow behavior of liquids but also the deformation of solids.

Rheology is an interdisciplinary subject. It is used not only in physics where it originates from but also in other fields of science such as material science, mechanical and chemical engineering, food science, and more recently biology [4-6].

The wide spread use of rheology in different fields indicates its importance. In industrial applications, process and quality control is often based on rheological parameters. For example, ketchup pasteurization through a heating pipe can be insufficient if the viscosity is too low and so the ketchup flows too quickly. We would also like to have butter that can be spread easily on the bread but does not flow like water. A very recent paper shows that we can distinguish cancerous cells from normal ones by measuring cell stiffness even when they show similar shapes [6].

Rheology is concerned with the response of the materials to applied stresses and deformations. An ideal viscous material flows as we apply a shear stress σ. This type of material is known as a Newtonian liquid. The shear stress σ is linearly proportional to the applied shear rate $\dot{\gamma}$ with its viscosity η as the proportionality constant. Whereas an ideal elastic material deforms elastically when a shear stress (σ) is applied. Now the shear strain (γ) itself is linearly proportional with the applied shear stress σ. The ratio between the two is the elasticity constant of the material. Also the deformation is fully recovered when the stress is released. However, most of the materials that we find in our daily life show some characteristics of both ideal materials. Depending on the time scale, they behave more viscous or elastic and they are known as viscoelastic materials.

A rheometer is an instrument to measure the rheological properties of materials. Depending upon the shear strain profile applied, we can perform steady state rotational and oscillatory measurements. A rotational measurement is carried out by imposing the shear strain in one direction. Whereas an alternating shear strain with a certain frequency ω is used in oscillatory measurements.

A flow curve and a stress relaxation curve can be obtained from the rotational measurements. The flow curve is obtained when a constant shear rate is applied and the shear stress σ is plotted as function of the applied shear rate $\dot{\gamma}$. For a Newtonian liquid, the viscosity, which is the proportionality constant of the flow curve, is independent of the shear rate. However, the viscosity of a non-Newtonian liquid depends on the shear rate. The stress relaxation curve shows the evolution of the shear stress when a constant shear strain is applied. From the stress relaxation curve we can extract the relaxation time of the material.

The linear viscoelastic properties of a material can be obtained by applying a harmonic shear strain $\gamma(t) = \gamma_0 \sin(\omega t)$ with sufficiently small amplitude γ_0 and measuring the stress response $\sigma(t) = \sigma_0 \sin(\omega t + \varphi)$, see figure 1. (With sufficiently small we mean the stress response σ_0 is linear with γ_0). The elastic storage modulus G' and the viscous loss modulus G'' are obtained by extracting the components in phase with $\gamma(t)$ and in phase with $\dot{\gamma}(t)$:

$$\sigma(t) = \sigma_0 \cos(\varphi) \sin(\omega t) + \sigma_0 \sin(\varphi) \cos(\omega t)$$

where

$$\begin{aligned} \sigma_0 \cos\varphi &= G'\gamma_0 \quad \text{and} \\ \sigma_0 \sin\varphi &= G''\gamma_0. \end{aligned}$$

The real and imaginary parts of the complex viscosity η^* are defined as

$$\begin{aligned} \eta' &= G''/\omega \\ \eta'' &= G'/\omega. \end{aligned}$$

For an ideal elastic solid, the stress response is in phase with the applied strain ($\varphi = 0$) and therefore it contains only G'. On the other hand, the phase lag φ of an ideal viscous material is $\pi/2$ which result in $G' = 0$ and the system contains only G''. By performing an oscillatory measurement at a fixed frequency but progressively increasing the stress amplitude, we can determine the linear and non-linear regime of the viscoelastic moduli.

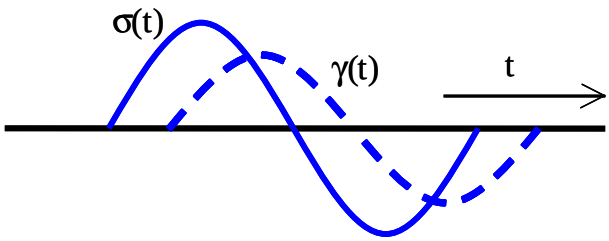

Figure 1. A schematic picture of a stress $\sigma(t)$ and a strain $\gamma(t)$ profile in an oscillatory measurement.

The constitutive equation for a linear viscoelastic material reads

$$\sigma(t) = \int_{-\infty}^{t} G(t - t')\dot{\gamma}(t')dt'$$

where $G(t)$ is a relaxation modulus of the material [7]. For a material with several relaxation times (τ_k) one can express $G(t)$ as

$$G(t) = \eta'_\infty \delta(t) + G'_0 + \sum_{k=1}^{N} G_k \exp(-t/\tau_k).$$

Substituting $G(t)$ into the constitutive equation in case $\dot{\gamma}(t) = \omega\gamma_0 \cos(\omega t)$ gives

$$G'(\omega) = G'_0 + \sum_{k=1}^{N} G_k \frac{\omega^2\tau_k^2}{(1+\omega^2\tau_k^2)} \tag{1.1}$$

$$G''(\omega) = \eta'_\infty \omega + \sum_{k=1}^{N} G_k \frac{\omega\tau_k}{(1+\omega^2\tau_k^2)} \tag{1.2}$$

where G_k is the relaxation strength at a relaxation time τ_k , G'_0 is the zero frequency elastic modulus and η'_∞ is high frequency limit of the real viscosity. Figure 2(a) shows the G' and G'' calculated from equation 1.1 and 1.2 with a single relaxation time and neglecting contributions from G'_0 and η'_∞. A fluid that behaves like this is called a Maxwell fluid. The G' increases with a slope of 2 for $\omega \ll 1/\tau$ and flattens at high frequency. The G'' increases with a slope of 1 at low frequencies and decreases with a slope of -1 at high frequencies. The crossing between the G' and the G'' indicates the relaxation time of the material ($\tau = \omega_c^{-1}$).

Figure 2(b) shows the G' and G'' of system with three relaxation times. The G' increases with a slope of 2 at low frequencies $\omega < 1/\tau_{longest}$. The slope decreases gradually as ω increases until finally reaches a plateau at high frequencies $\omega > 1/\tau_{shortest}$. The G'' increases with a slope of 1 at low frequencies. The slope gradually decreases and becomes -1 at high frequencies. Such behavior of G' and G'' is normally found in polymers with a wide molar mass distribution [3]. The average relaxation time $\langle\tau\rangle$ can be calculated as

$$\langle\tau\rangle = \frac{\sum_{k=1}^{N} \tau_k G_k}{\sum_{k=1}^{N} G_k} = \frac{\eta'_0 - \eta'_\infty}{G'_\infty - G'_0} \simeq \frac{\eta'_0}{G'_\infty}$$

as indicated by the arrow in figure 2(b). At the indicated crossing of the two asymptotes G'_∞ is equal to $\eta'_0\omega$ or $1/\omega_{cr} = \eta'_0/G'_\infty = \langle\tau\rangle$.

Complementary to conventional rheometry where one measures the bulk properties of the material, a technique called micro-rheology has been introduced to measure the local rheological properties. This technique requires a very small amount of sample, typically 1 μl, and covers a wide frequency range [4]. Essentially, the motion of probe particles is recorded and by analyzing

the characteristics of the observed particle tracks information of the local viscoelastic properties of the material is retrieved [8]. Because one probes the local properties it gives also information about the heterogeneity of the sample. One way to observe the particle motion is video microscopy. The measurement is done by following the displacements of the probe particles embedded in the system using a microscope equipped with a CCD camera [9], as further explained in chapter 2.

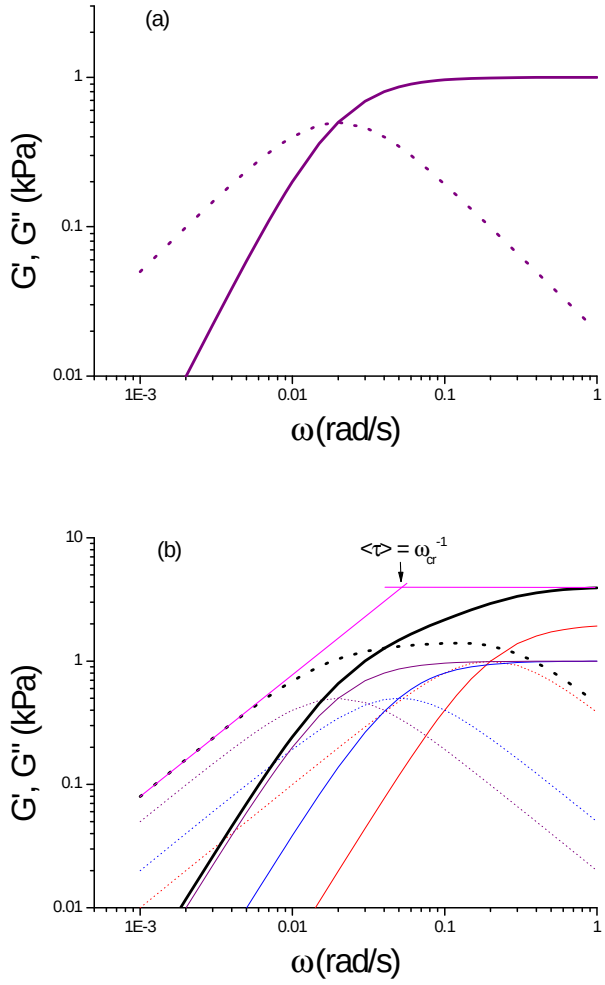

Figure 2. (a) The G' (solid line) and G'' (dotted line) of a material with a single relaxation time. (b) The G' (solid line) and G'' (dotted line) of a material with three relaxation times ($\tau_1 = 50$ s, $\tau_2 = 20$ s, $\tau_3 = 5$s and $G_1 = 1$ kPa, $G_2 = 1$ kPa, $G_3 = 2$ kPa) shown by the thin solid and dotted lines.

1.3 Soft glassy rheology (SGR) model

The SGR model, based on Bouchaud's trap model [10], is intended to describe the rheological properties of soft glassy materials (SGMs) [11-13]. Typical for these materials are metastability and structural disorder; the particles are too compressed to relax independent of each other and so, the particles are trapped by their neighboring particles. The trapped particle can be thought to be surrounded by an energy barrier which the particle has to overcome before it can escape from the trap resulting in a local relaxation and rearrangement of particles.

In the SGR model, the material is conceptually divided into many mesoscopic elements. An element may be seen as the representation of a particle or a cluster of particles. The macroscopic strain γ applied to a system is distributed homogeneously throughout the system and therefore the macroscopic strain rate is equal to the local strain rate $\dot{l}$ experienced by an element: $\dot{\gamma} = \dot{l}$.

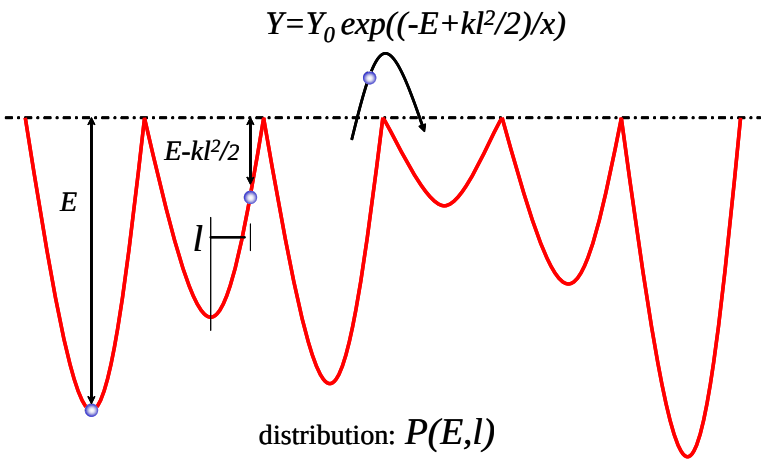

Figure 3. A schematic picture of the yielding of an element in an energy landscape.

The yielding of an element from the trap created by the neighboring elements drives the evolution of the rheological properties. Figure 3 shows a schematic picture of the yielding process. The energy barrier E of an element, or the trap depth, is equal to $kl_y^2/2$ where k is the elastic constant and l_y is the yield strain of an element. The yielding in an unsheared or unstrained material is accompanied by the rearrangement of the neighboring particles. This type of yielding is termed noise-induced yielding and is controlled in the model by an "effective noise temperature" x. The yielding rate Y is proportional to: $\exp(-E/x)$. The yielding rate increases if a macroscopic strain is applied. This type of yielding is termed strain-induced yielding and proportional to:

$\exp(-(E-\frac{1}{2}kl^2)/x)$. Even though strain-induced and noise-induced yielding are discussed in different ways, the SGR model captures them both; due to the local strain l, the barrier to overcome is reduced to $E-\frac{1}{2}kl^2$. Due to the disordered nature of the soft glassy material, each element will have a different yield strain.

The probability $P(E,l)$ to find an element with energy E and local strain l at time t follows from the evolution equation

$$\frac{\partial P}{\partial t} = -\frac{dl}{dt}\frac{\partial P}{\partial l} - Y_0 \exp\left(\left(-E+\tfrac{1}{2}kl^2\right)/x\right) P + Y(t)\,\rho(E)\,\delta(l)$$

The first term on the right hand side describes the straining of the element in between the yielding events. The second term describes the yielding process caused by the applied strain and the activation process due to the collective rearrangement of the neighboring elements. The last term on the right hand side represents the re-birth of the element after the yielding. $\rho(E)$ represents the distribution of available trap depths and $Y(t)$ represents the total yielding rate over all trapped elements.

The macroscopic strain-stress relation is given by

$$\begin{aligned} \sigma &= G_p \langle l \rangle \\ \sigma &= G_p \iint l P(E,l) dE dl. \end{aligned}$$

By evaluating the last expression, the model provides detailed predictions of the rheological properties. The degree of glassiness is quantified by the effective temperature x where $x=1$ marks the glass transition. An equilibrium state ($P_{eq}(E)$) exist above the glass transition ($x>1$). Below the glass transition, an equilibrium state is never reached and this results in aging effects. One of the most common rheological tests is the measurement of the linear viscoelastic moduli (G' and G''). For these moduli, the model provides the following predictions:

$$\begin{aligned} G^*(\omega,t) &= \Gamma(x)\Gamma(2-x)(i\omega)^{x-1} \quad \text{for } 1<x<2 \\ G^*(\omega,t) &= 1+\frac{\ln(i\omega)}{\ln(t)} \quad \text{for } x=1 \\ G^*(\omega,t) &= 1-\frac{1}{\Gamma(x)}(i\omega t)^{x-1} \quad \text{for } x<1 \end{aligned}$$

where $G^* = G' + iG''$, Γ is the gamma function, ω is the frequency, and t is the age of the system. For $2<x<3$, the $G' \sim \omega^{x-1}$ and the $G'' \sim \omega$. The system is Maxwell-like at low frequencies ($G' \sim \omega^2$ and $G'' \sim \omega$) for $x>3$.

Figure 4 shows the evolution of the G' and G'' behavior as a system evolves from the glassy state ($x<1$) to the liquid state ($x>1$). Below the glass

transition ($x < 1$), the moduli are frequency (ω) and age (t) dependent as indicated by the ωt scaling. This is known as aging. Whereas above the glass transition, the moduli depend only on the frequency and they are independent of the age of the system.

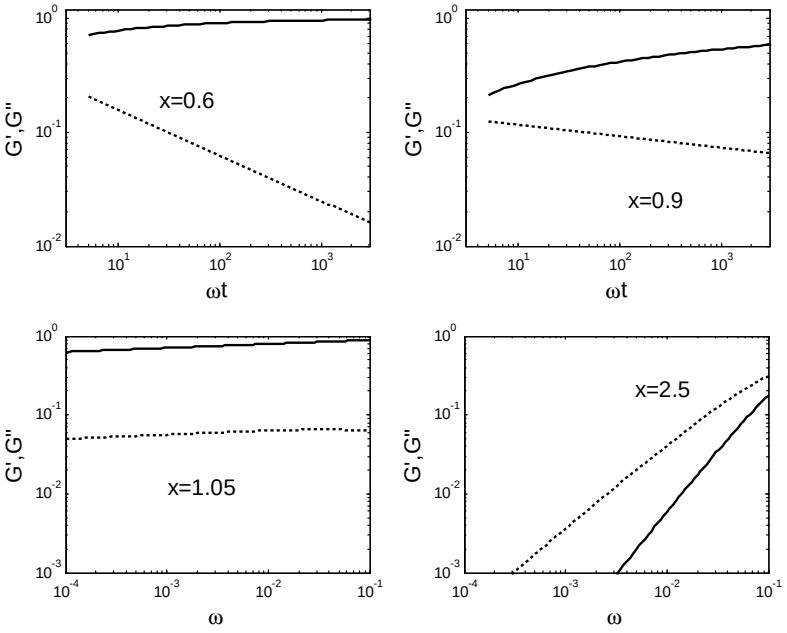

Figure 4. The G' (full lines) and G'' (dashed lines) at different x values.

1.4 State of the art

Most soft glassy materials are out of equilibrium which means that the mechanical properties and the microscopic dynamics continuously evolve with time [14]. In other words, the system is aging. Many different aspects of the soft glassy materials have been studied including the effect of aging on the rheological properties [11-13,15], the microscopic dynamics of colloidal hard sphere suspension near the glass transition [1], the spatial and temporal dynamic heterogeneity [1,16], the role of mobile particles in the break up of the structure and the role of immobile particles on the elasticity of a system [17], the evolution of the structural length scale [18,19], and the increase of the relaxation time [20-25].

One of the early experimental studies showing the connection between the aging and the rheology is done on densely packed suspensions of polyelectrolyte

microgel particles [15]. Cloitre *et al.* [15] show that the strain evolution curves of the suspensions depend on their age, which is controlled by a stress pulse (quench) far above the yield stress of the material. The waiting time t_w between the quench and the start of the experiment is defined as the age of the system. The curves can be collapsed onto a master curve when they are plotted as function of $(t - t_w)/t_w$ where $t - t_w$ is the time elapsed since the probe stress is applied. Even though the authors are aware of the SGR model [11-13], they do not compare their results with the detailed predictions of the model.

Understanding this rheological behavior of SGMs is very important due to the wide spread use of SGMs in practical applications. From theoretical point of view, two competing theories namely mode coupling theory (MCT) and the SGR model can be used to describe the rheological behavior of glassy materials. The mode coupling theory has been successfully applied to describe quantitatively the flow curve of thermosensitive system as the system approaches the glass transition [26] and the behavior of the elastic and loss modulus of a dense hard-sphere suspension as function of the applied strain amplitude [27]. However, this mode coupling theory still lacks to account for the inherent effect of aging on the evolution of the rheological properties [28]. On the other hand, the phenomenological soft glassy rheology model predicts the rheological behavior as the system approaches the glass transition and also deep in the glassy state including the aging effects [11-13] as discussed in section 1.3. This model has been used to describe the viscoelastic moduli of a laponite suspension [29]. In that study, the effective noise temperature obtained by comparing the slope of the moduli as function of frequency with the predictions of the model is 1.1, which indicates that the suspension is just above the glass transition. The model has been used also to describe the relative elasticity ($G'_n = G'/G'_{eq.}$) of living cells after rejuvenation where G' is the elasticity after rejuvenation and $G'_{eq.}$ is the elasticity just before the rejuvenation [24]. The G'_n of different cells and after different drug interventions form a master curve when G'_n is plotted against the phase lag between the applied harmonic strain and the stress response just before the rejuvenation (δ_0). The model captures the trend but fails to describe the results quantitatively.

From the experimental side, light scattering, optical microscopy and rheology are the most widely used techniques to study this class of materials. The light scattering techniques including static and dynamic light scattering, x-photon correlation spectroscopy, and diffusing wave spectroscopy provide information on the sample dynamics by measuring the time autocorrelation function of the scattered intensity $g_2(t)$ [30]. With the optical microscopy technique, one can follow the dynamics of the particles and extract further information such as the mean squared displacement, temporal and spatial heterogeneity and structural length scales [1]. From the rheological measurements one ob-

tains information on how the aging inherently affects the mechanical properties of the sample [13] and also how the relaxation time increases as a glassy sample ages [23].

Colloidal systems are often used as model systems to study glassy behavior since the particles are larger than the atoms and molecules in molecular glasses that intrinsically have larger time scales. Moreover, their physical and chemical properties can be manipulated to suit different interests of research [31]. Among many colloidal systems, laponite and poly-(methylmethacrylate) (PMMA) are probably the most widely used model systems to understand the unique properties of soft glassy materials. Laponite is a synthetic clay containing disc-shaped colloidal particles (typically 30 nm in diameter and 1 nm thick) [32]. PMMA particles are spherical with a typical radius of 1.18 μm and behave as hard spheres. These particles are often stabilized with a thin layer of poly-12-hydroxystearic acid and can be dyed with rhodamine to allow fluorescent visualization [1].

Both Laponite and PMMA systems show a glass transition and aging behavior [1,18,29,32]. Typically, with PMMA systems one can approach the glass transition by increasing the mass concentration [1], whereas the Laponite system enters the glassy state not only by the increase of the mass concentration but also due to aging. The release of ions at low pH is responsible for the glass transition of Laponite during aging [32]. Typically the glass transition of these systems is accompanied by a rapid increase of their viscosity [1,2,29].

Response sensitive systems have also attracted attention as they can be tuned for example by changing the pH, temperature, ionic strength, electric field, or solvent quality. Suspensions of soft thermosensitive colloidal particles are an example these response sensitive systems. Unique for these systems is the controllability of the particle size by tuning the temperature. The particles are swollen at low temperature and their size decreases as one increases the temperature. In the swollen state the particle is soft as it absorbs more water. Upon increasing the temperature the particle shrinks, the polymer density inside the particle increases and so the particle softness decreases. This temperature dependence of the size provides a unique and simple way to control the volume fraction of its suspension. More interestingly, by controlling both the temperature and the concentration one can vary both the volume fraction and the softness independently. Therefore such a soft colloidal system is very suited to study glassy behavior, although most of the studies were only carried out using hard colloidal systems.

If one considers the interaction potential between colloidal particles in a dense suspension one has two classes of glasses namely repulsive and attractive glasses. The attractive glasses (gel) can be obtained for example by adding non-adsorbing polymer to a repulsive suspension to increase the attraction forces

through depletion process. The phase diagrams of these repulsive glasses and attractive gels have been theoretically established in [33] and experimentally shown in [34].

Soft glassy materials are also often considered as jammed systems due to their dynamic arrest. A unifying picture of a jamming phase diagram has been proposed by Liu and Nagel [35]. In this phase diagram one can bring a jammed system into an unjammed state by decreasing the particle density (volume fraction), increasing temperature, or applying a certain load in the form of stress or strain. The realization of this idea has been realized for attractive gels by Trappe *et al.* [5].

In figure 5 we show a very similar jamming phase diagram for our thermosensitive system which is a repulsive glass. In the T vs 1/concentration plane (stress $\sim$ 0 Pa) we define the transition line where the relative effective noise temperature $x = 1$. This noise temperature is obtained by comparing the rheological data to the soft glassy rheology model. In the other planes, the transition lines indicate the minimum stress to flow the system (yield stress). In this figure, the space underneath the curved surface formed by the transition lines indicates the jamming phase. We can unjam the system by increasing the temperature, decreasing the concentration (particle density), or applying a stress that is larger than its yield stress (see chapters 3 - 5 of this thesis for the details).

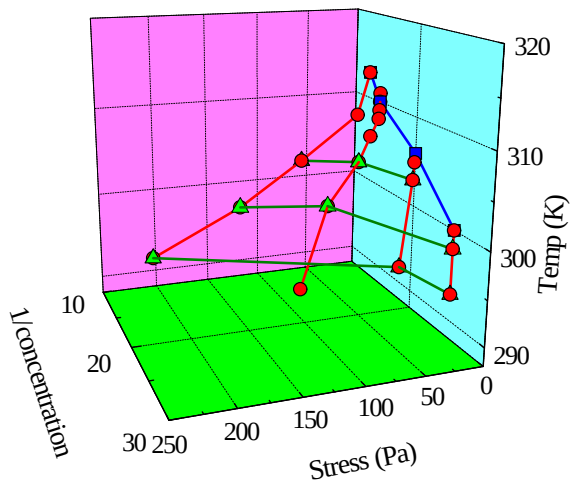

Figure 5. Jamming phase diagram of thermosensitive systems.

1.5 Purpose and Outline

Aging that has been observed in very diverse materials ranging from model systems to living cells, inherently affects the rheological properties of the material. A quantitative understanding of the aging is of an importance due to the wide use of systems that show the aging behavior.

The main purpose of this research is to study the rheological properties of aging soft glassy materials experimentally. To achieve this main objective we measure the rheological properties of highly concentrated suspensions of thermosensitive microgel particles at different temperatures and mass concentrations. We use the SGR model to describe and to understand our experimental findings. In order to investigate further the microscopic dynamics of this soft glassy system, we study the dynamics of probe particles embedded in to the suspension using confocal scanning laser microscopy (CSLM).

This thesis is organized as follow. In chapter 2 we describe the characteristics of the instruments used in this study (rheometer and CSLM), the thermosensitive systems, and the rejuvenation techniques. The characterization mainly focuses on the limits the instruments, the thermosensitive properties of the systems, and the ability of different rejuvenation techniques to obtain a well defined initial state. In chapter 3 we present the oscillatory measurements of the aging system and their quantitative comparison to the prediction of the SGR model. From this quantitative comparison we extract an effective noise temperature (x) which is a measure of glassiness. Other oscillatory measurements on different batches of the thermosensitive systems and creep tests are presented in chapter 4. In this chapter we show that both the oscillatory and creep tests show the aging behavior and can be quantitatively described by the SGR model. The tunability of the rheological behavior of the system between the aging glassy and liquid state is shown in chapter 5. In this chapter we emphasize the effect of particle softness on the glass transition behavior. In chapter 6 we turn to the microscopic study of the particle dynamics using video microscopy particle tracking to investigate the glass transition and the evolution of the microscopic dynamics as the system ages. We show that the relaxation time of the aging system, measured using particle tracking, increases almost linearly with the age of the suspension. From the distribution of the particle displacements we observe dynamic heterogeneity in the glassy system at time scales shorter than the relaxation time.

References

[1] E.R. Weeks *et al.,* Science **287**, 627 (2000)

[2] C.A. Angell, Science **267**, 1924 (1995)

[3] T.G. Mezger, *The Rheology Handbook* (Hannover, 2000)
[4] P. Cicuta and A.M. Donald, Soft Matter **3**, 1449 (2007)
[5] V. Trappe *et al.,* Nature **411**, 772 (2001)
[6] S.E. Cross *et al.,* Nature Nanotech. **2**, 780 (2007)
[7] C.W. Macosko, *Rheology Principles, Measurements, and Applications* (New York, 1994)
[8] T.G. Mason and D.A. Weitz, Phys. Rev. Lett. **74,** 1250 (1995)
[9] J.C. Crocker and D.G. Grier, J. Colloid Interface Sci. **179,** 298 (1996)
[10] J.P. Bouchaud, J. Phys. I **2,** 1705 (1992)
[11] P. Sollich *et al.,* Phys. Rev. Lett. **78,** 2020 (1997)
[12] P. Sollich, Phys. Rev. E. **58**, 738 (1998)
[13] S.M. Fielding *et al.,* J. Rheol. **44**, 323 (2000)
[14] L. Cipelletti and L. Ramos, J. Phys. Condens. Matter. **17,** R253 (2005)
[15] M. Cloitre *et al.,* Phys. Rev. Lett. **85,** 4819 (2000)
[16] Y. Gao and M.L. Kilfoil, Phys. Rev. Lett. **99**, 078301 (2007)
[17] J.C. Conrad *et al.,* Phys. Rev. Lett. **97**, 265701 (2006)
[18] R.E. Courtland and E.R. Weeks, J. Phys. Condens. Matter. **15,** S359 (2003)
[19] L. Berthier *et al.,* Science **310**, 1797 (2005)
[20] B. Chung *et al.*, Phys. Rev. Lett. **96**, 228301 (2006)
[21] L. Ramos and L. Cipelletti, Phys. Rev. Lett. **94**, 158301 (2005)
[22] V. Viasnoff and F. Lequeux, Phys. Rev. Lett. **89**, 065701 (2002)
[23] L. Ramos and L. Cipelletti, Phys. Rev. Lett. **87**, 245503 (2001)
[24] X. Trepat *et al.*, Nature **447**, 592 (2007)
[25] R. Bandyopadhyay *et al.*, Phys. Rev. Lett. **93**, 228302 (2004)
[26] J. J. Crassous *et al.,* J. Chem. Phys. **125**, 204906 (2006)
[27] K. Miyazaki *et al.*, Europhys. Lett. **75**, 915 (2006)
[28] J. M. Brader *et al.,* Phys. Rev. Lett. **98**, 058301 (2007)
[29] D. Bonn *et al.,* Europhys. Lett. **59,** 786 (2002)
[30] L. Cipelletti and L. Ramos, J. Phys. Cond. Matt. **17,** R253 (2005)
[31] F. Sciortino and P. Tartaglia, Advances in Physics **54**, 471 (2005)
[32] F. Schosseler *et al.*, Phys. Rev. E **73**, 021401 (2006)
[33] K. Dawson *et al.,* Phys. Rev E. **63**, 011401 (2001)
[34] K.N. Pham *et al.,* Science **296**, 104 (2002)
[35] A.J. Liu and S.R. Nagel, Nature **396,** 21 (1998)

Chapter 2

Instrument and system characterization

Abstract In this chapter we describe the characteristics of the instruments and experimental techniques used in this study. Special attention has been paid to the thermal stability and the accuracy and resolution of the measured quantities. Moreover, we discuss the properties of the model suspensions used. We explain how we determined properties like particle radius and volume fraction of the thermosensitive microgel particles that we used as a function of the applied temperature and polymer mass concentration. Eventually we consider three different techniques to rejuvenate samples in the glassy state.

2.1 Introduction

In this chapter, we describe the characterization of the instruments and experimental techniques used in this study (rheometer and confocal scanning laser microscope). The rheometer was characterized for its temperature distribution inside the geometry, its torque stability, and its capability in oscillatory experiments. The displacement resolution of the confocal scanning laser microscope (CSLM) was characterized by measuring the dynamics of the probe particles glued on a culture disc. The application of the CSLM set up in particle tracking microrheology was tested by measuring the dynamics of the probe particles in a Newtonian liquid (glycerol). To characterize the model suspensions used in this study, we started with finding the proper concentration of microgel particles to measure their radius using light scattering techniques. At this concentration we measured their radius at different temperatures during heating and cooling. Also the stability of the model system was tested by measuring its tempera-

ture dependence after 3 years of storage. Moreover, we determined the volume fraction of these suspensions using Einstein's relation by measuring the viscosity at low concentrations. Using Einstein's relation the viscosity value was converted to a volume fraction. In the last section of this chapter we describe rejuvenation of aging samples by applying a stress or temperature quench to the material.

2.2 Instruments

2.2.1 Rheometer

A rheometer is an instrument used to study the rheological properties of a material by imposing a shear stress (σ) and observing the resulting shear strain (γ) or strain rate ($\dot{\gamma}$) and vice versa. The shear stress (σ) is defined as a shear force (F) per unit area (A). The shear strain is the gradient of deformation ($\gamma = \Delta d/\Delta y$). For an ideally elastic material, the work done by the external stress is stored reversibly in the system. Whereas for an ideally viscous liquid, the work done by the stress is fully dissipated. In between these two types of materials, there is a viscoelastic material that shows both elastic and viscous behavior.

In this study, we use a stress-controlled Haake RS600 rheometer equipped with a home-built vapor lock to create a stable local environment. This rheometer uses an air bearing system where the rotor of the drive and the motor axis float in air due to the continuous supply of compressed air. The rheometer uses the air bearing system to minimize the bearing friction. Figure 1 shows a schematic picture of the rheometer.

A cone and plate geometry as indicated in figure 1 was used in all the experiments if not stated otherwise. For this cone and plate geometry, we can calculate the shear stress (σ), the shear strain (γ), and the strain rate ($\dot{\gamma}$) from the applied torque and measured angular displacement (velocity) using the following equations:

$$\sigma = \frac{3M}{2\pi R^3} \tag{2.1}$$

$$\gamma = \frac{\phi}{\beta} \tag{2.2}$$

$$\dot{\gamma} = \frac{\dot{\phi}}{\beta} \tag{2.3}$$

where M is the torque applied to the sample, R and β are the radius and the angle of the cone respectively, ϕ is the angular displacement and $\dot{\phi}$ is the angular speed. Depending on the shear stress profile applied, we can perform both step stress (creep) and oscillatory (dynamic) experiments. In the step

stress experiments, a constant stress is applied at $t = 0$ and kept constant for time t ($\sigma(t) = \sigma_0\Theta(t)$) where Θ is the Heaviside step function. On the other hand, an oscillating shear stress ($\sigma(t) = \sigma_0 e^{i\omega t}$) is applied to the sample in an oscillatory experiment.

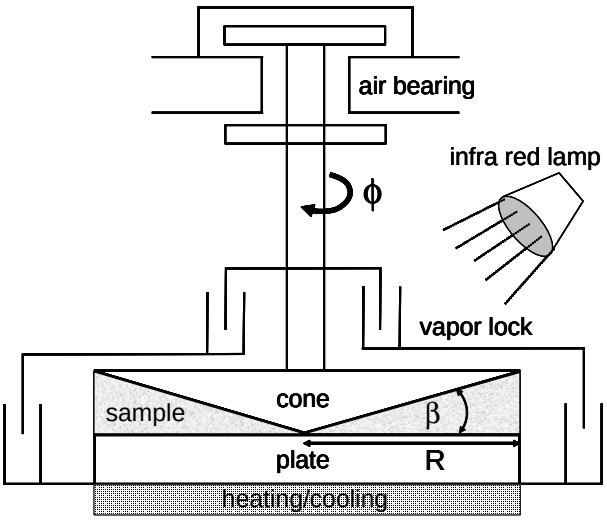

Figure 1. The schematic picture of the rheometer equipped with a home-built vapor lock.

Three different tests were done to characterize the rheometer. First, the temperature distribution inside a plate-plate geometry was studied. The temperature distribution is important since thermosensitive microgel particles will be used in the aging study. Second, the torque stability of the instrument was measured to ensure the suitability of the instrument for aging studies in which very low stress will be applied to avoid aging interruption. Third, the performance of the instrument in the oscillatory experiments was tested.

Temperature distribution

The temperature distribution inside the plate-plate geometry with diameter of 60 mm (PP/60) and a gap of 2 mm was measured using a calibrated thermocouple. The temperature distribution study was performed at a plate temperature of 40 °C. The temperature was measured at nine different positions (see figure 2). A vapor lock was used to avoid sample evaporation. In order to prevent condensation on the shield, its temperature was kept at ~ 45 °C using an infra red lamp.

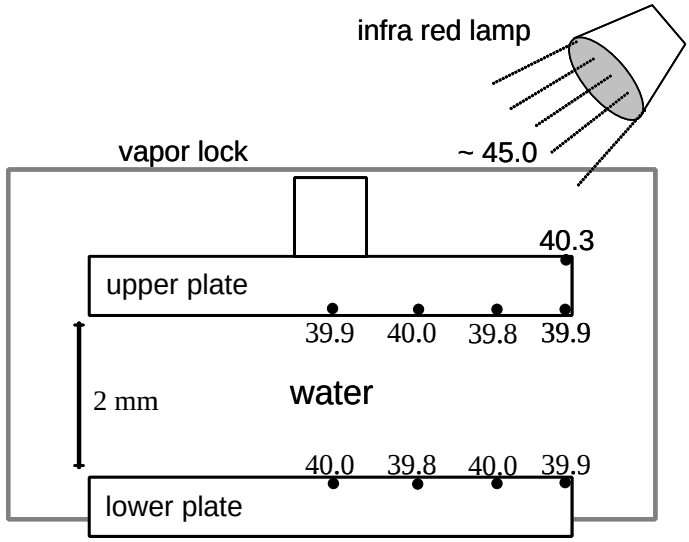

Figure 2. Temperature distribution inside the PP/60 geometry measured at a setting temperature of 40 °C.

The temperature distribution inside the PP/60 geometry, as shown in figure 2, shows that the maximum temperature difference in the vertical and horizontal direction is only 0.2 °C. The relatively homogenous temperature distribution inside the geometry ensures the homogeneity of the sample temperature within 0.2 °C.

Torque stability and oscillatory test

Since the aging process in this study is monitored by applying small shear stresses, the rheometer should be able to provide a well defined low amplitude constant shear stress over a long time scale. To test this small stress stability, the torque balance of the rheometer has been considered. The torque balance on the moving part of the rheometer reads:

$$M_{motor} = M_{bearing} + M_{sample} + I\ddot{\phi} \tag{2.4}$$

where M_{motor} is the driving torque from the motor, $M_{bearing}$ is the torque due to the air bearing, M_{sample} is the torque due to the sample, and $I\ddot{\phi}$ is the torque due to the inertia. For a Newtonian liquid, $M_{sample} = b\eta\dot{\phi}$ and therefore the angular speed $\dot{\phi}$ is:

$$\dot{\phi} = \frac{M_{sample}}{b\eta} = \frac{M_{motor} - M_{bearing} - I\ddot{\phi}}{b\eta} \tag{2.5}$$

where $b = 2\pi R^3/3\beta$ is a geometrical constant and η is the viscosity. Error analysis of equation 2.5 gives:

$$\left|\frac{\Delta\dot{\phi}}{\dot{\phi}}\right| = \left|\frac{\Delta M_{sample}}{M_{sample}}\right| \tag{2.6}$$

This equation shows that the torque fluctuation experienced by the sample is directly proportional to the angular speed fluctuation. This relation is used to identify the torque stability of our instrument.

To characterize the torque stability, three different constant torque amplitudes (0.5, 2.5, and 5.6 μNm) were applied to rotate the cone geometry. According to the manufacturer, the minimum applicable torque of this rheometer is 0.5 μNm. Figure 3 shows the relative angular speed fluctuation ($\Delta\dot{\phi}/ < \dot{\phi} >$) at different torque amplitudes where $\Delta\dot{\phi} = \dot{\phi} - < \dot{\phi} >$ and $< \dot{\phi} >$ is the average of $\dot{\phi}$ over all ϕ. The amplitude of the relative fluctuation decreases as the applied torque increases, however the curves fluctuate in very similar pattern.

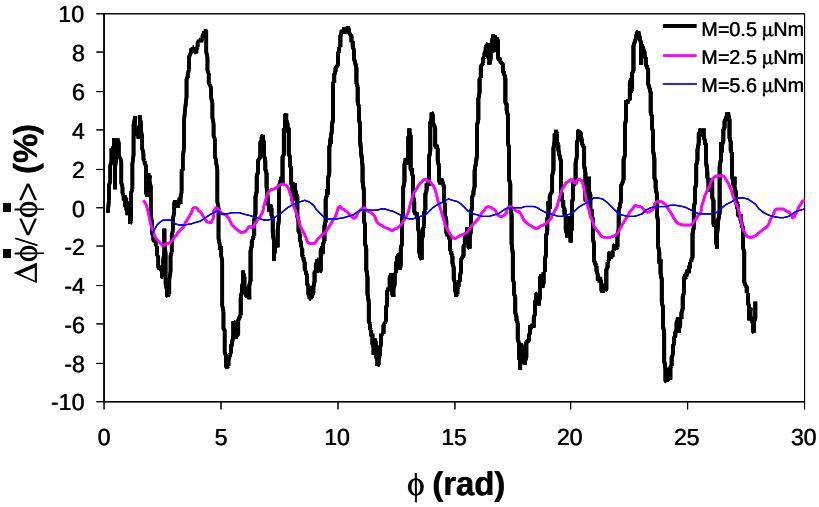

Figure 3. The relative angular speed fluctuation of Haake RS600 measured at different torques using silicone oil M10^{TM} at 22 ^{o}C.

When the rheometer is used at its minimum torque (0.5 μNm), it shows that the maximum angular speed fluctuation is 9%, which directly corresponds to its torque fluctuation (see equation 2.6). The relative fluctuation decreases dramatically as the applied torque increases. At $M_0 = 2.5$ μNm, the maximum error is 1.6% and becomes 0.5% at $M_0 = 5.6$ μNm. Therefore, the expected maximum experimental error of the instrument when used in its lower torque limit is $\sim 9\%$. This relative experimental error is related to torque fluctuation of 0.045 μNm and, for the cone and plate geometry, a shear stress of 0.8 mPa. The possible sources of the angular speed fluctuation are the torque fluctuation of the motor, the imperfectness of the air bearing system, and the inertia of the moving parts as indicated by equation 2.5.

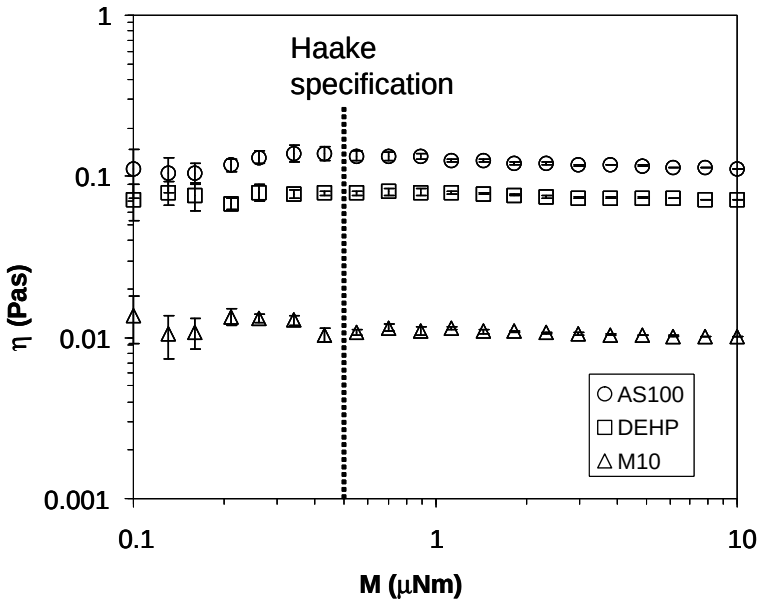

Figure 4. Viscosity of Newtonian liquids measured with Haake RS600 at 22 °C. The dashed line indicates the minimum torque specified by the manufacturer.

In addition to the measurement of the angular speed fluctuation during rotation, we also measure the viscosity of Newtonian liquids (Di(2-ethylhexyl) phthalate (DEHP), M10^{TM}, and AS100^{TM}) in the vicinity of the torque limit ($0.1 - 10$ μNm) and $T = 22$ °C. Figure 4 shows the viscosity of the three different Newtonian liquids. The viscosity of the liquids is constant at torques well above 0.5 μNm but deviates up to $\sim 10\%$ at lower torques as indicated by the error bars. This result indicates that the 9% torque fluctuation measured in the torque stability test is also observed in the viscosity measurements.

The instrument is also tested for its ability in an oscillatory experiment. For oscillatory experiments, an oscillating torque ($M_{motor} = M_0 e^{i\omega t}$) is applied and the resulting angular displacement ϕ with a phase lag δ ($\phi = \phi_0 e^{i(\omega t - \delta)}$) is recorded. Since $M_{sample} = cG^*\phi$ and neglecting the torque due to the air bearing, from equation 2.4 we obtain

$$M_{motor} - I\ddot{\phi} = cG^*\phi \tag{2.7}$$

and therefore the complex modulus $G^* = G' + iG''$ is

$$
\begin{aligned}
G^* &= \frac{iM_0\sin(\delta)}{c\phi_0} + \frac{M_0\cos(\delta)+\omega^2 I\phi_0}{c\phi_0} \\
G' &= \frac{M_0\cos(\delta)+\omega^2 I\phi_0}{c\phi_0} \\
G'' &= \frac{M_0\sin(\delta)}{c\phi_0}.
\end{aligned}
$$

The corresponding real (η') and imaginary (η") part of the complex viscosity $\eta^* = G^*/i\omega = \eta' - i\eta$" are given by:

$$\eta' = \frac{M_0\sin(\delta)}{\omega c\phi_0} \tag{2.8}$$

$$\eta" = \frac{M_0\cos(\delta)}{\omega c\phi_0} + \frac{I}{c}\omega \tag{2.9}$$

where c is a constant, M_0 is the torque amplitude applied at a frequency ω and ϕ_0 is the amplitude of the angular displacement.

To test the instrument in an oscillatory experiment, we measured the real (η') and imaginary (η") viscosity of a Newtonian sample (DEHP). The viscosities were measured at $M_0 = 50$ μNm, $T = 25$ ^{o}C, and $\omega = 0.062 - 100$ rad/s.

Figure 5 shows the real (η') and the imaginary viscosity (η") of the Newtonian sample. The real viscosity is more than 2.5 decades higher than the imaginary viscosity over the entire observed frequency (ω). The real viscosity is independent of the frequency whereas the imaginary viscosity decreases as function of frequency.

For an ideal Newtonian liquid, the phase lag (δ) between the torque and the angular displacement is $\pi/2$ and therefore the imaginary viscosity is theoretically zero. However, figure 5 shows that the imaginary viscosity of DEHP is systematically bigger than zero.

In order to investigate the source of the imaginary viscosity (η"), we considered the phase lag between the torque and the angular displacement. Over the entire frequency range, we found that the phase lag (δ) is always smaller than its ideal value ($\pi/2$). In figure 5 we plot the extra phase lag ($\varepsilon = \pi/2 - \delta$) as a function of the frequency. We found that ε decreases as a function of its frequency. By Incorporating ε into equation 2.8 and 2.9 we obtain:

$$\eta' = \frac{M_0\sin(\pi/2-\varepsilon)}{\omega c\phi_0} = \frac{M_0}{\omega c\phi_0} \tag{2.10}$$

$$\eta" = \frac{M_0\cos(\pi/2-\varepsilon)}{\omega c\phi_0} = \frac{M_0\varepsilon}{\omega c\phi_0}, \tag{2.11}$$

and therefore $\varepsilon = \eta"/\eta'$. In figure 5, we plot the ratio between the imaginary and the real viscosity ($\eta"/\eta'$) as a function of the frequency and we found that

they are in agreement with the extra phase lag ε calculated from the phase lag difference between the torque and the angular displacement. Therefore, this result shows that the η" observed in a Newtonian liquid measurement is due to the deviation from the ideal phase lag of a Newtonian liquid.

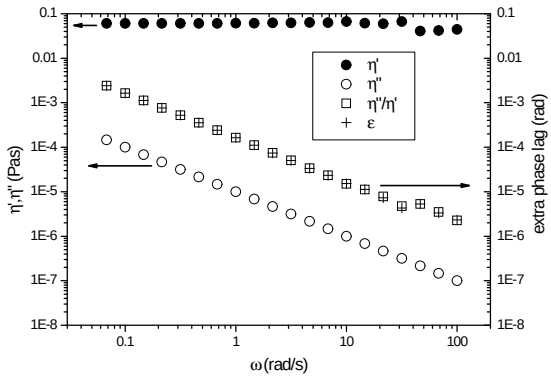

Figure 5. The η' (filled circles) and η" (open circles) of DEHP measured at 25 °C.

In conclusion, from this characterization we found that the temperature distribution inside the geometry is within 0.2 °C, the maximum torque fluctuation at its lower limit (0.5 μNm) is 9% which is related to shear stress fluctuation of 0.8 mPa for the cone and plate geometry, and the rheometer is suitable for oscillatory experiments as indicated by its performance in the oscillatory test.

2.2.2 Confocal scanning laser microscope (CSLM)

A confocal scanning laser microscope (CSLM) is a microscope that uses laser light to illuminate the sample (figure 6). The confocal microscope produces sharp and clear images by illuminating the specimen point-by-point and rejecting the light that does not come from the focal point [1]. The laser light is directed by the CSLM unit that scans the sample in a horizontal xy plane. The light passes through the microscope objective and excites the fluorescent particles. The fluoresced light from the sample partially passes back through the objective and measured by a detector in the CCD camera. In this way, an image is reconstructed in the CCD camera. Due to its ability to produce sharp images and its versatility, confocal microscopy has been used to track the particle dynamics in hard sphere colloidal glasses [2], living cells [3], and F-actin networks [4-7].

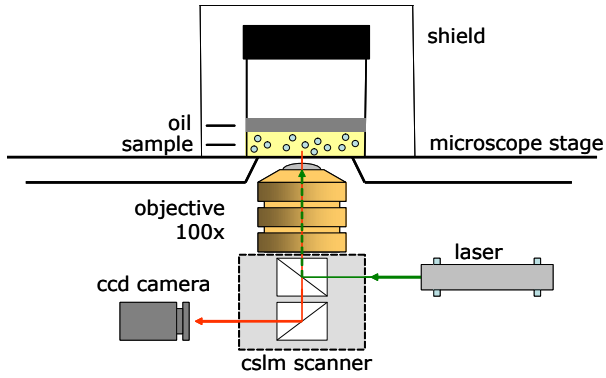

Figure 6. A schematic picture of a CSLM set up.

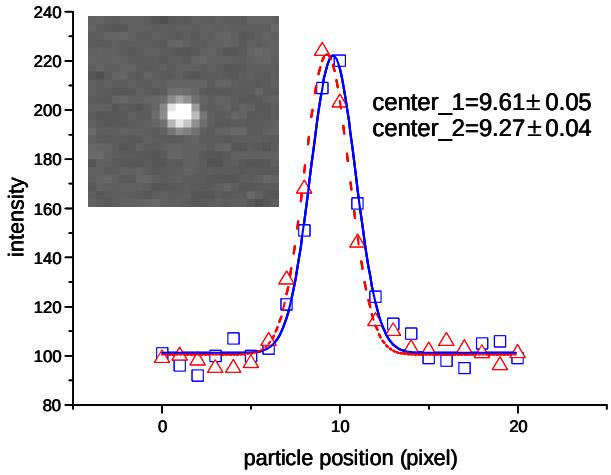

Figure 7. Particle position of an particle in two consecutive images. The inset shows an image of a fluorescent particle.

The fluorescent particle appears as an extended airy disk that spread over several pixels, typically 5×5 (inset of figure 7). By fitting this intensity plot with a 2D Gaussian profile, the position of the center of the particle can be determined on sub pixel level with a resolution of 0.05 pixel, which corresponds to $0.05 \times 0.13\ \mu m = 6$ nm. The dynamics of probe particles embedded in the sample are followed by taking the images of the probe particles at a certain frequency rate. The image is analyzed to find the center of mass of the probe particles as shown in figure 7. By knowing the particle position in two consecutive images, we can determine the particle displacement. A track of an particle is constructed by following the position of the particle over a certain time t. From the track we can calculate the mean squared displacement (MSD) in 2D $\langle \Delta r^2(t) \rangle = \langle [x(t_0 + t) - x(t_0)]^2 + [y(t_0 + t) - y(t_0)]^2 \rangle$.

Displacement resolution

In aging glassy systems, the expected displacements are very small. Therefore, it is necessary to determine the displacement resolution of our CSLM to ensure that we obtain reliable data.

The displacement resolution of the CSLM was studied by measuring the displacement of the particles glued on a Delta T culture dish (Bioptechs, Butler, PA, USA) as a function of time. The fluorescence particles (sulfate modified polystyrene from invitrogen^{TM} with a diameter of 227 nm) were glued to the dish by adding one drop of probe suspension (0.0001 w/w) and drying in an oven at 80 ^{o}C for about 4 hours. The position of the probe particles was followed with the CSLM by taking 2600 images at a rate of 1 image per second using a 100× objective. The images were analyzed using IDL^{TM} software to determine the center of mass of the individual probe particles in every image and to construct the trajectory of every single particle. The MSD of the glued particles is calculated by taking the ensemble and time average of the squared displacements.

Figure 8 shows the MSDs of the probe particles glued on the dish. At short times ($t \leqslant 500$ s) the MSDs stays constant at $\sim 4 \times 10^{-5}$ μm^2, which corresponds to a displacement as small as 6 nm. This corresponds with the accuracy of the position determination. However, at long times ($t \sim 1000$ s), the MSD increases up to $\sim 7 \times 10^{-5}$ μm^2, which corresponds to a displacement of $\sim$ 9 nm. The increase of the MSD at long time can be due to a drift for instance of the microscope stage. From this we conclude that we can detect displacement in the order of 6 (9) nm or larger at short (long) time scale.

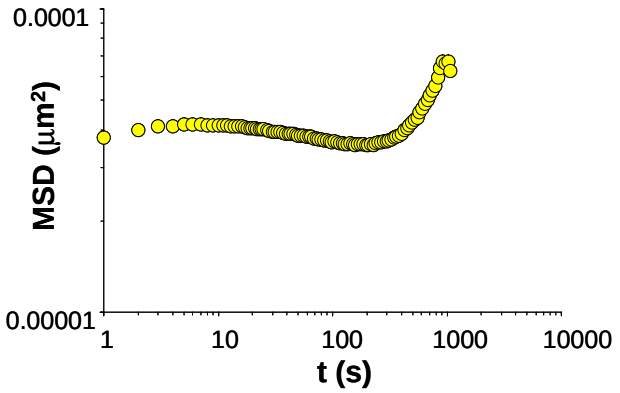

Figure 8. The mean squared displacement of probe particles glued on the Delta T culture dish.

Particle tracking microrheology (PTM)

Particle tracking microrheology is one of the techniques used to measure the local rheological properties of a sample. In PTM, the rheological properties are determined from the observed dynamic of the embedded probe particles. The motion of these particles is driven purely by thermal energy k_BT in the case of passive particle tracking. For a purely Newtonian liquid, the mean squared displacement (MSD) of the probe particles scales linearly with time $\left(\left\langle \Delta r^2(t)\right\rangle \sim t\right)$. For a viscoelastic material, the probe particle motion is sub-diffusive $\left\langle \Delta r^2(t)\right\rangle \sim t^n$ where $n < 1$. Faster than linear growth of MSD (superdiffusive) is only obtained if an active force drives the particle motion such as adenosine triphosphate (ATP) in living cells [3].

In the following we describe briefly the basics of microrheology and the formulas used to calculate the rheological quantities from the MSD following Mason *et al.* [8,9]. The dynamics of a single particle in a complex fluid is described by the generalized Langevin equation:

$$m\dot{v} = f_R(t) - \int_0^t dt'\zeta(t-t')v(t') \tag{2.12}$$

where m and $v(t)$ are the particle mass and velocity, respectively and $f_R(t)$ is the random force that drives the particle motion. The second term on the right hand side represents the history dependent friction force assuming that $\zeta(t) = 6\pi aG(t)$ where a is the radius of the particle and $G(t)$ is the relaxation modulus. Equation 2.12 can be solved using the unilateral Laplace transform defined as:

$$g(s) = \mathcal{L}\left\{g(t)\right\} = \int_0^\infty g(t)\exp(-st)dt.$$

The solution of equation 2.12 in the Laplace domain is :

$$\tilde{v}(s) = \frac{\tilde{f}_R(s) + mv(0)}{\tilde{\zeta}(s) + ms}. \tag{2.13}$$

Multiplying equation 2.13 with $v(0)$ and averaging yields:

$$\tilde{\zeta}(s) = \frac{k_BT}{\langle v(0)\tilde{v}(s)\rangle} - ms \tag{2.14}$$

where k_BT stems from the equipartition of energy ($k_BT = m\left\langle v^2(0)\right\rangle$). Since $\langle v(0)\tilde{v}(s)\rangle = s^2\left\langle \Delta\tilde{x}^2(s)/2\right\rangle$ [8], with $\left\langle \Delta\tilde{x}^2(s)\right\rangle$ the Laplace transform of $\left\langle \Delta x^2(t)\right\rangle$, we obtain:

$$\tilde{\zeta}(s) = 6\pi a\tilde{G}(s) = \frac{2k_BT}{s^2\left\langle \Delta\tilde{x}^2(s)\right\rangle} - ms. \tag{2.15}$$

In two dimensions and for small particles in which case inertia can be neglected, we have:

$$\tilde{G}(s) = \frac{4k_BT}{6\pi as^2\left\langle \Delta\tilde{r}^2(s)\right\rangle}. \tag{2.16}$$

Using equation 2.16, we can determine in principle $\tilde{G}(s)$ from the MSD ($\langle \Delta r^2(t) \rangle$). However, in practice it is hard to determine the Laplace transform of the $\langle \Delta r^2(t) \rangle$ due to the limited experimental time range and inaccuracies. Therefore Mason [9] suggests an approximating method that is based on a local power law description of $\langle \Delta r^2(t) \rangle$. By assuming that

$$\langle \Delta r^2(t) \rangle = \langle \Delta r^2(t_0) \rangle \left(\frac{t}{t_0} \right)^{\alpha(t_0)}$$

where

$$\alpha(t_0) = \left[\frac{d \ln \langle \Delta r^2(t) \rangle}{d \ln t} \right]_{t_0}$$

we calculate the Laplace transform of $\langle \Delta r^2(t) \rangle$ at $s = 1/t_0$ and obtain:

$$\tilde{G}(s) \simeq \frac{4k_B T}{6\pi a s \langle \Delta r^2(1/s) \rangle \Gamma[1 + \alpha(s)]} \tag{2.17}$$

where Γ is the gamma function, which is well estimated by: $\Gamma[z] \approx 0.457(z)^2 - 1.36(z) + 1.90$ for $1 \leqslant z \leqslant 2$.

From equation 2.16 we arrive via analytic continuations at:

$$\eta^*(\omega) = \tilde{G}(i\omega) = \frac{4k_B T}{6\pi a (i\omega)^2 \langle \Delta \tilde{r}^2(i\omega) \rangle} \tag{2.18}$$

and

$$G^*(\omega) = i\omega \tilde{G}(i\omega) = \frac{4k_B T}{6\pi a (i\omega) \langle \Delta \tilde{r}^2(i\omega) \rangle} \tag{2.19}$$

Using the same power law approximation but with $t_0 = 1/\omega$ we obtain:

$$G^*(\omega) = i\omega \eta^*(\omega) = \frac{4k_B T}{6\pi a \langle \Delta r^2(1/\omega) \rangle} \frac{\exp\left(\frac{i\pi}{2}\alpha(\omega)\right)}{\Gamma[1 + \alpha(\omega)]} \tag{2.20}$$

with

$$\alpha(\omega) = \left[\frac{d \ln \langle \Delta r^2(t) \rangle}{d \ln t} \right]_{t=1/\omega}.$$

For the real and the imaginary parts we find:

$$G'(\omega) = \frac{4k_B T}{6\pi a \langle \Delta r^2(1/\omega) \rangle} \frac{\cos(\pi\alpha(\omega)/2)}{\Gamma[1 + \alpha(\omega)]} \tag{2.21}$$

$$G''(\omega) = \frac{4k_B T}{6\pi a \langle \Delta r^2(1/\omega) \rangle} \frac{\sin(\pi\alpha(\omega)/2)}{\Gamma[1 + \alpha(\omega)]} \tag{2.22}$$

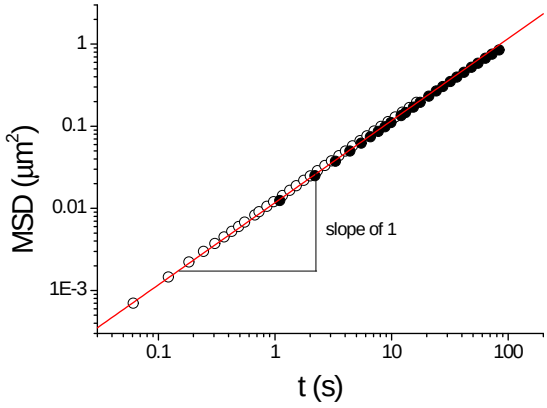

Figure 9. The MSD of the probe particles in a glycerol solution. The open and closed symbols are the MSD obtained from the fast and slow recordings respectively.

To study the capabilities of our CSLM we measured the rheological properties of a Newtonian liquid. We used a glycerol solution embedded with probe particles. The sample was prepared by adding 0.2 grams of suspension of 0.5% w/w probe particles (sulfate modified polystyrene which has a diameter of 227 nm) into 9.8 gram of 100% glycerol. The sample was stirred overnight to mix the probe particles homogeneously. One milli-liter of sample was loaded to the sample container and the particle tracking was performed at room temperature ($\sim$ 25 ^{o}C). To avoid any wall effects, the particle dynamics was monitored by taking images at 30 μm from the bottom of the sample container. Two different recording rates (16.7 and 1 image per second) were used to capture both the short and long time scale behavior.

Figure 9 shows the MSD, $\langle \Delta r^2(t) \rangle$, of the probe particles in 98% glycerol as a function of time t. The MSD obtained either from fast or slow recording scales with t shows that the probe particles behave diffusively. The combination of the fast and slow scanning covers more than three decades of t and they are quantitatively in agreement. The minimum t is set by the maximum recording speed of the CCD camera. The maximum t is determined by the maximum time the particles stay in the focal plane. The data shows that a MSD as low as $\sim 5 \times 10^{-4}$ μm^2 can be detected with the set up. This MSD is still one order of magnitude higher than the displacement resolution ($\sim 4 \times 10^{-5}$ μm^2).

Using equations 2.21 and 2.22, the viscoelastic properties ($G'(\omega)$ and $G''(\omega)$) of the sample can be calculated from the MSD as presented in figure 10. The loss modulus ($G''(\omega)$) is $\sim$1.5 order of magnitude higher than the elastic modulus ($G'(\omega)$) over the entire observation frequency. Theoretically, the $G'(\omega)$ is

zero for a purely Newtonian liquid. The observed $G'(\omega)$ in figure 10 is due to the slope of the MSD curve in figure 9, which is not exactly one but 0.98. In this figure we also plot the loss modulus calculated from the viscosity of the solution using the Stokes-Einstein relation $G''(\omega) = \eta\omega = 4\omega K_B T t/6\pi a \left\langle \Delta x^2(t) \right\rangle$. This loss modulus is in agreement with the loss modulus calculated using the approximation method (equation 2.22) indicating that the approximation method especially for a Newtonian liquid is reliable.

Now, we compare the particle tracking microrheology with the macrorheology. The viscosity obtained from the particle tracking method is 0.623 ± 0.003 Pas whereas the viscosity measured using Haake RS600 rheometer is 0.498 ± 0.001 Pas. Two possible sources for this viscosity difference are the absorption of water to the sample during measurement using the rheometer [10] and the precision of the particle radius.

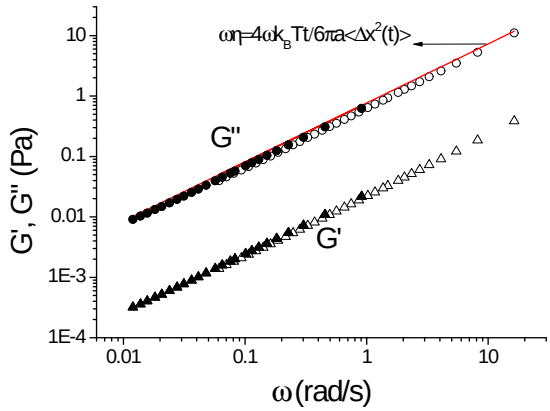

Figure 10. The loss modulus ($G''(\omega)$) and the elastic modulus ($G'(\omega)$) of 98% glycerol calculated from the MSD obtained from the fast (open symbols) and slow recording (closed symbols). The solid line is the loss modulus calculated from the viscosity of the solution ($G''(\omega) = \eta\omega = 4\omega K_B T t/6\pi a \left\langle \Delta x^2(t) \right\rangle$).

In conclusion, from the glued particle sample we found that the displacement resolution is 6 nm at short times and rises to 9 nm at long times. The set up has been also successfully tested to measure the MSD of the probe particles in a Newtonian liquid that increases linearly with t. We found that the minimum t of the MSD is set by the speed of the camera whereas the maximum t is determined by the diffusion of the particles in the vertical direction. Moreover, we have shown that from the MSD we can calculate the rheological moduli of a Newtonian liquid using the approximation method of the generalized Stokes-Einstein equation.

2.3 Systems

2.3.1 Literature review

As model systems for the aging study we used suspensions of thermosensitive microgel particles, which include two batches of poly-N-isopropylacrylamide (PNIPAM) particles (P-1 [11] and P-2 [12]) and one batch of core-shell microgel particles (P-P [13-15]). The core-shell particles (P-P) consist of a poly-N-isopropylacrylamide (PNIPAM) core and a poly-N-isopropylmethacrylamide (PNIPMAM) shell.

PNIPAM is a cross-linked polymer with N-isopropylacrylamide (NIPAM) as the building block. The crosslinker normally used in the PNIPAM synthesis is N,N'-methylene bis(acrylamide). However, PNIPAM particles without the use of cross-linker have also been successfully synthesized [16,17].

The PNIPAM microgel particles are in a swollen state below its lower critical solution temperature ($\sim 32\,^{o}$C) and shrink very sharply above it. In the swollen state, the internal structure of the PNIPAM microgel is not homogenous. The radial density of the polymer is higher in the center of the particles. Whereas in the shrunken state the PNIPAM particles have a box profile and the polymer density is homogenous from the center to the surface [18].

Gao and Hu [19] report the structural properties as obtained from light scattering measurements of PNIPAM microgel particles in water. They find that, at room temperature, as the mass concentration m increases, the microgel suspension goes from a liquid ($m < 3\%$ w/w), to a crystalline ($3\% < m < 5\%$), and then a glass state ($5\% < m < 14\%$) while the optical appearance of the dispersion changes progressively from transparent to cloudy to colored (pink, green, blue, and purple gradually) and to transparent again.

Senff and Richtering [20] report the rheological properties of different cross-linking density of PNIPAM particles. In the low volume fraction (<50%), the PNIPAM particles behave like hard spheres. However, at higher volume fractions the rheological behavior deviates from the hard sphere behavior. They find that the crystallization of the swollen PNIPAM particles start at effective volume fraction of around 0.59 [21] . This transition is bigger than the freezing transition of hard sphere which is 0.494, which strongly indicates that the swollen PNIPAM particles are soft.

For the core-shell particles (P-P), both the core and the shell are thermosensitive but with different lower critical solution temperatures (LCST). This is a new microgel particle that synthesized for the first time in 2003 [13]. In D_2O, the core PNIPAM has LCST of 34 ^{o}C, whereas the LCST of the shell PNIPMAM is 44 ^{o}C. The shell prevents the aggregation of the microgels up to 44 ^{o}C. Depending on the mass ratio of the shell and the core, the microgel particles may have different properties. Microgel particles with thin shells show

two transition temperatures associated with the transition temperature of the core (PNIPAM) and the shell (PNIPMAM). The transition temperature of the core is less pronounced in a microgel particle with a thicker shell [15].

2.3.2 System characterization

In order to characterize the model systems, the temperature dependence of the particles size is determined using light scattering techniques. Static light scattering (SLS) and dynamic light scattering (DLS) are used to measure the radius of gyration and the hydrodynamic radius, respectively. The radius of gyration, R_g, obtained from SLS is defined as $R_g = \sqrt{\left(\Sigma m_i r_i^2\right)/\Sigma m_i}$ where m_i is the mass of the i^{th} fraction of the particles and r_i is the distance of the i^{th} fraction from the center of mass of the particle. Practically, the radius of gyration is extracted from the form factor using a Guinier's plot $\left(\ln\left(I\left(q\right)\right) - \ln\left(I\left(0\right)\right) = -q^2 R_g^2/3\right)$, where $I(q)$ and $I(0)$ is the light intensity measured at an angle θ and at zero angle respectively, with $q = 4\pi n \sin(\theta/2)/\lambda_0$ where n is the solution refractive index and λ_0 is the incident wavelength in vacuum [22].

On the other hand, the hydrodynamic radius is defined as the radius of the hypothetical hard-sphere that diffuses with the same speed as the particle under examination. In fact, the measured quantity in dynamic light scattering is the intensity fluctuation of the scattered light as function of time. The autocorrelation function of the scattered light intensity provides information about the diffusion coefficient of the particle. The Stokes-Einstein's equation $(D = kT/6\pi\eta_0 R_h)$ provides the relation to extract the hydrodynamic radius R_h from the diffusion coefficient D.

The system was characterized by studying on the effect of mass concentration of the suspension on the measured radius. Then, using the suitable mass concentration, the reversibility of the temperature dependent radius was studied by measuring the particle size during heating and cooling. In order to study the stability of the systems during storage at high mass concentration, the size of the particles was measured directly after the synthesis and 3 years later. After characterizing the temperature dependence of the particles size, we determined the volume fraction of the particle suspensions by measuring the viscosity of the solvent (η_s) and that of the suspensions η using the Haake RS600 rheometer. The volume fraction ϕ of the diluted suspensions was determined using Einstein's relation: $\eta/\eta_s = 1 + 2.5\phi$ for $\phi \ll 1$.

Figure 11 shows the hydrodynamic radius of the P-1 system at different mass concentrations measured as a function of temperature. The radius of the particle decreases as temperature increases. The radius decreases steadily from 20 to 30 °C, followed by a sharp decrease with a transition temperature of about 32 °C. At temperatures above 35 °C, the radius stays almost constant.

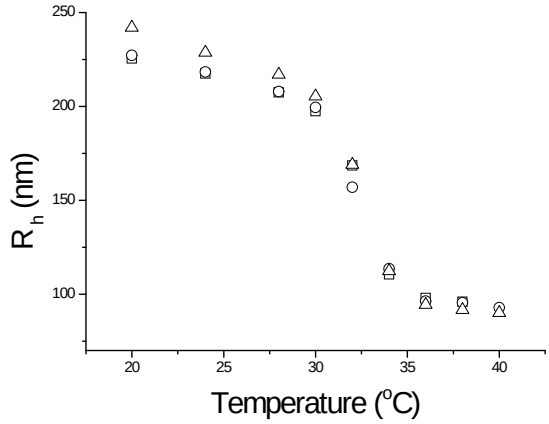

Figure 11. The temperature dependent hydrodynamic radius $R_h(T)$ of P-1 particles measured at different mass concentrations ($\square$ = 0.005% w/w, $\bigcirc$ = 0.01% w/w, $\triangle$ = 0.05% w/w). The error bars are smaller than the symbols

At low temperatures (T<32 ^{o}C), the P-1 particles are swollen because there is a strong interaction between the PNIPAM polymer and water (solvent). In other words, water is a good solvent for the P-1 particles at low temperatures. On the other hand, at high temperatures (T>32 ^{o}C) water is a poor solvent for P-1 particles and therefore they shrink [23,24]. The transition from the swollen to the shrunken state near 32 ^{o}C is in very good agreement with the previous studies [23,24].

Figure 11 also shows that the hydrodynamic radius of 0.05% w/w P-1 particles is slightly higher than the other mass concentrations especially at low temperature, which indicates hydrodynamic interactions between neighboring particles. However, for mass concentration $\leqslant$ 0.01% w/w the hydrodynamic radius is independent of mass concentration and depends only on the temperature. Therefore, 0.01% w/w suspension is used as our standard mass concentration for the rest of the study.

Figure 12 shows the dependence of the hydrodynamic radius of P-1 and P-P on the temperature during heating and cooling. The hydrodynamic radius decreases during the heating and increases during cooling. The transition from the swollen state at low temperatures to the shrunken state at high temperatures is very sharp for P-1 samples, whereas the radius of core-shell (P-P) particles decreases gradually as the temperature increases. Both samples show the collapse of the heating and the cooling curves.

It is known that above the transition temperature, the PNIPAM particles shrink resulting in a higher density and thus a greater Hamaker constant [23]. The increase of the Hamaker constant increases the attractive van der Waals

forces which cause aggregation. In addition, the shrinking of the particles also collapses the dangling PNIPAM tails on the surface of the particles diminishing their steric stabilization. However, the reversible size of the particles during heating and cooling indicates that this aggregation is reversible.

The reversible dependence of the particle size on temperature provides a convenient way to control the volume fraction of such a thermosensitive particles. The volume fraction of a suspension of the thermosensitive particles can be increased by decreasing the temperature and vice versa. The P-P system provides wider temperature range to control the volume fraction gradually due to the gradual change of the P-P radius.

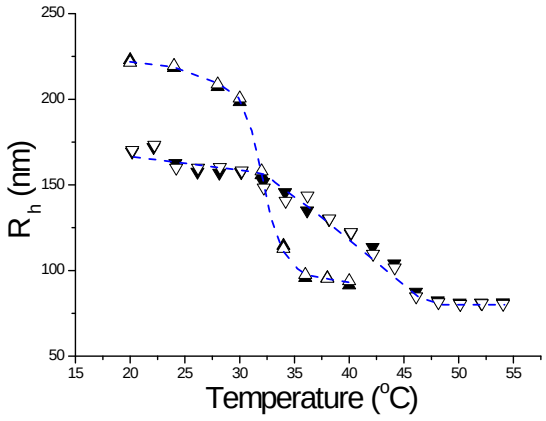

Figure 12. $R_h(T)$ of P-1 ($\triangle$) and P-P ($\bigtriangledown$) measured during heating (filled symbols) and cooling (empty symbols). The error bars are smaller than the symbols. The dashed lines are drawn to guide the eye.

Figure 13 shows the radius of gyration of 0.01% P-1 systems measured directly after the synthesis and the system that was stored for 3 years at high mass concentration ($\sim$ 4% w/w) in the refrigerator ($\sim$ 4 ^{0}C). We observe that both the fresh and the stored P-1 system have similar temperature dependence behavior. The size of the particle and its transition temperature stay constant for three years. This result strongly indicates that the system is both chemically and physically very stable.

After knowing the temperature dependence of the radius of the microgel particles and their stability, now we consider their volume fraction measured rheologically using the Einstein's relation. Figure 14 shows the volume fraction of the systems as a function of their concentration. The volume fraction ϕ of a dilute suspension increases linearly with the mass fraction m i.e. $\phi = a \times m$. The proportionality constant a is determined from the slopes of the

curves in figure 14: $a = 124 \pm 11$, 59 ± 4 and 42 ± 1 for the system P-1, P-2 and P-P, respectively. From this relation we can can calculate the volume fraction at higher mass concentrations that can easily exceeds unity. This is because we assume that the particles are undeformable. However, because the microgel particles are soft and deformable the effective volume fraction $\phi_{eff.}$ can not exceeds unity. Increasing the mass fraction m only increases the degree of compression between the particles. More over, by combining with the temperature-dependence radius we can calculate the volume fraction ϕ as function of the mass concentration and the temperature.

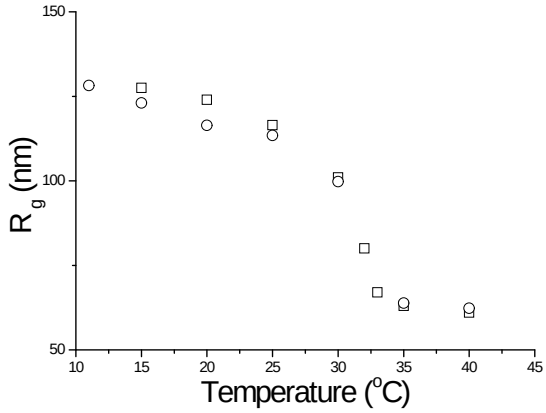

Figure 13. The radius of gyration (R_g) of P-1 measured directly after synthesis (□) and 3 years later (◯). The error bars are smaller than the symbols.

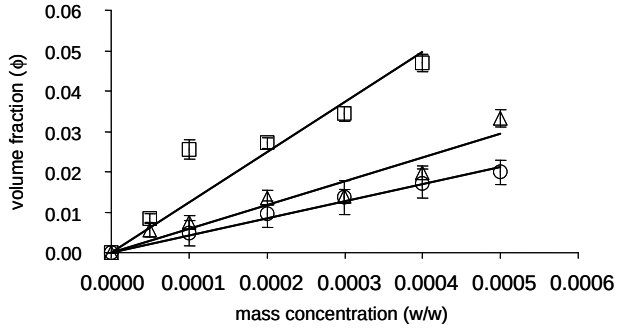

Figure 14. The volume fraction ϕ as calculated from the viscosity data using the Einstein relation of dilute P-1 (□), P-2 (△), and P-P (◯) suspensions as function of their mass fraction m (w/w) measured at 24, 20, and 24 °C respectively. The lines indicate the linear regressions of the corresponding data.

2.4 Rejuvenation

Aging is one of the unique properties of materials in glassy state. The rheological properties of an aging system evolve continuously and never reach an equilibrium [25]. An important condition for the characterization of an aging material is to prepare the sample in a well-defined initial state. Commonly this is achieved by exposing the sample to a large strain or stress (larger than the yield stress) for a sufficiently long time [26-31]. In the terminology of the jamming phase diagram proposed by Liu and Nagel [32], we can rejuvenate a system by bringing the system out of the jammed state. This can be achieved not only by applying a stress larger than the yield stress, but also decreasing the volume fraction and increasing the temperature. The rejuvenation randomizes the structure and erases all internal stresses introduced to the system earlier.

2.4.1 Mechanical vs thermal rejuvenation

Since we have a thermosensitive model system, we can rejuvenate the sample either mechanically or thermally. In the mechanical rejuvenation, the system is submitted to a shear stress larger than the yield stress. Whereas in thermal rejuvenation, the volume fraction of the system decreases as the temperature increases. This is because the size of the particle decreases as function of the temperature (see figure 12). The cessation of the shear stress and the fast re-cooling of the system bring it back to the glassy state.

We compare mechanical and thermal rejuvenation using a 7% P-1 system at 15 °C. Two milliliters of the system at 36 °C was injected into a Haake RS600 rheometer using cone-plate geometry with a cone angle of 2° and diameter of 60 mm. Subsequently the rheometer was cooled down to 15 °C. For the mechanical rejuvenation, the system was first sheared vigorously ($\sigma = 100$ Pa) for 60s. Whereas for the thermal rejuvenation, the sample was heated to 34 °C, i.e. above the volume transition temperature, for 60 s and then cooled back down to the measurement temperature at a rate of 0.7 °C/min. After the rejuvenation ($t = t_w = 0$), we allowed the system to rest for a waiting time $t_w = 10000$ s. Next, an oscillatory probe stress ($\sigma_p = 1$ Pa) was applied to determine $G'(\omega)$ and $G''(\omega)$, with ω increasing from 6.28×10^{-3} rad/s up to 6.28×10^{1} rad/s.

Figure 15 shows $G'(\omega)$ and $G''(\omega)$ of the system at $t_w = 10000$ s that was prepared by mechanical and thermal rejuvenation. The $G'(\omega)$ and $G''(\omega)$ presented in the figure is an average of three measurements. We do not observe significant variation between them as indicated by the error bar of $G'(\omega)$ and $G''(\omega)$ that is smaller than the symbols. This indicates that the measurements are reproducible and both the mechanical and the thermal rejuvenation provide a well defined initial state.

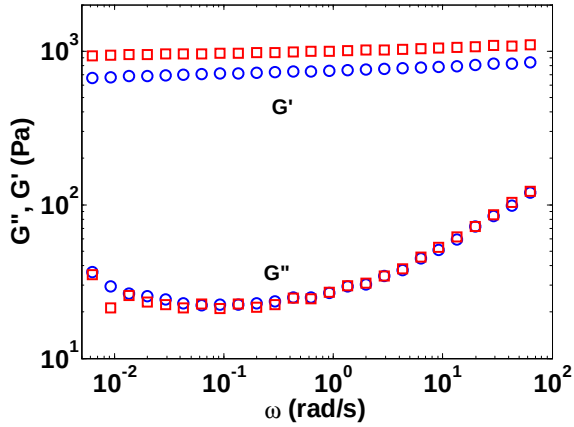

Figure 15. The $G'(\omega)$ and $G''(\omega)$ of P-1 suspensions (0.07 w/w) rejuvenated mechanically (O) and thermally (□). The moduli were measured at $T = 15$ °C and $t_w = 10000$ s.

Nevertheless, there is an interesting quantitative difference. $G'(\omega)$ of the thermally rejuvenated system is consistently higher than for a mechanically rejuvenated sample. The qualitative explanation for this difference is because the mechanical rejuvenation may create a slightly different structure giving rise to somewhat smaller yield energies and therefore decreasing $G'(\omega)$. On the other hand, due to the limited cooling rate, the temperature rejuvenation drives the sample into the glassy state more gradually. This gradual process results in a system with a more stable configuration and therefore has a higher $G'(\omega)$. From the observed difference in $G'(\omega)$ we may say that even though the two rejuvenation methods erase the sample memory, the initial states are not exactly the same. The average initial yield energies of the sample prepared thermally seems to be higher as indicated by higher $G'(\omega)$.

2.4.2 Step vs fading stress rejuvenation

We have shown that the mechanical rejuvenation prepares an aging system into a well defined initial state by applying a single step-up step-down stress well above the yield stress. We call this protocol step rejuvenation. However, the sudden cessation of the shear stress results in a strained system. Since the system is viscoelastic, the remaining strain causes a strain recovery in the creep experiments [26,31]. To overcome this problem a second protocol was developed in which the amplitude of an oscillating stress progressively decreases to zero.[1] This fading stress rejuvenation prepares a sample into a stress and strain free state after the rejuvenation and therefore eliminating the strain recovery effect.

[1] The idea of a fading stress rejuvenation was suggested by H. Rathgen

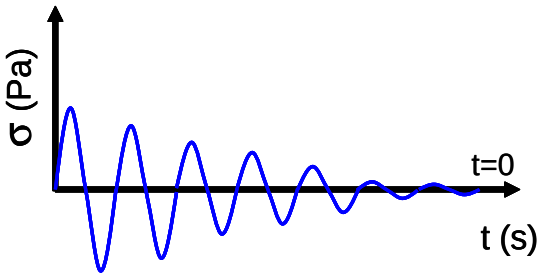

Figure 16. The schematic protocol for the fading stress rejuvenation.

Using a Haake RS600 rheometer with a cone-plate geometry (2^o angle and 60 mm diameter) we measured the strain evolution of a 7% P-P suspension at 25 ^{o}C. The system was prepared using a step stress and a fading stress rejuvenation without applying a probe stress (σ_p). In the step stress rejuvenation, a shear stress ($\sigma = 20$ Pa) was applied for 120 s to flow the sample. In the fading stress oscillation, a progressively decreasing oscillation stress (from 30 Pa to 0 Pa) was applied at $\omega = 6.28$ rad/s (see figure 16). The strain evolution ($\gamma(t) - \gamma(0)$), where $\gamma(t)$ is a strain at time t and $\gamma(0)$ is a strain at $t = 0$, was recorded. Initial time t=0 is defined as the end of the rejuvenation.

Figure 17 shows the strain evolution of the 7% w/w P-P suspension directly after the step stress and the fading stress rejuvenation. In the case of the fading stress rejuvenation, the strain stays constant at around zero over the observation time. In contrast, the strain decreases as function of time for the system prepared with the step stress rejuvenation.

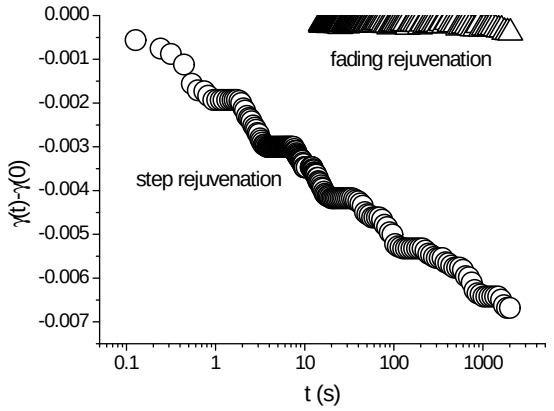

Figure 17. The strain evolution ($\gamma(t) - \gamma(0)$) of a 7% w/w P-P sample at 25 ^{o}C directly after the step stress and the fading stress rejuvenation.

The decrease of $\gamma(t) - \gamma(0)$ as function of time t shows a strain recovery. This is because the remaining strain after the step stress rejuvenation recovers due to the elasticity of the system. Whereas the absence of strain recovery from the sample prepared using fading rejuvenation indicates that the system is not strained after the rejuvenation.

Now we apply the fading stress rejuvenation method to prepare the system before a creep experiment. In the creep experiment, a constant probe stress ($\sigma_p = 0.05$ Pa) was applied and the strain evolution as a function of time was monitored. The probe stress was applied 30 s after the end of the rejuvenation ($t_w = 30$ s) for 2000 s.

Figure 18 shows the evolution of the strain ($\gamma(t) - \gamma(t_w)$) as a function of $t - t_w$. The strain continuously increases as t-t_w increases and shows no reversal. The absence of the strain reversal is because the system is strain-free after the rejuvenation.

This result is in contrast to the creep data reported in [26,31] which was prepared with step stress rejuvenation . The strain increases at short times ($t - t_w < t_w$) but decreases at longer times $t - t_w$. The decrease of the strain at longer times originates from the strain recovery due to the remaining strain after the rejuvenation.

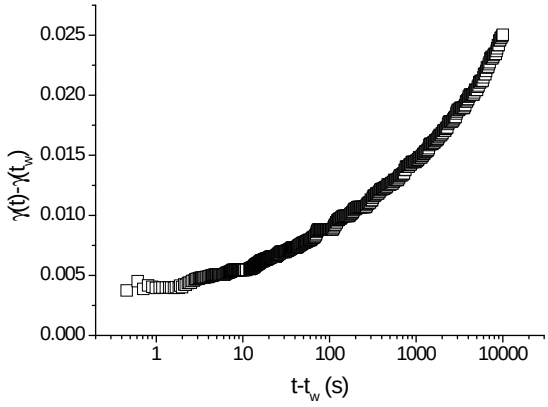

Figure 18. The strain evolution ($\gamma(t) - \gamma(t_w)$) of a 7% w/w P-P sample at 25 ^{o}C prepared with the fading stress rejuvenation; σ_p=50 mPa.

We also measured $G'(\omega)$ and $G''(\omega)$ of the system at 3000 s after a step stress and a fading stress rejuvenation ($t_w = 3000$ s). An oscillating stress with an amplitude of 1 Pa was applied to the system to measure $G'(\omega)$ and $G''(\omega)$ at $0.0628 \leqslant \omega \leqslant 62.8$ rad/s. Figure 19 shows the $G'(\omega)$ and $G''(\omega)$ of the system that was prepared using both the step stress and the fading stress rejuvenation. The $G'(\omega)$ is around one order of magnitude higher than

$G''(\omega)$ over three decades of frequency. The $G'(\omega)$ is almost constant over all frequencies, whereas $G''(\omega)$ shows a minimum at $\omega \sim 2$ rad/s.

The figure also shows that the $G'(\omega)$ and $G''(\omega)$ of the system prepared using fading stress rejuvenation is not significantly different from those prepared using step stress rejuvenation. This means that in principle we can use both the step stress and the fading stress rejuvenation before an oscillatory measurement of an aging system. However, using the fading stress rejuvenation we can not probe a system at very short t_w due to the finite time for the oscillatory stress to decrease to zero.

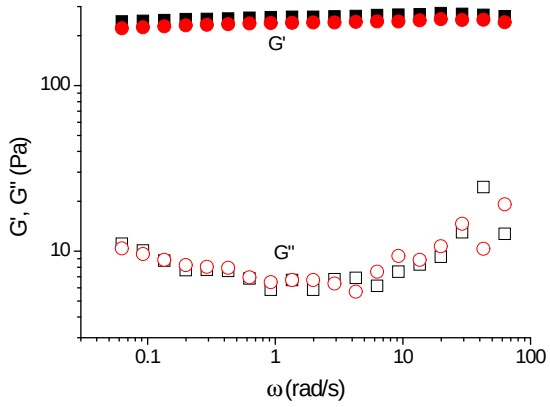

Figure 19. $G'(\omega)$ and G"(ω) of a 7% w/w P-P sample at 25 °C prepared with the step stress (□) and the fading stress (◯) rejuvenation.

In conclusion, we find that our aging thermosensitive system can be rejuvenated mechanically and thermally to obtain reproducible results. However, the mechanical and the thermal rejuvenation do not result in the same initial state as indicated by the difference in the amplitude of $G'(\omega)$.

The mechanical rejuvenation can be stopped either abruptly (step stress rejuvenation) of gradually (fading stress rejuvenation). A step stress rejuvenation produces a strained system at the end of the rejuvenation, whereas a fading stress rejuvenation produces a strain and stress free system.

For the oscillatory experiments, both the step stress and the fading stress rejuvenation result in almost the same behavior of $G'(\omega)$ and $G''(\omega)$. However, in the creep experiments, the fading stress rejuvenation results in a continuous increase of strain. On the other hand, the strain in the step stress rejuvenation increases only for short times $t - t_w < t_w$ and recovers for $t - t_w > t_w$.

References

[1] V. Prasad *et al.,* J. Phys. Condens. Matter **19,** 113102.(2007)

[2] R.E. Courtland and E.R. Weeks, J. Phys. Condens. Matter **15,** S359 (2003)

[3] P. Bursac *et al.,* Nature. Matter. **4,** 557 (2005)

[4] T. Gisler and D. A. Weitz, Phys. Rev. Lett. **82,** 1606 (1999)

[5] T.G. Mason *et al.,* J. Rheol. **44,** 917 (2000)

[6] H. Salman *et al.,* Chem. Phys. **284,** 389 (2002)

[7] M. L. Gardel *et al.,* Phys. Rev. Lett. **96,** 088102-1 (2006)

[8] T. G. Mason *et al.,* J. of Mol. struc. **383**, 81 (1996)

[9] T.G. Mason, Rheol. Acta **39,** 371 (2000)

[10] P.N. Shankar and M. Kumar, Proc. R. Soc. Lond. A **444,** 573 (1994)

[11] J. Gao, and Z, Hu, Langmuir **18,** 1360 (2002)

[12] R.H. Pelton, and P. Chibante, Colloids and Surface **20,** 247 (1986)

[13] I. Berndt and W. Richtering, Macromolecules **36**, 8780 (2003)

[14] I. Berndt *et al.*, J. Am. Chem. Soc. **127**, 9372 (2005)

[15] I. Berndt *et al.,* Langmuir **22**, 459 (2006)

[16] J. Gao and B.J. Frisken, Langmuir **19**, 5212 (2003)

[17] J. Gao and B.J. Frisken, Langmuir **19,** 5217 (2003)

[18] M. Stieger *et al.,* J. Chem. Phys. **120,** 6197 (2004)

[19] J. Gao and Z. Hu, Langmuir **18,** 1360 (2002)

[20] H. Senff and W. Richtering, Coll. and Polymer Sci. **278,** 830 (2000)

[21] H. Senff and W. Richtering, J. of Chem. Phys. **111,** 1705 (1999)

[22] K.S. Birdi, *Handbook of Surface and Colloid Chemistry* (Boca Raton, 1997)

[23] R. Pelton, Adv. in Coll. and Interface Sci. **85,** 1 (2000)

[24] T.G. Mazon and M.Y. Lin, Phys. Rev. Lett., **71** 040801 (2005)

[25] S.M. Fielding *et al.,* J. Rheol. **44,** 323 (2000)

[26] M. Cloitre, *et al.,* Phys. Rev. Lett. **85,** 4819 (2000)

[27] C. Derec *et al.,* Phys. Chem. **1,** 1115 (2000)

[28] C. Derec *et al.,* Phys. Rev. E. **67,** 061403-1 (2003)

[29] V. Viasnoff and F. Lequeux, Phys. Rev. Lett. **89,** 065701-1 (2002)

[30] P. Bursac *et al.,* Nature mater. **4,** 557 (2005)

[31] E.H. Purnomo *et al.,* Phys. Rev. E. **76,** 021404 (2007)

[32] A.J. Liu and S.R. Nagel, Nature **396, 21** (1998)

Chapter 3

Linear viscoelastic properties of aging suspensions

Abstract We have examined the linear viscoelastic behavior of poly-N-isopropyl acrylamide (PNIPAM) microgel suspensions in order to obtain insight in the aging processes in these densely packed suspensions at various temperatures below the volume transition temperature. The system is found to display a strong aging behavior. The viscoelastic moduli are compared to the predictions of the soft glassy rheology model. The model predicts quantitatively the loss modulus G"(ω,t), the elastic modulus G'(ω,t) and their ratio G"(ω,t)/G'(ω,t). A relative noise-temperature of $(X/X_g) \approx 0.62$ is obtained. Despite the fact that the microgel particles are more compressed and hence less mobile at a lower thermodynamic temperature T, (X/X_g) is found to be essentially independent of T within the range of 5 to 10 °C, which is below the volume transition temperature.[1]

A material undergoing aging never achieves thermodynamic equilibrium because the relaxation times increase with the age of the system. The dynamics in the material slow down with age but never stop. Aging and "close to aging" phenomena have been observed experimentally in polymers [1], colloidal suspensions [2-7], foams [8], and living cells [9-11]. When driven far from equilibrium, e.g. by applying a quench in mechanical strain or a thermal quench, the mechanical properties of these systems depend strongly on the waiting

[1] This chapter has been published in: Europhys. Lett. **76**, 74 (2006)

time t_w before the measurement. Frequently, the mechanical properties can be scaled onto each other by scaling the time with $(t_w)^\mu$ just as in case of amorphous polymers. However, the explanation given in the past for the aging of amorphous polymers does not hold for colloidal suspensions because the energies involved in the restructuring and equilibration processes are much larger than the thermal energy k_BT. Mode-coupling theory has been quite successful at describing various aspects of glassy materials, including soft glassy materials [12,13]. Explicitly time-dependent (aging) mechanical properties, however, are most directly described in the so-called soft glassy rheology (SGR) model developed by Sollich and co-worker [14-16] specifically for this class of materials. This model has been used to describe qualitatively or semi quantitatively the rheological properties of various systems, such as acrylate-metacrylic acid (AMA) [2], laponite [7], and living cells [9-11]. The key characteristic of the SGR model is an effective noise temperature which allows individual elements of the system to overcome yield energies substantially larger than k_BT. This effective noise temperature is related to the complex mechanical coupling between the densely packed individual elements in the systems.

In spite of the detailed level of predictions made by the SGR model, most comparisons to experimental data to date remained rather qualitative. In this chapter we compare quantitatively, the prediction of the SGR model to the linear viscoelasticity of Poly-N-isopropylacrylamide (PNIPAM) microgel particle suspensions. Owing to the thermosensitivity of this material, we can tune in situ the volume fraction by varying the temperature and thereby test the conjecture of Liu and Nagel [17] that both increasing abruptly the volume fraction and shearing the system mechanically can be used to produce similar well defined initial states in soft glassy materials. The paper is organized as follows: after a brief introduction into key elements of the SGR model, we describe our experimental procedures, followed by the presentation of the rheological measurements. We show that the SGR model can be fitted to the experimental results and we extract the effective noise temperature of our system for various conditions.

Sollich and co-workers [14-16] attribute similarities in the rheology of soft glassy materials (SGM) to the sheared features of structural disorder and metastability. Small domains (elements) are defined which can only relax under interaction with neighboring domains. The SGR model uses an effective noise temperature $\mathcal{X}$ to take into account the stochastic interaction of elements with their environment. In the model, the constitutive equation in one dimension is expressed as

$$\sigma(t) = G_p \langle l \rangle = G_p \int \int l\, P(E, l, t)\, dE\, dl$$

where G_p is the element elasticity and $P(E, l, t)$ is the probability for an element to be in a state with yield energy E and internal strain l at time t. For a small amplitude harmonic shear $\gamma(t) = \gamma_0 e^{i\omega t}$ this results in $\sigma(\omega, t) = \gamma_0 e^{i\omega t} G^*(\omega, t)$ with the time dependent dynamic moduli defined as

$$G^*(\omega, t) = G_p \left(1 - \int_0^t Y\,(t-s)\; G_\rho\,(s)\; e^{-i\omega s}\, ds\right). \tag{3.1}$$

Here Y is the yielding rate, and $G_\rho(s) = \int_0^\infty e^{(-s\exp(-E/\mathcal{X}))} \exp(-E)\; dE$. Equation 3.1 can be evaluated numerically to calculate the elastic modulus $G'(\omega, t)$ and the loss modulus $G''(\omega, t)$.

The system studied here is a suspension of poly-N-isopropylacrylamide (PNIPAM). This system displays a volume transition, which offers a unique way to control the degree of steric hindrance in the system. The PNIPAM particles were synthesized following the procedure described by Gao and Hu [18]. The sample was purified by centrifugation (15000 rpm, 2.5 hours) and redispersed at 25 °C. This procedure was repeated four times.

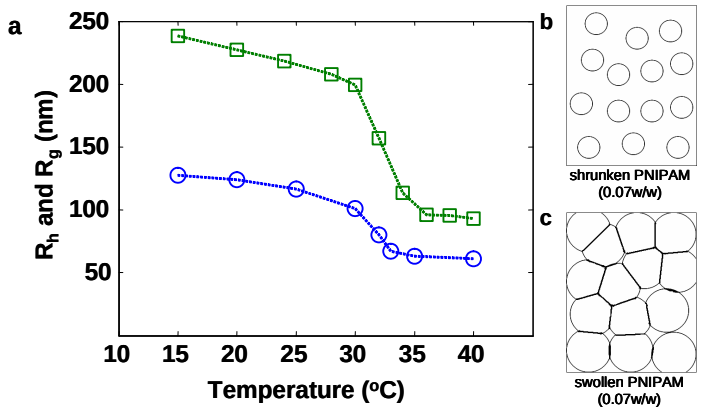

Figure 1. (a) The hydrodynamic radius (□) and the gyration radius (◯) of PNIPAM (0.0001 w/w). The schematic picture of the 0.07 w/w PNIPAM in shrunken (b) and swollen (c) state.

To characterize the volume transition we measured the radius of gyration (R_g) and the hydrodynamic radius (R_h) of the microgel particles as a function of temperature (15-40 °C) using static and dynamic light scattering, respectively, from very dilute suspensions (0.0001 (w/w)), see fig. 1(a). Between the highest and the lowest temperature, both radii vary by a factor of 2 to 2.5, corresponding to a variation of the particle volume of 8 to 15 times. It is worth noting that the ratio of the radii ($R_g/R_h = 0.55$ at 21 °C and 0.66 at 40 °C) is smaller than for hard-spheres (0.77), which indicates that the polymer density inside the particle is not homogenous, in agreement with earlier reports

by others [18,19]. The rheological experiments were performed as follows: at 36 °C (i.e. in the shrunken state; see fig. 1(b)) two milliliters of concentrated PNIPAM suspensions (typically 0.07 w/w corresponding to a volume fraction of $\simeq 0.55$) were injected into a Haake RS600 cone plate rheometer with a cone angle of 2°. Subsequently the system was cooled down to the desired measurement temperature. Due to the geometric confinement inside the rheometer, the swelling of PNIPAM is suppressed giving rise to a very dense system of highly compressed microgel particles with strong mutual repulsion, see fig. 1(c). The data shown here are averages of typically three or more independent experimental runs.

One of the main challenges in the characterization of aging systems is to prepare the samples in a well-defined initial state. Commonly this is achieved by submitting the sample to a large strain or stress (larger than the yield stress) for a sufficiently long time [2,4-6,10]. The applied stress or strain randomizes the structure and erases all internal stresses introduced to the system earlier. This procedure is referred to as mechanical quenching in analogy to thermal quenches of ordinary glasses. It is usually argued that mechanical quenching and thermal quenching are equivalent with respect to erasing the memory of the system - a conjecture that we will come back to later.

Let us consider a system that was quenched mechanically by imposing a stress protocol (typically 100 Pa, 60s) as indicated on fig. 2(a): the system was first sheared vigorously to provide a reproducible highly disordered initial state. After stopping the mechanical quench (time t=0), we left the system at rest for a waiting time t_w. Then a probe stress was applied to determine $G'(\omega, t)$ and $G''(\omega, t)$, beginning at low frequencies. We verified that the probe stress was sufficiently small (typically 1 Pa) to avoid any measurable influence on the mechanical response, such as rejuvenation or overaging [2,6]. The integration time per point was set to $T = 3{\cdot}2\pi/\omega$. Figure 2(b) shows a typical result for four different waiting times for a sample at 21°C. (The data for other temperatures look similar.) The response obviously depends on the waiting time, i.e. the samples displays indeed aging behavior. Additional step stress experiments show also the t_w-dependence of the strain responses [20]. Younger samples have a somewhat lower $G'(\omega, t)$ and (at low frequencies) a distinctly higher $G''(\omega, t)$ than older ones. At fixed frequency, a weak increase in $G'(\omega, t)$ with t_w is found, which is consistent with both a weak algebraic growth or a logarithmic growth reported by others [5]. As a function of frequency, $G'(\omega, t)$ is found to be almost constant with an increase of no more than 20% over almost three decades in frequency. $G''(\omega, t)$, however, shows much more characteristic features: for short waiting times $G''(\omega, t)$ first decreases with increasing frequency and then increases again. The older the sample, the less pronounced is the decrease in the low frequency range. At high frequencies, all G'' curves collapse and

approach a universal positive slope of ≈ 1, independent of t_w. This universal high frequency behavior is commonly attributed to a combination of both the local viscosity of the system and the Brownian motion of particles [12]. Since both elements involve only the motion of particles within their cages they can be modeled by an age-independent contribution $G''_{ps} = \omega\eta'_\infty + c\omega^{1/2}$. In the following, we will focus on the age-dependent low frequency range (up to $\omega \approx 1$ rad/s).

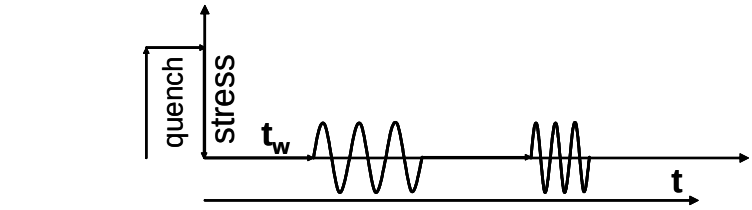

a

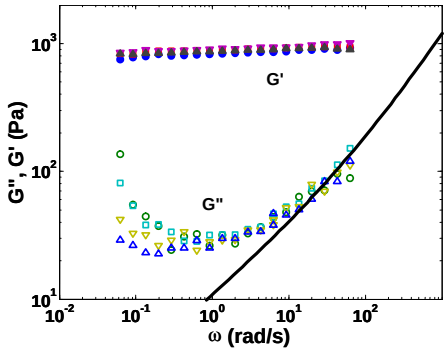

b

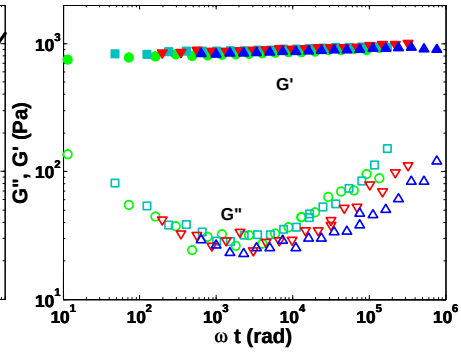

c

Figure 2. (a) The schematic procedure of oscillatory measurement. (b) The G' (filled symbols) and G'' (open symbols) of concentrated PNIPAM (0.07 w/w) as function of frequency measured at different waiting times at 21 ^{o}C: t_w= 30 s(O), 600 s(□), 3000 s(∇), 10000 s(Δ). The solid line represents the contribution from Brownian motion ($\sim \omega^{1/2}$) and local viscous effect ($\omega\eta'_\infty$) to $G''(\omega)$. (c) The same as the left figure but plotted as function of ωt.

Qualitatively, the behavior of $G'(\omega, t)$ and $G''(\omega, t)$ can be understood based on the elastic deformation and the yielding (or rearrangement) of the microgel particles, respectively. A freshly prepared sample is in a highly disordered state and thus rearranges continuously. If the sample is probed at a low frequency,

many rearrangement processes take place while the system is being probed thus giving rise to substantial energy dissipation and a high value of $G''(\omega, t)$. The higher the probe frequency, the fewer rearrangement processes take place per oscillation cycle, hence the smaller the $G''(\omega, t)$. As the sample is probed after longer waiting times, more and more of the spontaneous rearrangements have already taken place, and hence fewer take place while the system is being probed. Hence $G''(\omega, t)$ decreases and becomes less frequency-dependent (in the low frequency range). The same reasoning holds for the increase of $G'(\omega, t)$ as function of the frequency. At higher frequency, the time available for the yielding is shorter and hence more particles contribute to the elastic response and the system will appear somewhat stiffer.

To interpret the data quantitatively, one may first be tempted to replot them by plotting G' and G'' as a function of ωt_w. However, such a scaling is not successful because it neglects the finite time required to perform the oscillatory measurements. As noted above, the data were acquired by sweeping the excitation frequency from low to high frequencies. This means that data points recorded at low frequencies probe the sample in an earlier stage than those recorded at higher frequencies. Collapsing the data is only possible if we plot the data as a function of ωt, where $t = t(\omega_n) = t_w + \delta t(\omega_n)$ is the total time expired between the end of the mechanical quench and the acquisition of the data at the frequency ω_n. For our measurement protocol, $\delta t(\omega_n)$ increases linearly from $293s$ to $2140s$ between our lowest ($\omega_1 = 0.063$ rad/s) and our highest ($\omega_{25} = 63$ rad/s) measurement frequency. With this scaling, the curves for different waiting times collapse indeed onto a single master curve in the low frequency range (see fig. 2 (c)), i.e. up to $\omega t \approx 1000$. The success of the scaling further corroborates that the probe stress was indeed chosen sufficiently small not to induce overaging or rejuvenation.

Let us now compare to the results obtained by quenching the system thermally. In those experiments, the samples were heated to 34 ^{o}C, i.e. above the volume transition temperature, for 60 s and then cooled back down to the measurement temperature at a rate of 0.7 ^{o}C/min. The finite time required to cool the system impedes measurements at sample life times younger than $\approx$ 4600 s. All the qualitative observations described above also hold for the thermally quenched systems. The system displays aging, which appears particularly prominently in the low frequency behavior of $G''(\omega, t)$. The data for identical sample ages are very reproducible upon consecutive temperature sweeps, which proves that the memory is indeed erased completely by the thermal protocols (data not shown). Provided that the fraction of the cooling time, which the system spent in the glassy state (i.e. below 32 ^{o}C), is properly included in the sample age t both G' and G'' collapse if plotted versus ωt (data not shown). Nevertheless, there is an interesting quantitative difference (see

fig. 3). $G'(\omega, t)$ is consistently higher than for mechanically quenched samples at the same temperature. The qualitative reasoning for this difference is because the mechanical quench may create a slightly different structure giving rise to somewhat smaller yield energies and therefore decreases $G'(\omega, t)$. On the other hand the temperature quench drives the sample into the glassy state more gradually. This gradual process results in a system with a more stable configuration and therefore has a higher $G'(\omega, t)$. From the observed difference in $G'(\omega, t)$ we may say that even though the two quench methods erase the sample memory, the initial states are not exactly the same. The average initial yield energies of the sample prepared thermally seems to be higher as indicated by higher $G'(\omega, t)$.

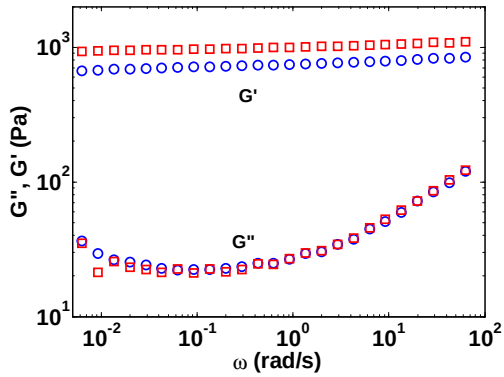

Figure 3. The elastic modulus G' and the loss modulus G'' of PNIPAM suspensions (0.07 w/w) quenched mechanically (O) and thermally (□). The moduli were measured at $T = 15$ °C and $t_w = 10000s$.

Regardless of the difference in the $G'(\omega, t)$, the temperature and the mechanical quench rejuvenate the sample totally. However, the time when the system enters the glassy state is better defined in the mechanical quench than in the temperature quench. In the mechanical quench, the system directly enters the glassy state after the flow cessation. Therefore the mechanical quench is easier to use.

For a quantitative analysis we compare the experimental data to the SGR model. It seems natural to identify the measured moduli with the time dependent complex dynamic modulus (equation 3.1) in the theory. However, the time scales associated with aging and the finite measurement time unavoidably introduce additional transients, which are particularly prominent at the lowest measurement frequencies where aging is most pronounced. The experimentally

measured quantities are given by [20]:

$$\tilde{G}'(\tilde{\omega},\tau_s) = 1-\frac{\tilde{\omega}}{\pi m}\int_{\tau_s-m\pi/\omega}^{\tau_s+m\pi/\omega}\int_0^{\tau} G_\rho(\tau-s)\,y(s)\,\cos(\tilde{\omega}s)\,ds\cos(\tilde{\omega}\tau)d\tau \quad . \tag{3.2}$$

$$\tilde{G}''(\tilde{\omega},\tau_s) = \frac{\tilde{\omega}}{\pi m}\int_{\tau_s-m\pi/\omega}^{\tau_s+m\pi/\omega}\int_0^{\tau} G_\rho(\tau-s)\,y(s)\,\cos(\tilde{\omega}s)\,ds\sin(\tilde{\omega}\tau)d\tau \tag{3.3}$$

where the stress signal has been probed over m periods of oscillation. To account for the high frequency behavior, we include the Brownian motion ($G'_D(\omega) = G''(\omega) = c\omega^{1/2}$) and local viscosity contribution ($G''_s(\omega) = \eta'_\infty\omega$) as discussed above, where η'_∞ is the high shear rate viscosity or the real viscosity at high frequency. In Fig. 4 we compare the model prediction with the experimental data for thermodynamic temperatures of 21, 24, and 27 °C using three fit parameters, namely the prefactor c in the Brownian term, the elasticity G_p of the individual microgel particles, and the effective noise temperature $\mathcal{X}/\mathcal{X}_g$, where X_g is the average depth of the potential barriers. ($\eta'_\infty = 0.883, 0.345$, and $0.134 Pa.s$ were measured independently at $21, 24$ and 27 °C.) As expected, the data do not collapse at high frequencies. To incorporate the Brownian motion and the local viscous contribution into the scaled plot, characteristic times of $t = 2186, 2756, 5160$, and$12155s$ were used. In the low frequency range, the value of $\mathcal{X}/\mathcal{X}_g$ can be determined in two independent ways, either from the slope of G'' or from the (frequency-dependent) ratio of G' and G'' at low frequencies. Both methods yield consistent results: from the slopes we obtained $\mathcal{X}/\mathcal{X}_g$ as 0.63 ± 0.04, 0.64 ± 0.05, 0.62 ± 0.07 at 21, 24, and 27 °C respectively. From the ratio of the moduli we obtain $\mathcal{X}/\mathcal{X}_g = 0.61 \pm 0.02$, 0.62 ± 0.03, 0.63 ± 0.08 at 21, 24, and 27 °C respectively. Notwithstanding a weak trend, the relative noise temperature is thus essentially independent of the thermodynamic temperature within the range investigated here. In contrast, the elastic constant of the particles G_p (that has been scaled to 1 in the SGR model) seems to decrease slightly with increasing temperature: ($G_p = 909 \pm 54$ Pa, 484 ± 38 Pa, and 600 ± 138 Pa at 21, 24, and 27 °C respectively). These values reflect the decrease in the absolute values of both G' and G''.

We interpret these findings as follows: the lower the temperature, the more the particles like to swell, i.e. the stronger they are compressed inside the rheometer. On the individual particle level this gives rise to a somewhat higher elastic modulus. On the collective level, the thermodynamic temperature affects the relative noise-temperature $\mathcal{X}/\mathcal{X}_g$ in two ways. Primarily the particles are more compressed and thus more hindered by each other at lower temperatures, which should give rise to deeper traps and thus higher energy barriers to be overcome during configurational rearrangements. Furthermore the thermal energy avail-

able for the yielding is also decreased at lower temperatures. Although both effects point in the same direction, we found $\mathcal{X}/\mathcal{X}_g$ to be essentially independent of T. Since the average trap depth is expected to increase this suggests that the absolute noise temperature $\mathcal{X}$ increases as well. The latter can be rationalized in the sense that a stiffer system at lower T is more likely to display stronger and longer range coupling of rearrangement processes across the system. A separation of these opposing trends is currently not possible.

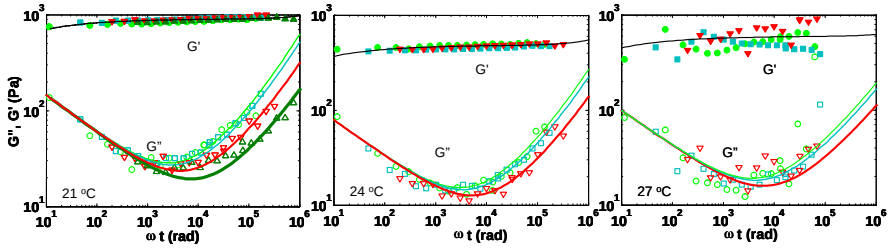

Figure 4. The $G'(\omega, t)$ and $G''(\omega, t)$ of the concentrated PNIPAM suspensions (0.07 w/w) plotted as function of ωt at 21, 24, and 27 ^{o}C. Different symbols show different experimental waiting times as in figure 2. Solid lines show model calculations (see text for details).

In conclusion, we found that concentrated PNIPAM suspensions display aging behavior. Well-defined initial states could be produced by both conventional mechanical shearing as well as thermal quenching across the volume transition temperature ($\approx$ 32 ^{o}C), which corresponds effectively to a quench in volume fraction. Except for a slightly higher elastic modulus of the thermally quenched systems both systems behave similarly. In particular, the aging behavior of the linear viscoelastic moduli ($G'(\omega, t)$, $G''(\omega, t)$, and $G''(\omega, t)/G'(\omega, t)$) is found to be in quantitative agreement with the SGR model. The system was found to display a relative effective noise temperature (in units of the average trap depth) of ≈ 0.62 for mechanically quenched systems, independent of the thermodynamic temperature. The quantitative agreement obtained is the first step to the physical understanding of the idea of effective noise temperature $\mathcal{X}$ and aging in general. Attempts to determine the absolute effective noise temperature are in progress.

References

[1] L.C.E. Struik, Ann. N.Y. Acad. Sci., **279** (1976) 78

[2] M. Cloitre, *et al.*, Phys. Rev. Lett., **85** (2000) 4819

[3] R.E. Courtland and E.R. Weeks, J. Phys. Condens. Matter., **15** (2003) S359

[4] C. Derec *et al.,* Phys. Chem., **1** (2000) 1115
[5] C. Derec *et al.,* Phys. Rev. E., **67** (2003) 061403-1
[6] V. Viasnoff and F. Lequeux, Phys. Rev. Lett., **89** (2002) 065701-1
[7] D. Bonn *et al.,* Europhys. Lett., **59** (2002) 786
[8] S. Cohen-Addad *et al.,* Phys. Rev. E **57** (1998) 6897
[9] B. Fabry *et al.,* Phys. Rev. E., **68** (2003) 041914-1
[10] P. Bursac *et al.,* Nature mater., **4** (2005) 557
[11] R.E. Laudadio *et al.,* Am. J. Physiol. Cell Physiol., **289** (2005) C1388
[12] T.G. Mason and D.A. Weitz, Phys. Rev. Lett., **75** (1995) 2770
[13] P. Hébraud and F. Lequeux, *Phys. Rev. Lett.,* **81** (1998) 2934
[14] P. Sollich *et al.,* Phys. Rev. Lett., **78** (1997) 2020
[15] P. Sollich, Phys. Rev. E., **58** (1998) 738
[16] S.M. Fielding *et al.,* J. Rheol., **44** (2000) 323
[17] A.J. Liu and S.R. Nagel, Nature, **396** (1998) 21
[18] J. Gao and Z. Hu, Langmuir, **18** (2002) 1360
[19] M. Stieger *et al.,* J. Chem. Phys., **120** (2004) 6197
[20] E.H. Purnomo *et al.,* Phys. Rev. E., **76** (2007) 021404

Chapter 4

Rheological properties of aging thermosensitive suspensions

Abstract Aging observed in soft glassy materials inherently affects the rheological properties of these systems and has been described by the soft glassy rheology (SGR) model [S.M. Fielding et al., J. Rheol. **44**, 323 (2000)]. In this paper, we report the measured linear rheological behavior of thermosensitive microgel suspensions and compare it quantitatively with the predictions of the SGR model. The dynamic moduli [G'(ω,t) and G"(ω,t)] obtained from oscillatory measurements are in good agreement with the model. The model also predicts quantitatively the creep compliance J(t-t_w,t_w), obtained from step stress experiments, for the short time regime [(t-t_w) < t_w]. The relative effective temperature X/X_g obtained from both the oscillatory and the step stress experiments is indeed less than 1 ($X/X_g < 1$) in agreement with the definition of aging. Moreover, the elasticity of the compressed particles, G_p, increases with increased compression, i.e. the degree of hindrance and consequently also the bulk elasticity (G' or 1/J) increases with the degree of compression.[1]

4.1 Introduction

Pastes are not the simple materials as they appear to be. It seems that they have a 'memory': after a force has been applied, they recover and move back in the opposite direction, as David Weitz stated in a comment [1] on an inves-

[1] This chapter has been published in: Phys. Rev. E. **76**, 021404 (2007)

tigation of the long time mechanical behavior of highly concentrated microgel suspensions by Cloitre *et al.* [2]. Pastes are highly concentrated suspensions of soft particles: due to excluded volume effects the particles are deformed and possibly compressed by their neighbors. Microgel particles form a class of macromolecules intermediate between highly branched polymers and macroscopic polymer networks [3]. A microgel particle is an intramolecularly cross-linked, soluble macromolecule of colloidal dimensions. The size depends on the degree of cross-linking and the nature of the solvent and is comparable to very high molecular weight polymers; its internal structure is that of a swollen network. Therefore the effective volume fraction of the microgel particles in the suspension can be controlled during the experiment by adjusting the temperature and/or solvent quality. Microgels are used as binders in organic coatings and in food products, while pastes in general are applied in various area's, like pharmaceutical, food and cosmetic industries.

The relaxation times of aging materials, like the microgel particle pastes, increase as the material ages and therefore a thermodynamic equilibrium will never be achieved. Experimental evidence for aging and "close to aging" behavior stems from a wide range of soft glassy materials such as polymers [4,5], colloidal suspensions [2,6-11], foams [12], and also living cells [13-16]. The mechanical properties of aging materials depend on the age of the system just as in case of amorphous polymers. However, the explanation given in the past for the aging of amorphous polymers does not hold for colloidal suspensions, because the energies involved in the restructuring and equilibration processes are larger than the thermal energy k_BT [17,18].

In an earlier paper [11] we have shown that a thermosensitive PNIPAM (poly-N- isopropylacrylamide) microgel suspension is a good model system for a colloidal glass exhibiting aging behavior. We also have shown, by exploiting their thermosensitive properties, that these suspensions can be rejuvenated not only by shearing the sample mechanically but also by a thermal quench. The viscoelastic properties of these PNIPAM suspensions can be described quantitatively quite well with the soft glassy rheology (SGR) model. In this paper, we extend this quantitative comparison to step stress experiments. We also measure the viscoelastic moduli for two other thermosensitive microgel particle systems, another PNIPAM with slightly larger particles and a PNIPAM-PNIPMAM (poly-N-isopropylacrylamide - poly-N-isopropylmethacrylamide) core-shell system. Also for these systems both the linear oscillatory response and the step stress response are in quantitative agreement with the model. The relative effective temperature $\mathcal{X}/\mathcal{X}_g$ extracted from both types of experiments is less than 1 which indeed shows, according to the SGR model, that the suspensions are in the aging state.

The paper is organized as follows. In section 2 we describe the experimental

systems and the method and procedures used in this study. In section 3 we report our results and explain them qualitatively. In section 4 we introduce the key elements of the SGR model and finally in section 5 a quantitative comparison between the SGR model and the experimental results is discussed. From this comparison, we extract the relative effective temperature $\mathcal{X}/\mathcal{X}_g$ of our systems for various conditions as well as the elasticity G_p of the compressed particles. Our conclusions are formulated in section 6.

4.2 Experimental Method

4.2.1 Sample Synthesis

The original PNIPAM system (hereafter called P-1) has been prepared following the procedure described in [19] using 1.18×10^{-4} g/ml of sodium dodecyl sulfate as surfactant. The sample is purified by centrifugation (15000 rpm, 2.5 hours) and redispersed in ultra pure water at 25 ^{o}C. This procedure is repeated four times.

The second PNIPAM system (hereafter called P-2) was obtained from the Materials Science and Technology of Polymers group at the University of Twente. P-2 was synthesized according to the method described in [20]. After synthesis the microgel particles were dialyzed using a semi permeable membrane (molecular weight cut off = 12000-14000) for one week.

The core-shell PNIPAM-PNIPMAM sample (hereafter called P-P) was obtained from the Complex Fluids group of the RWTH Aachen University. The core of these particles consists of crosslinked PNIPAM while the shell contains the PNIPMAM component. The method to synthesize these particles is described in [21]. After synthesis the sample was purified in three cycles of ultracentrifugation (50000 rpm, 45 minutes) and redispersion in bidistilled water. The solid concentrations of these three suspensions have been determined using gravimetry.

4.2.2 Sample Characterization

Light scattering

Static light scattering experiments are performed to determine the radius of gyration R_g of the microgel particles as function of the temperature. Very dilute suspensions (mass fraction 0.0001 w/w) are used for these experiments. The radius of gyration is determined from the form factor $P(q) = I(q)/I(0)$ where q is the wave number and I the measured intensity, using a Guinier's plot, i.e. plotting $\ln(I)$ versus $-q^2R_g^2/3$.

The radius of gyration of the three different soft microgel particles has been given in figure 1 as a function of the temperature T. The microgel particles are swollen at low temperatures and the radius of gyration decreases with increasing temperature. For $T > 35$ °C, the radius of gyration does not decrease any further for both the P-1 and the P-2 system. This indicates that the particles are fully shrunken which is in agreement with earlier reports [19,20,22]. For the core-shell P-P system, R_g continues to decrease up to $T \sim 45$ °C. This further decrease stems from the shrinking of the PNIPMAM shell which has a transition temperature of about 44 °C [21].

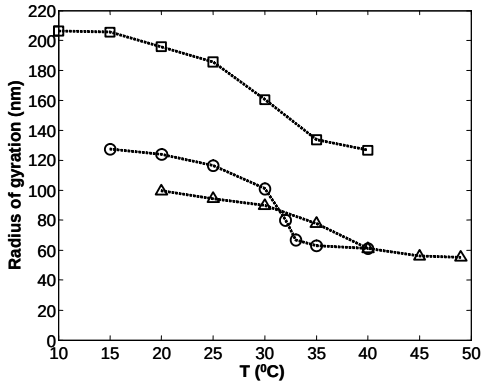

Figure 1. The radius of gyration R_g of the thermosensitive P-1(◯), P-2 (□), and P-P (△) microgel particles. The lines are a guide for the eye.

Effective volume fraction

The volume fraction ϕ of the diluted suspensions is determined using Einstein's relation: $\eta/\eta_s = 1 + 2.5\phi$ for $\phi \ll 1$. This equation describes the linear increase of the viscosity due to the increase of the volume fraction of the suspended particles. The viscosity of water η_s and that of the suspensions η are measured with a Haake RS600 using a cone and plate geometry (cone angle: 2°, diameter: 60 mm). The viscosity of the P-1 and P-P suspensions are measured at 24 °C and the viscosity of the P-2 suspension at 20 °C. At these temperatures the microgel particles are swollen and do not show any attractive interaction [23]. The shear rate used to measure the viscosity is kept below 200 s^{-1} to avoid secondary flow effects.

The data presented in figure 2 show that the volume fraction ϕ of a dilute suspension increases linearly with the mass fraction m i.e. $\phi = am$. The proportionality constant a is determined from the slopes of the curves in figure 2: $a = 124$, 59 and 42 for the system P-1, P-2 and P-P, respectively.

For the rheological aging experiments samples of P-1, P-2 and P-P are used with mass fractions of 0.07, 0.10 and 0.07 (w/w), respectively. According to

the linear relation, found above for very low mass fractions, the corresponding volume fraction ϕ is about 8.7, 5.9 and 2.9, respectively. For these high mass fractions this means that the volume available for a single microgel particle in the suspension is only a fraction of its free volume at that temperature: 0.11, 0.17 and 0.34 for P-1, P-2 and P-P, respectively. So the particles are strongly compressed in these suspensions, feeling a high mutual repulsion which increases with increasing mass fraction and the effective volume fraction is $\phi_{\text{eff}} \sim 1$.

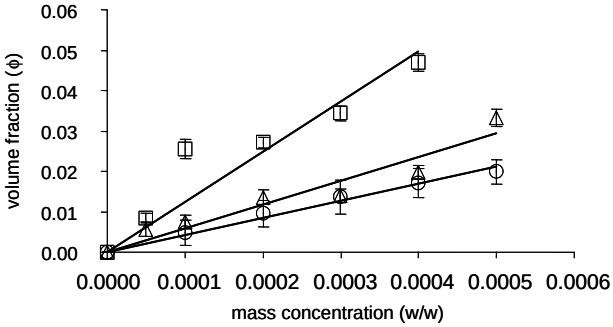

Figure 2. The volume fraction ϕ as calculated from the viscosity data using the Einstein relation of dilute P-1 (□), P-2 (△), and P-P (◯) suspensions as function of their mass fraction m (w/w). The lines indicate the linear regressions of the corresponding data.

4.2.3 Rheological aging experiments

The Rheological experiments are also performed with the Haake RS600 rheometer using the cone and plate geometry, mentioned above. The general protocol for rheological aging studies involves: sample loading, quenching, waiting, and measuring the rheological properties. Sample loading is performed as follows: At 36 °C (i.e. in the shrunken state) two milliliters of concentrated suspension are injected on the lower plate of the rheometer. Subsequently, the cone is positioned at the right height and the system is cooled down to the desired temperature.

After loading and cooling the sample, it is mechanically quenched: a stress σ_q well above the yield stress σ_y is applied for 60 s to erase the memory of the sample. The end of the quench is defined as $t = 0$.

Before the rheological measurements are performed, the sample is kept at rest for a certain waiting time t_w, during which no stress is applied. After this waiting time, a step or oscillatory stress $\sigma_p \ll \sigma_y$ is applied to examine the rheological properties of the sample. In the step stress scenario (figure 3a), a constant small stress is applied and the strain response is measured. In the

oscillatory measurements, an oscillating probe stress $\sigma_p \ll \sigma_y$ is applied to measure the elastic and loss modulus (figure 3b). The results shown are an average over typically three or more independent experimental runs.

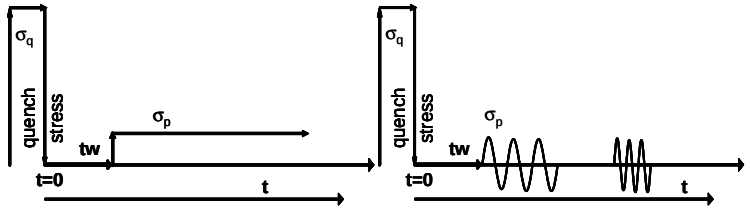

a b

Figure 3 (a) Schematic procedure of a step stress and (b) an oscillatory stress measurement in the aging study.

4.3 Experimental results

4.3.1 Quench

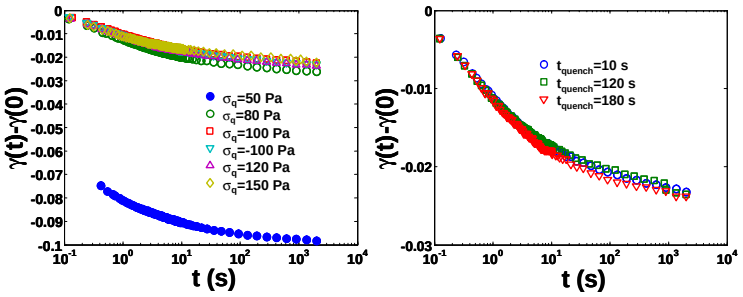

a b

Figure 4. (a) The effect of quench stress ($t_q = 60$ s) and (b) quench duration on the strain recovery of the P-1 suspensions after the flow cessation ($T = 24$ ^{o}C).

Since an aging material never reaches thermodynamic equilibrium, the only way to achieve a well defined initial state is to prepare the sample far from equilibrium. One way to achieve this is by applying a stress well above the yield stress such that the sample undergoes a strong shear flow. Figure 4 shows the effect of amplitude σ_q and duration t_q of the quench on the strain recovery of the material. After the quench, the strain decreases with the elapsed time $t-t_0$ due to the elasticity of the sample. Figure 4 (a) shows that for stresses σ_q well

above the yield stress $\sigma_y \sim 48$ Pa, the measured strain recovery is independent of the applied stress σ_q, i.e. all the curves measured at different σ_q collapse on each other. However, if the quench stress $\sigma_q = 50$ Pa is close to the yield stress $\sigma_y \sim 48$ Pa, the strain recovery is different from the other curves: because the structure is hardly destroyed by these stresses the elasticity of the sample is much larger. Figure 4 (b) shows that the strain recovery is independent of the quench duration t_q too, provided that $\sigma_q \gg \sigma_y$. In this study we use $\sigma_q = 100$ Pa.

The collapse of the strain recovery curves obtained from the samples quenched with different stress amplitudes well above the yield stress and stress durations indicates that the system has been prepared in a well defined initial state. On the other hand, when the stress is close to the yield stress ($\sigma_q = 50$ Pa), the quench is insufficient to erase the sample memory as shown by the fast elastic jump at short time in the strain recovery curve. Moreover it is also observed that the absolute strain recovery obtained from a quench with $\sigma_q = -100$ Pa does not differ from the recovery obtained from a $\sigma_q = +100$ Pa quench. This means that the recovery process is independent of the stress direction.

4.3.2 Step stress

In a step stress experiment, after some time t_w measured from the cessation of the quench, a small stress, typically $\sigma_p = 1$ Pa, is applied to the sample and the strain response is recorded. In figure 5 (a) a typical strain response $\gamma(t) - \gamma(t_w)$, where $\gamma(t_w)$ is the strain just before the probe stress was applied, has been plotted as a function of $t - t_w$ at $T = 24\ ^{o}$C for the P-1 suspension and four different waiting times. Curves measured at other temperatures look similar.

Typically, in the first stage of the recovery process the strain increases due to the step stress applied at t_w. At a certain moment the strain reaches a maximum and the recovery direction reverses because the sample still feels the effect of the initial quench, due to its long relaxation times. For $t_w = 30$ s, the strain peaks at $t - t_w = 10$ s. The peak shifts to longer times $t - t_w$ as the waiting time increases and is hardly visible for the samples with $t_w = 3000$ s and 10^4 s. It is also observed that in the first stage, before the peak is reached, $\gamma(t) - \gamma(t_w)$ is lower for older samples (longer t_w).

The decrease of $\gamma(t) - \gamma(t_w)$ as the sample ages shows that the sample is more elastic at longer t_w. This behavior can be explained in terms of yielding events of the particles caged by their neighbors. The cage can be considered as an energy well. When no shear is applied the yielding is purely driven by the "effective noise temperature". Due to this yielding the elastic energy stored in the particle is dissipated. Because on the average the new cage will represent

a deeper trap (less deep traps are faster depopulated) the escape rate goes down and accordingly the relaxation times increase. Therefore an old sample undergoes fewer yielding events, resulting in less energy dissipation. Moreover, the tendency towards deeper traps as time evolves implies also an increase of the elasticity of the sample.

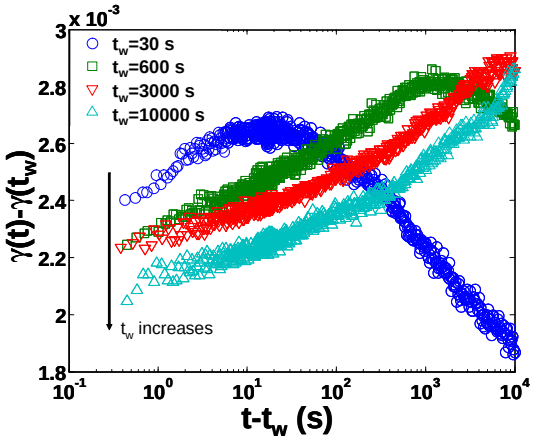

a

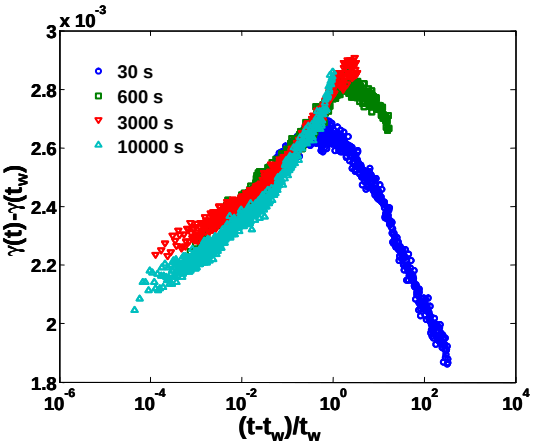

b

Figure 5. (a) The strain response of the P-1 suspension at 24 °C measured at different waiting times when the probe stress is smaller than the critical stress. (b) The same data plotted as function of $(t - t_w)/t_w$.

Figure 5 (a) shows that $\gamma(t) - \gamma(t_w)$ depends not only on the elapsed time $t - t_w$ but also on the age of the sample t_w. Therefore, in figure 5 (b) $\gamma(t) - \gamma(t_w)$ has been plotted as function of $(t - t_w)/t_w$. Now all the curves collapse onto a

single master curve for $(t - t_w)/t_w < 1$. For longer times, $(t - t_w)/t_w > 1$, the curves do not collapse because here the initial quench dominates the recovery process so it will depend only on the elapsed time t and not on the waiting time t_w.

4.3.3 Linear viscoelasticity

Figure 6 shows the viscoelastic moduli G' and G'' of the P-2 suspension for different waiting times t_w measured at 20 °C. The data for the P-1 and the P-P suspension look very similar; moreover the P-1 results have been published in [11]. The elastic modulus G' increases only slightly with frequency in the interval considered . On the other hand, the loss modulus G'' is at least one order of magnitude smaller and passes through a minimum.

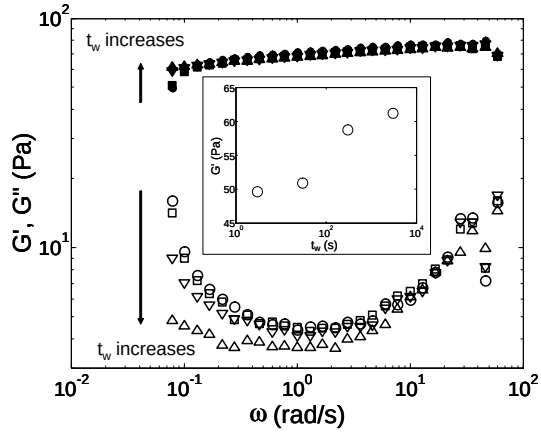

Figure 6. The moduli G' (filled symbols) and G'' (open symbols) of a concentrated P-2 suspension (0.10 w/w) as a function of the frequency measured at 20 °C for different waiting times: $t_w = 3$ s (O), 30 s (□), 300 s (∇), 3000 s (△). Inset: the increase of G' as function of t_w at $\omega = 0.0628$.

The effect of waiting time t_w is most pronounced in the behavior of G'' at low frequencies ($\omega < 1$ rad/s). The loss modulus G'' decreases with increasing waiting time. The effect of t_w is also observed, but less pronounced, in G'. The elastic modulus of older samples is slightly higher than that of a fresh sample (see the inset in figure 6). Again, the increase of G', at a fixed frequency, and the decrease of G'' with sample age can be explained by the growth of the relaxation times as the sample ages. The older sample with longer relaxation times undergoes fewer yielding events and therefore less energy will be dissipated, i.e. G'' goes down with age while the elasticity G' increases due to the increasing trap depth.

The same line of reasoning can be used to explain the decrease of G'' as function of ω. As ω increases, the time available for yielding during one cycle decreases and therefore less yielding events will occur. This results in a lower dissipation rate and a decrease in the loss modulus G''. The behavior of G'' at high frequencies is attributed to the local viscous effect and the Brownian motion of the particle [11]. These contributions are not due to particle-particle interactions, so age independent and can be represented as $G'' = \omega\eta'_\infty + c\omega^{0.5}$ where η'_∞ is the high frequency viscosity of the suspension and c is a fitting parameter.

4.4 SGR model

For a more quantitative analysis, we compare the experimental data with the SGR model [24-26]. The SGR model, based on Bouchaud's trap model, is intended to describe the rheological properties of repulsive glasses. The shared properties with soft glassy materials are metastability and structural disorder; the particles are too compressed to relax independent of each other and so, the particles are trapped by their neighboring particles. The traps can be thought to be surrounded by an energy barrier which the trapped particle has to overcome before it can escape from the trap resulting in a local rearrangement of particles.

In the SGR model, the material is conceptually divided into many mesoscopic elements. An element may be seen as the representation of a particle or a cluster of particles. The macroscopic strain γ applied to a system is distributed homogeneously throughout the system and therefore the macroscopic strain rate is equal to the local strain rate $\dot{l}$ experienced by an element: $\dot{\gamma} = \dot{l}$.

The energy barrier E of an element, or the trap depth, is equal to $kl_y^2/2$ where k is the elastic constant and l_y is the yield strain of an element. The yielding in an unsheared or unstrained material is accompanied by the rearrangement of the neighboring particles. This type of yielding is termed noise-induced yielding and is represented in the model by a "effective temperature" x and proportional to: $\exp(-E/x)$. The yielding probability increases if a macroscopic strain is applied. This type of yielding is termed strain-induced yielding and proportional to: $\exp(-(E - \frac{1}{2}kl^2)/x)$. Even though strain-induced and noise-induced yielding are discussed in different ways, the SGR model captures them both; due to the local strain l, the barrier to overcome is reduced to $E - \frac{1}{2}kl^2$. Due to the disordered nature of the soft glassy material, each element will have a different yield strain. Therefore, to obtain the number of elements that yield over a certain time interval, we need to use the average yielding rate of the elements. In the model, the probability $P(E, l, t)$ that an element will be in a

state with yield energy E and internal strain l is given by:

$$\begin{aligned} P(E,l,t) &= \int_{-\infty}^{\infty} P_q(E,l,t,m)dm \\ &+ \int_0^{\tau}\int_{-\infty}^{\infty} P_r(E,l,t,m,s)dmds \end{aligned} \tag{4.1}$$

where $P_q(E,l,t,m)dE\,dl\,dm$ is the distribution of elements with a yield energy between E and $E+dE$, and a strain between l and $l+dl$, present at time t which were formed in the quench with an initial strain between m and $m+dm$. $P_r(E,l,t,m,s)dE\,dl\,dm\,ds$ represents the distribution of elements with a yield energy between E and $E+dE$, and a strain between l and $l+dl$, present at time t which were formed in the time interval $(s, s+ds)$ with an initial strain between m and $m+dm$. Evaluation of the integral in Eq. 4.1 [26] and assume that the elements are born with strain free gives:

$$\begin{aligned} P(E,l,t) &= P_0(E)\, e^{-\Omega\, Z(t,0,0)}\, \delta\left(l-\gamma(t)\right) \\ &+ \int_0^t Y(s)\rho(E)\, e^{-\Omega\, Z(t,s,-\gamma(s))} \\ &\delta\left(l-[\gamma(t)-\gamma(s)]\right) ds \end{aligned} \tag{4.2}$$

where $P_0(E)$ is the distribution of yield energies E directly after the quench, $\Omega = \exp(-E/\mathcal{X})$ and Z is defined as

$$Z\left(t,s,u\right) = \int_s^t \exp(\frac{1}{2x}(u+\gamma(t'))^2)dt'$$

$Y(s)$ represents the yielding rate and

$$\rho(E) = \frac{1}{\mathcal{X}_g}\exp(-E/\mathcal{X}_g)$$

is the renewal distribution for the yield energies E, with $\mathcal{X}_g = \langle E\rangle$, while $x = \mathcal{X}/\mathcal{X}_g$.

Once $P(E,l,t)$ is known, the constitutive equation (in one dimension) can be expressed as:

$$\sigma(t) = G_p\left\langle l\right\rangle = G_p \int\int l\, P(E,l,t)\, dE\, dl \tag{4.3}$$

which results in:

$$\sigma\left(t\right) = G_p\left(\gamma\left(t\right) - \int_0^t G_\rho\left(t-s\right) Y\left(s\right)\, \gamma\left(s\right)\, ds\right) \tag{4.4}$$

where

$$G_\rho(s) = \int_0^\infty e^{-s\Omega}\, \Omega^x dE$$

Since we consider pastes that are far from equilibrium, we can not define, strictly speaking, G' and G'' on the basis of a memory relaxation function. Therefore, we use a practical definition for G' and G''. Experimentally, G' and $G''$are determined by correlating the measured stress response $\sigma(t)$ with the oscillatory shear $\gamma(t) = \gamma_0 \cos(\omega t)$ over m periods via:

$$G' = \frac{\omega}{m\pi\gamma_0} \int_{t_0 - m\pi/\omega}^{t_0 + m\pi/\omega} \sigma(t) \cos(\omega t) dt \tag{4.5}$$

$$G'' = \frac{-\omega}{m\pi\gamma_0} \int_{t_0 - m\pi/\omega}^{t_0 + m\pi/\omega} \sigma(t) \sin(\omega t) dt. \tag{4.6}$$

Substitution of the constitutive equation, Eq. 4.4, in the expressions for G' and G'' yields:

$$G'(\omega, t_0) = G_p - \frac{G_p \omega}{m\pi} \int_{t_0 - m\pi/\omega}^{t_0 + m\pi/\omega} M(t) \cos(\omega t) dt \tag{4.7}$$

$$G''(\omega, t_0) = \frac{G_p \omega}{m\pi} \int_{t_0 - m\pi/\omega}^{t_0 + m\pi/\omega} M(t) \sin(\omega t) dt. \tag{4.8}$$

where $M(t)$ is defined by:

$$M(t) = \int_0^t G_\rho (t - s) Y(s) \cos(\omega s) \, ds \tag{4.9}$$

The numerical integration of Eqs. 4.7 and 4.8 is not straight forward due to the functional dependence of $G(s)$ and $Y(s)$ on s. In the appendix, an efficient and accurate method is described to evaluate $G'(\omega, t)$ and $G''(\omega, t)$. For quick comparison with the experimental data, using the exact asymptotic form of the yielding rate ($Y(t) = t^{x-1}/x\Gamma(x)\Gamma(x)\Gamma(1-x)$) the following asymptotic relation as given by [26 can be used:

$$G^*(\omega, t) = G_p \left(1 - \frac{1}{\Gamma(x)} (i\omega t)^{x-1} \right) \text{ for } x < 1 \tag{4.10}$$

where Γ is the well known gamma function.

The same SGR model can be applied to a step stress experiment. However, since the overall strain recovery due to the quench is not described in the model, only the extra contribution due to the small probe stress is predicted. For a step stress experiment, the stress as a function of time is given by $\sigma(t) = \sigma_0 H(t - t_w)$ and the strain response can be written as $\gamma = \sigma_0 J(t - t_w, t_w; \sigma_0)$. Dividing Eq. 4.4 by the applied stress $\sigma(t)$ results in:

$$1/G_p = J(t - t_w, t_w) - \int_{t_w}^t J(s - t_w, t_w) Y(s) G_\rho (t - s) \, ds \tag{4.11}$$

Solving this integral equation will result in an expression for $J(t - t_w, t_w)$. For comparison with the experimental results, however, again a more simple asymptotic relation can be used [26]:

$$J(t - t_w, t_w) = \frac{1 + c[(t - t_w)/t_w]^{1-x}}{G_p} \quad (4.12)$$
$$\text{for } \frac{(t - t_w)}{t_w} \ll 1$$

where c is a constant.

4.5 Experiment vs model

It has been shown in figure 6 that the viscoelastic moduli G' and G'' of the P-2 suspension depend on both the frequency ω and the age t_w. Due to the experimental protocol used, in which we apply a frequency sweep from low to high frequency, the total age t of the sample includes not only the waiting time t_w but also the time required to perform the oscillation at its frequency and the preceding frequencies. In figure 7, we show G' and G'' of the P-2 that are plotted as function of ωt. The G' and G'' measured at different ages collapse onto a single master curve especially at $\omega t < 10^3$ where the particle-particle interactions dominate the behavior of the moduli. The deviation of G'' from the master curve is again due to the contribution from the local viscous effect and the Brownian motion.

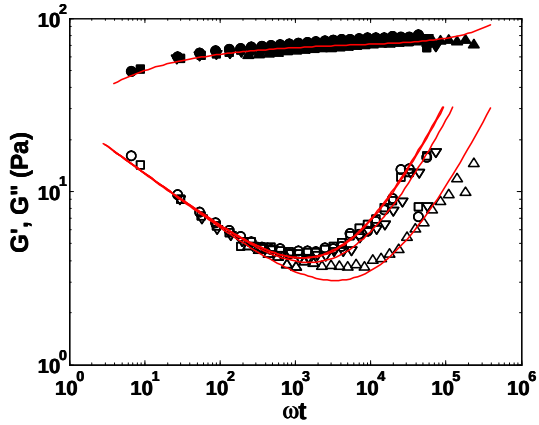

Figure 7. $G'(\omega, t)$ and $G''(\omega, t)$ plotted as function of ωt for the concentrated P-2 suspension (0.10 w/w). Different symbols correspond to different experimental waiting times, as in figure 6. Solid lines show model calculations, see text for details.

The viscoelastic moduli of the aging P-2 suspension is then compared quantitatively to the prediction of the SGR model presented as lines in figure 7. The viscoelastic moduli can be calculated either from equation 4.7 and 4.8 or equation 4.10. In addition to the G' and G'' calculated from the SGR model, we also include the Brownian motion $G'_D(\omega) = G''_D(\omega) = c\omega^{1/2}$ and the local viscosity contribution $G''_s(\omega) = \eta'_\infty\omega$ to account for the behavior at high frequency. The high frequency viscosity $\eta'_\infty = 0.2$ Pas is independently measured and then used in the calculation.

The relative effective temperature $x = \mathcal{X}/\mathcal{X}_g$ and the elasticity of the compressed particles G_p obtained from this comparison are 0.68 and 80 Pa respectively. The relative effective temperature which is smaller than unity means that the sample is indeed in the aging state. In this state, the sample never achieves an equilibrium because the average relaxation time, $\tau(t) = x\Gamma(x)\Gamma(x)\Gamma(1-x)/t^{x-1}$, grows with its age.

The quantitative comparison of the predictions of the SGR model to the step stress data is presented in figure 8. The data is presented as a creep compliance: $J = (\gamma(t) - \gamma(t_w))/\sigma_p$. The comparison is made only for $(t-t_w)/t_w << 1$ because the SGR model only predicts the evolution of the strain caused by the applied stress and neglect the strain recovery originating from the quench step. The model assumes that the sample is strain free after the stress removal in the quench stress, which is not the case in our experiments. Due to the elasticity of the sample, the remaining strain exist in the sample relaxes back as observed in decrease of the strain at $(t-t_w)/t_w > 1$. Incorporating the strain recovery originating from the quench step to the model is expected to describe the creep compliance not only for $(t-t_w)/t_w \ll 1$ but also for $(t-t_w)/t_w \gg 1$. However, this is beyond the scope of this paper.

The model presented as solid lines in figure 8 can be calculated numerically using equation 4.12. Two parameters, $x = \mathcal{X}/\mathcal{X}_g$ and G_p, are fitted in this comparison. The relative noise temperatures, $x = 0.58 \pm 0.05$, 0.60 ± 0.03 and 0.88 ± 0.01 as obtained for $T = 15$, 21 and 24 °C, respectively, show that the suspensions are in the aging regime. The x value of P-1 suspension at 24 ^0C obtained from the step stress method is higher than the one obtained from the oscillatory method ($x \approx 0.62$ [11]). We speculate that the difference stems from the fact that the probe stress applied in one direction (step stress) partially rejuvenates the sample and increases the x value.

The elasticity of the compressed particles increases with decreasing temperature: $G_p = 1002 \pm 11$, 778 ± 5 and 536 ± 16 Pa for $T = 15$, 21 and 24 °C, respectively. The result is comparable to the compressed particle elasticity G_p obtained from the dynamic measurements [11]. The elasticity of the particle increases as the particles are more compressed due to the increase of R_g while the macroscopic volume is preserved.

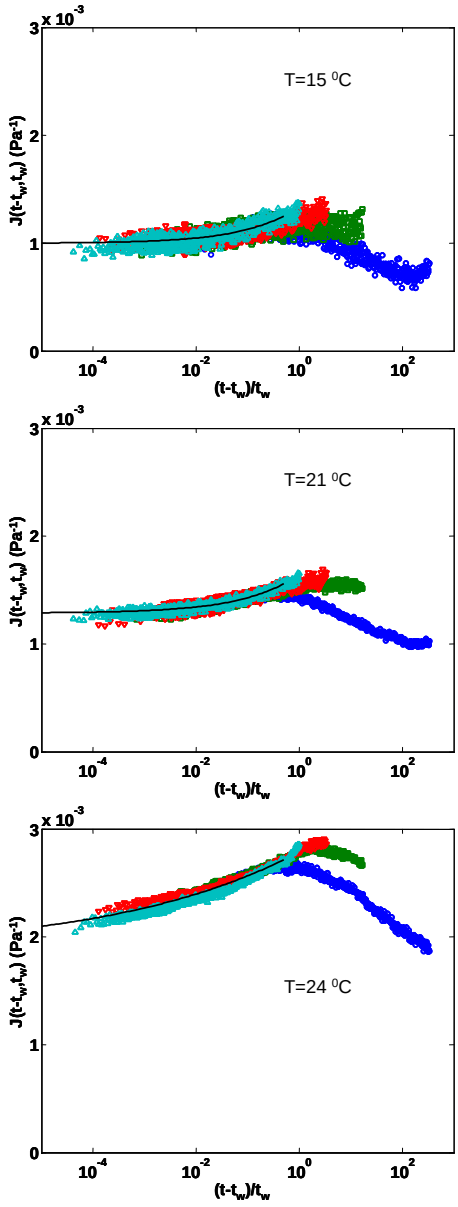

Figure 8. $J(t-t_w, t_w)$ as a function of $(t-t_w)/t_w$ for the P-1 suspension at different ages (30 s - 10^4 s) and measured at different temperatures. The solid lines represent the predictions of the SGR model.

Figure 8 also shows that the sample at lower temperature has smaller $J(t-t_w, t_w)$ which means that the sample is more elastic. In figure 9 we plot the elasticity of the P-1 suspension measured both with oscillatory G' [11] and step stress experiments $1/J$ at $t_w = 600$ s. The data for different waiting

times look similar. The higher elasticity of the sample at lower temperature is related to the increase of the elasticity of its constituents which are the individual particles. The increase of the particles elasticity collectively increases the bulk elasticity. This increase in the bulk elasticity can also be described in term of the yielding process. At lower temperature the particles are more constrained and therefore there are less yielding which are responsible for the energy dissipation. Because the energy dissipation is small, the elasticity of the sample increases.

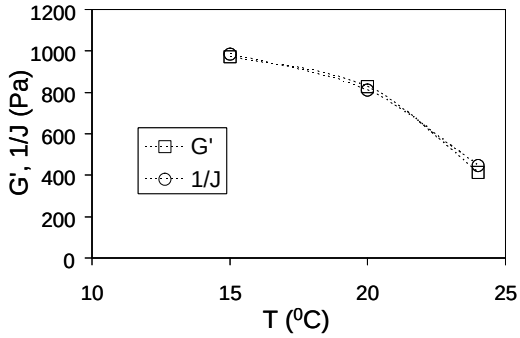

Figure 9. The elasticity, G' and $1/J$, of the P-1 suspension for $t_w = 600$ s at different temperatures.

4.6 Conclusions

In summary, we found that both $G'(\omega)$ and $G''(\omega)$ as well as the strain response in step stress experiments of highly concentrated soft microgel particles depend strongly on their age. The aging behavior is quantitatively described by the soft glassy rheology (SGR) model. It is in agreement with the model predictions for systems in the aging state, a relative effective temperature less than unity ($\mathcal{X}/\mathcal{X}_g < 1$) is found consistently for both types of measurements. Also with respect to the elasticity, we find a consistent behavior: the elasticity of the individual particles G_p is found to increase with decreasing temperature in accordance with decreasing bulk elasticity – for which we find $G' \simeq 1/J$ even though the system is not in equilibrium.

Overall, our measurements confirm that the SGR model correctly captures the aging behavior of microgel suspensions. The discrepancies seen in the long-term strain relaxation behavior show that the stress and strain free initial condition assumed in the SGR model is not fulfilled in the typical mechanical quench protocol in experiments. While this problem can probably be overcome by both improved quench protocols or extensions of the model, the deeper

question of the origin of the effective noise temperature and its absolute value still remain to be solved. We expect that non-linear rheological experiments currently in progress in our laboratory will provide information on both the absolute average energy barrier (and thus the noise temperature) and the evolution of the characteristic relaxation time (τ(t)) of the aging suspensions.

Appendix

Since both $G_\rho(s)$ and $Y(s)$ decay quickly with s but have also a long time tail, accurate integration of equation 4.7 and 4.8 has to be done with care. The integration interval $[0-t]$ is split up in subdomains to probe the product $G_\rho(s)Y(t-s)$ properly: $[0,10]$, $[10,100]$,.., $[10^m, t-10^m]$,.., $[t-100, t-10]$, $[t-10, t]$ where m was chosen such that $10^m < t/2 < 10^{m+1}$. Moreover, partial integration is used to handle the cosine and sine contributions correctly also if the time step becomes of the order of one period or even larger:

$$\int_{t_{n-1}}^{t_n} f(s)\cos(\omega s)\, ds = \left[\frac{1}{\omega^2} f'(s)\cos(\omega s) + \frac{1}{\omega} f(s)\sin(\omega s)\right]_{t_{n-1}}^{t_n} \tag{4.13}$$

$$\int_{t_{n-1}}^{t_n} f(s)\sin(\omega s)\, ds = \left[\frac{1}{\omega^2} f'(s)\sin(\omega s) - \frac{1}{\omega} f(s)\cos(\omega s)\right]_{t_{n-1}}^{t_n} \tag{4.14}$$

In these expressions, it has been assumed that the derivative of $f(s) = G_\rho(s)Y(t-s)$ is almost constant over the interval $[t_{n-1}, t_n]$: $f'(s) = [f(t_n) - f(t_{n-1})]/[t_n - t_{n-1}]$. Each sub-interval was again divided into 100 time steps over which Eqs. 4.13 and 4.14 were evaluated.

References

[1] D.A. Weitz, Nature **410,** 32 (2001)

[2] M. Cloitre, R. Borrega, and L. Liebler, Phys. Rev. Lett. **85,** 4819 (2000)

[3] H. Senff and W. Richtering, Colloid Polym. Sci. **278**, 830 (2000)

[4] L. C. E. Struik, Ann. N.Y. Acad. Sci. **279**, 78 (1976)

[5] H. Montes, V. Viasnoff, S. Jurine and F. Lequeux, J. Stat. Mech.: Theory Exp. **3**, 71 (2006)

[6] R.E. Courtland and E.R. Weeks, J. Phys. Condens. Matter **15,** S359 (2003)

[7] C. Derec, A. Ajdari, G. Ducouret, and F. Lequeux, Phys. Chem. **1**, 1115 (2000)

[8] C. Derec, D. Ducouret, A. Ajdari, and F. Lequeux, Phys. Rev. E. **67,** 061403 (2003)

[9] V. Viasnoff, and F. Lequeux, Phys. Rev. Lett. **89**, 065701 (2002)

[10] D. Bonn, P. Coussot, H. T. Huynh, F. Bertrand, G. Debrégeas, Europhys. Lett. **59,** 786 (2002)

[11] E.H. Purnomo, D. van den Ende, J. Mellema, and F. Mugele, Europhys. Lett. **76,** 74 (2006)

[12] S. Cohen-Addad, H. Hoballah, and R. Höhler, Phys. Rev. E **57,** 6897 (1998)

[13] B. Fabry, G. N. Maksym, J. P. Butler, M.Glogauer, D. Navajas, N. A. Taback, E. J. Millet, and J. J. Fredberg, Phys. Rev. E. **68**, 041914 (2003)

[14] P. Bursac, G. Lenormand, B. Fabry, M. Oliver, D. A. Weitz, V. Viasnoff, J. P. Butler, and J. J. Fredberg, Nat. mater. **4,** 557 (2005)

[15] R. E. Laudadio, E. J. Millet, B. Fabry, S. S. An, J. P. Butler, and J. J. Fredberg, Am. J. Physiol.: Cell Physiol. **289,** C1388 (2005)

[16] L. Deng, X. Trepat, J. P. Butler, E. Millet, K.G. Morgan, D. A. Weitz, and J. J. Fredberg, Nat. mater. **5,** 636 (2006)

[17] B. Abou and F. Gallet, Phys. Rev. Lett. **93,** 160603-1 (2004)

[18] P. Wang, C. Song, and H. A. Makse, Nat. Phys. **2,** 526 (2006)

[19] J. Gao, and Z, Hu, Langmuir **18,** 1360 (2002)

[20] R.H. Pelton, and P. Chibante, Colloids and Surf. **20,** 247 (1986)

[21] I. Berndt, J. S. Pedersen, P. Lindner, and W. Richtering, Langmuir **22,** 459 (2006)

[22] M. Stieger, W. Richtering, J. S. Pedersen, and P. Lindner, J. Chem. Phys. **120,** 6197 (2004)

[23] M. Stieger, J. S. Pedersen, P. Lindner, and W. Richtering, Langmuir **20,** 7283 (2004)

[24] P. Sollich, F. Lequeux, P. Hébraud, and M. E. Cates, Phys. Rev. Lett. **78,** 2020 (1997)

[25] P. Sollich, Phys. Rev. E. **58,** 738 (1998)

[26] S. M. Fielding, P. Sollich, and M. E. Cates, J. Rheol. **44,** 323 (2000)

Chapter 5

Glass transition and aging in particle suspensions with tunable softness

Abstract We report an aging soft colloidal system that can be tuned continuously and reversibly over a wide range between the glass at low temperature and the liquid state at high temperature, T, where the state is characterized by a noise temperature ranging from 0.5 to above 3.0. We show that volume fraction and the softness of the particles can be controlled independently by tuning the temperature and the mass concentration. Both the volume fraction and the particle softness determine the glass transition. More over, we find indications that aging stops after a certain time if we approach the hard sphere limit with our particle softness.

Soft glassy materials (SGMs) exhibit distinct rheological behavior. Under small stresses they behave like a solid ($G' > G''$) on experimental time scales. However, at very long time scales, they flow. Such rheological features characteristic of soft glassy behavior have been found in many materials including colloidal suspensions [1-8], emulsions [9], foams [10], and living cells [11]. The microscopic dynamics of these soft materials reveal signatures of glassy behavior including metastability, dynamic heterogeneities, intermittency and kinetic arrest [12]. On increasing the mass concentration of a suspension of colloidal hard spheres, the system undergoes a glass transition at a volume fraction of $\phi_{trans} \simeq 0.58$. In case of soft spheres, for which the softness and size can be controlled by for instance pH or temperature, one can tune the system to the glass transition by varying the mass concentration or the particle size (via

pH or temperature) [13]. More over for star polymers, another class of soft particles, it has been found that glass transition is determined not only by the volume fraction that can be higher than unity but also by the degree of compression [14]. Due to its softness and deformability, a suspension of soft particles may still flow on an experimental time scale at a volume fraction higher than 0.58. However, a systematic study of the effect of particle softness on the glass transition is still lacking.

Soft glassy materials often show rheological properties that evolve continuously with time, which is known as aging. In chapters 3 and 4 we have shown that the viscoelastic moduli of suspensions of soft colloidal particles in the glassy state scales linearly with their age. Aging has also been observed in colloidal hard sphere suspensions from measurements of the mean squared displacement (MSD) as a function of time, using video microscopy, at different ages of the sample [2]. The transition time from the caging plateau to the long time diffusive behavior increases sub linearly with the age of the suspension. This difference in behavior between soft colloidal particles and hard spheres raises an issue on the effect of particle softness on the aging behavior.

In this chapter, we address the issues mentioned above by systematically studying the glass transition and the aging behavior of thermosensitive colloidal suspensions, a unique class of SGMs, that are well suited for studying mechanical behavior in the vicinity of glass transition because their volume fraction and degree of mutual compression can be easily tuned by varying the temperature [7,8,13]. We first demonstrate that the glassiness (as quantified by the effective noise temperature x, prescribed by the soft glassy rheology (SGR) model) of a newly synthesized thermosensitive microgel suspension can be tuned continuously and reversibly by varying the thermodynamic temperature T. The aging behavior of the viscoelastic moduli observed deep in the glassy state vanishes upon approaching the glass transition. Above the glass transition, the material shows nearly Maxwellian liquid behavior. The viscoelastic moduli both below and above the glass transition can be quantitatively described by the SGR model [15-17]. By performing the same experiments at different mass concentrations, we study the effect of particle softness on the glass-liquid transition. The volume fraction ϕ_{trans} at which the transition occurs approaches that of a colloidal hard sphere system as the particles get harder (i.e. at a higher polymer concentration inside the particles). When measuring the viscoelastic moduli at different ages of the sample we observe that in the glassy state the aging stops after 6000 s for the highest mass concentration (8% w/w) while aging goes on for 3.9% w/w mass concentration . This indicates that when the softness approaches the hard sphere limit aging is not permanent, in line with observations by Crassous *et. al.* [18]

In this study aqueous suspensions containing thermosensitive core-shell microgel particles with a poly-N-isopropyl acrylamide (PNIPAM) core and a poly-N-isopropylmethacrylamide (PNIPMAM) shell [19-21] were used. The swelling of these particles decreases more gradually with increasing temperature than for pure PNIPAM particles, resulting in a broader temperature range to tune the volume fraction ϕ of the suspension continuously. At $T_0 = 24$ °C the volume fraction $\phi(T_0, c) = 42 \times c$ was obtained from the measured Einstein viscosity at known low mass concentrations c as described in chapter 2 (figure 14). For other temperatures ϕ was determined with $\phi\,(T, c) = \phi\,(T_0, c)\,(R_g(T)/R_g(T_0))^3$, where $R_g(T)$ was obtained from static light scattering experiments. All experiments were carried out using a Haake RS600 rheometer with a cone and plate geometry (diameter 60 mm, angle 2°). A vapor lock was used to avoid evaporation and the temperature of the shielding was kept approximately 5 °C above the plate temperature to prevent condensation. This was sufficient to keep the concentration constant for more than a week.

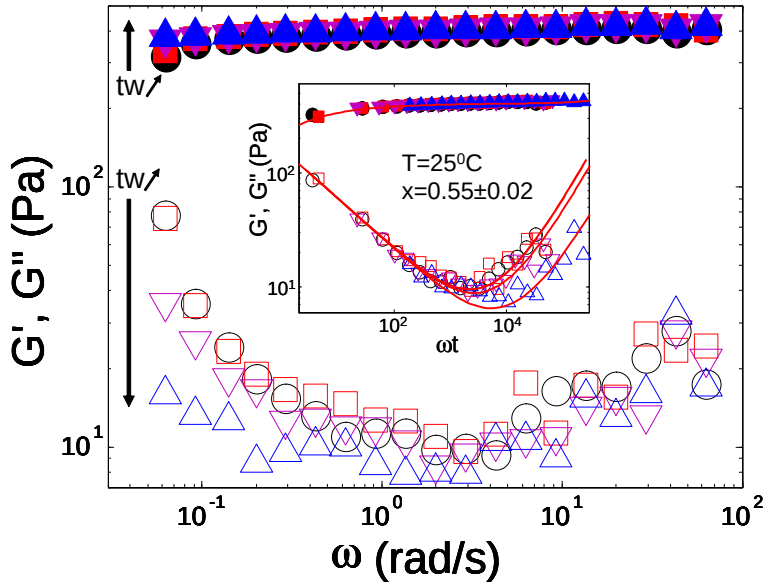

Figure 1. G' (filled symbols) and G'' (open symbols) of the 7% w/w suspension at 25 °C plotted as a function of ω for different waiting times $t_w = 3$ s (◯), 30 s (□), 300 s (▽) and 3000 s (△). Inset: the same data plotted as a function of ωt and compared with the SGR model extended by local viscous and Brownian effects (solid lines).

The rheometer was loaded at 44 °C and then cooled down to the experimental temperature. Prior to any oscillatory measurement, the suspension was rejuvenated by a mechanical quench i.e. a stress well above the yield stress was applied for 60 s. The time $t = 0$ is defined at the end of the quench. The

elastic modulus $G'(\omega)$ and the loss modulus $G''(\omega)$ were measured at several temperatures T and after different waiting times t_w. The age is defined as the total time since the end of the mechanical quench until the moment of data acquisition which includes the waiting time and the oscillation time so far [7,8].

In figure 1 we show the behavior of the moduli G' and G'' of an aging suspension at 25 °C. As we increase the frequency, G'' initially decreases but increases again at high frequencies. G' increases only slightly over the whole frequency range. At low frequencies the material becomes more elastic (higher G' and lower G'') with its age. For $\omega t < 10^3$ they collapse onto a master curve when plotted as a function of ωt as shown in the inset of figure 1. For $\omega t > 10^3$, where the moduli are dominated by local viscous and Brownian effects, they do not collapse, as discussed in more detail in chapter 3. Two fitting parameters (x and G_p) are used in the quantitative comparison. The best fit between the model and the experimental results is obtained from the χ^2 minimization of the parameters. The error of the parameters is determined as the half width at half maximum of χ^{-2}. This procedure is explained in more detail in the appendix.

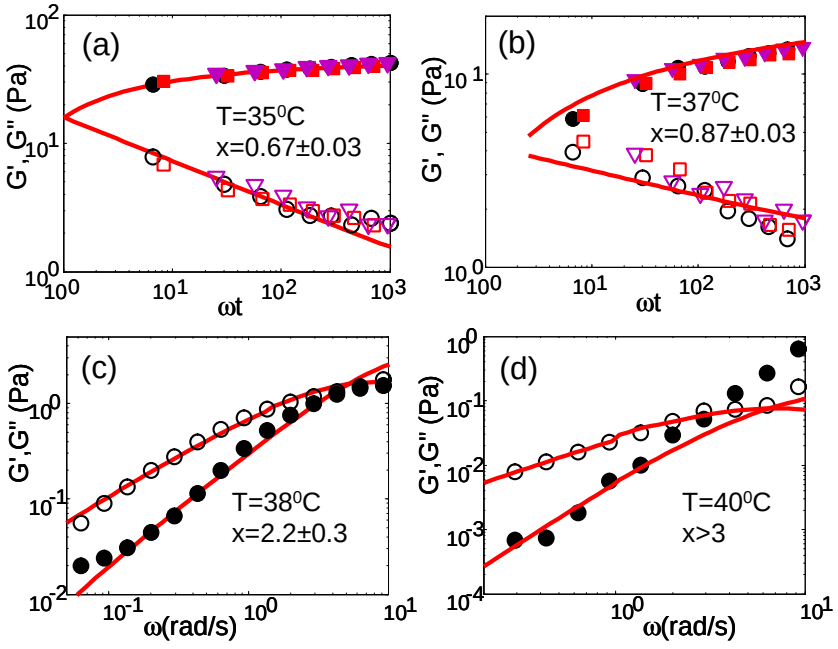

Figure 2. Evolution of G' (filled symbols) and G'' (open symbols) of a 7% w/w suspension from glassy behavior at low temperature ((a) and (b)) to liquid behavior at higher temperature ((c) and (d)). Note that the data in (a) and (b) were plotted vs. ωt to collapse curves for different sample ages (t_w = 3 s (◯), 30 s (□), 300 s (▽)), whereas data in (c) and (d) plotted versus ω.

The behavior of the moduli can be explained using the SGR model as described in chapter 1. In this model the steric hindrance against relaxation (or yielding) of internal stresses of individual elements is represented by a complex energy landscape. Relaxation is conceived as a jump of an element from one well to another. The jump probability depends on the depth of the well and is enhanced by straining the particle. As the elements escape more readily from shallower wells, the deeper ones become more populated as the system gets older. Simultaneously, the average escape time, i.e. the structural relaxation time, increases as well. The slight increase of G' and the decrease of G'' with increasing ω (for $\omega < 1$ rad/s) in figure 1 can be explained in terms of stress yielding of the particles. This yielding dissipates energy and lowers the number of strained particles. A sample with a higher yielding rate dissipates more energy and therefore has a higher G'' and lower G'. As ω increases, the time $1/\omega$ available for yielding during one cycle decreases resulting in a higher G' and lower G''. The same reasoning explains the decrease in G'' and the slight increase in G' upon aging, since the elements occupy increasingly deep traps implying a decreasing yielding rate. The quantitative agreement between the experimental data and the SGR model (inset of figure 1) yields the effective noise temperature $x = X/X_g$, where X is the absolute effective temperature and X_g is the average depth of the energy well. The value of 0.55 ± 0.02 indicates that the suspension is deep in the glassy state at $T = 25$ °C (see chapter 4 for modeling details).

To show the tunable glassiness of these suspensions we measured their viscoelastic moduli at different temperatures and waiting times (t_w = 3 s, 30 s, 300 s). In figure 2 we show the evolution of the moduli as we gradually increase the temperature. They are compared with the SGR model to obtain a value for the effective noise temperature x as a function of the temperature T. At 35 °C and 37 °C, the particles are sufficiently swollen and the suspension behaves solid-like ($G' > G''$). The moduli display aging behavior, as indicated by their dependence on ωt. Upon increasing to 38 °C and 40 °C, the suspension behaves liquid-like, i.e. $G' < G''$ and both moduli are independent of the age t. At 38 °C, G' increases faster than G'': $G' \sim \omega^{1.2}$ and $G'' \sim \omega$. At 40 °C, the suspension shows low frequency Maxwellian behavior: $G' \sim \omega^2$ and $G'' \sim \omega$.

The effective noise temperature x, obtained from a quantitative comparison between the experimental results and the predictions of the SGR model, provides a model-dependent parameter to identify the glass transition [15-17]. The suspension behaves like a glass when $x \leqslant 1$, and like a liquid for $x > 1$, as indicated in figure 2.

Fitting the SGR model to the moduli of the suspensions at different mass concentrations (c) measured at different temperatures T, we obtain the effective noise temperature x as a function of T, as shown in figure 3(a). The behavior

of $x(T)$ reflects the transition from glassy behavior at low T characterized by $x \leqslant 1$ to liquid-like behavior at high T with $x > 1$. This transition can be tuned reversibly without any noticeable hysteresis. We also observe that the transition occurs at a higher temperature as c increases. This indicates that the origin of the transition is not only related to the swelling behavior of the hydrogel particles (giving rise to a decreasing effective volume fraction ϕ with increasing T) but also depends on the polymer mass concentration, as figure 3(b) clearly shows. The effective volume fraction ϕ_{trans}, at the transition where $x = 1$, decreases as c increases.

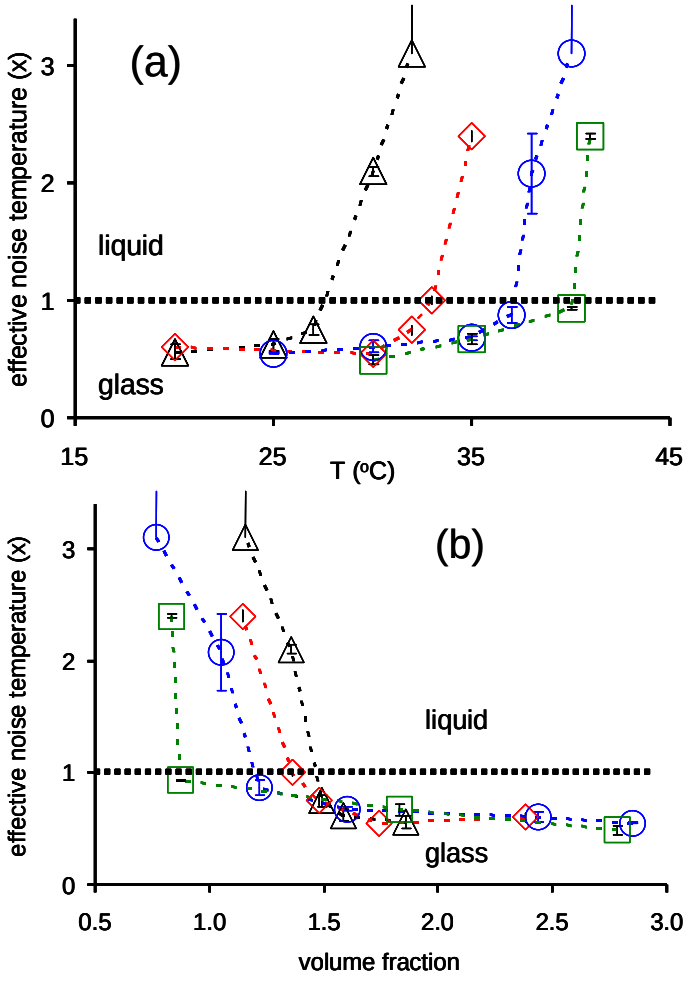

Figure 3. (a) The dependence of the effective noise temperature (x) as a function of T for the thermosensitive suspension at different mass concentrations (3.9% (△), 5.0% (◊), 7.0% (◯), and 8% (□)). (b) The same data shown as a function of the volume fraction at the corresponding temperature.

This dependence on the mass concentration can be explained in term of the particle softness. When we consider a microgel particle in the suspension, the particle shrinks as we increase the temperature. The shrinking of the particle consequently increases the polymer density inside the particle and therefore it behaves harder (i.e. has a higher elasticity) than a fully swollen particle. From figure 3(a) we observe that the transition occurs at higher temperature for a suspension with higher mass concentration which indicates that the individual particles are less swollen and so harder compared to those at a lower mass concentration. Since temperature controls both the size and the softness of the particles, plotting the glass transition curves $x(\phi, c)$ as function of their volume fraction ϕ does not result in a single curve.

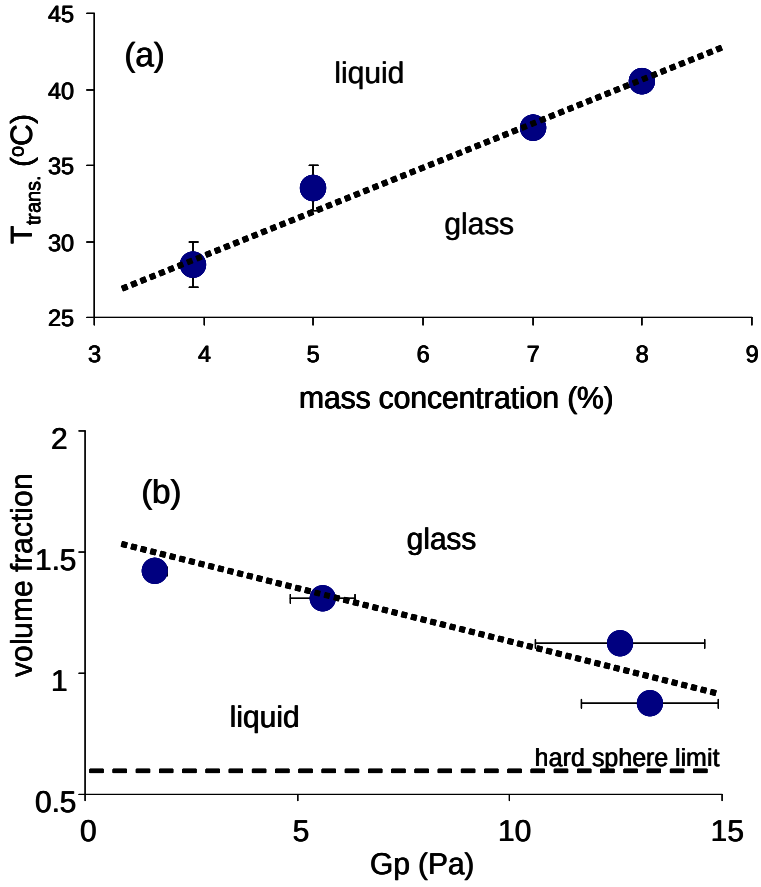

Figure 4 (a) The dependence of the transition temperature on the mass concentration. (b) The dependence of the transition volume fraction on the particle elasticity. The dashed lines are drawn to guide the eye.

We interpreted the glass transition in the frame work of the SGR modelling. However, without invoking SGR, we can determine the transition temperature

as a function of the mass concentration based on the behavior of the viscoelastic moduli. For $T > T_{\rm trans}(c)$, the moduli show no aging and the system is in the liquid state. While for $T < T_{\rm trans}(c)$ the moduli show aging and the system is in the glassy state. $T_{\rm trans}(c)$ obtained by interpolating the temperature values around $x = 1$ in figure 3(a) has been plotted in figure 4(a). In fact the two values used to estimate $T_{\rm trans}(c)$ are the upper and lower bound for $T_{\rm trans}(c)$ itself. We used $T_{\rm trans}(c) = ((T_{upper}+T_{lower})/2)\pm((T_{upper}-T_{lower})/2)$. Within the concentration range considered, the transition temperature increases almost linearly with the mass concentration in agreement with the dependence shown in figure 3 (a). Since the temperature and the mass concentration affect both the particle size and the particle softness, we plot in figure 4(b) the volume fraction as function of the particle elasticity, G_p. Figure 4(b) shows that the transition volume fraction decreases as G_p increases (particles get harder). The volume fraction at the transition comes closer to the hard sphere limit ($\phi^{HS}_{\rm trans} \sim 0.58$) as the particles become more elastic.

In order to investigate the effect of particle softness on the aging behavior we also measured the elastic and viscous moduli of two suspensions with an almost identical volume fraction but different particle softness. In contrast to previous measurements, we also measured the moduli at a much longer waiting time $t_w = 30000$ s ($\omega = 0.00628 - 6.28$ rad/s). Figure 5 shows the moduli of 3.9% and 8% w/w suspensions measured at 20 and 35°C respectively. The volume fraction of the two suspensions is almost equal ~ 1.8 which is calculated from the radius of gyration at very dilute suspensions. Although the volume fraction is the same, we observe that the elastic modulus of the 3.9% w/w suspension (figure 5(a)) is more than 1 decade lower than the one of 8% w/w (figure 5(b)). More interestingly, we find that the moduli of the 3.9% w/w suspension plotted as function of ωt form a master curve whereas for the 8% w/w suspension the curve with the longest waiting time $t_w = 30000$ s deviates from the master curve.

From the quantitative comparison with the model, we obtain that the elasticity of the particle (G_p) is 11.4±1.0 Pa and 227±25 Pa for mass concentration of 3.9% w/w and 8% w/w, respectively, which shows again that the particle is softer at 3.9% w/w suspension than the one at 8% w/w suspension. For the 3.9% w/w suspension, the particle density is lower therefore the particles have to be more swollen to achieve the same volume fraction as the 8% w/w suspension. As the particle is more swollen, it absorbs more water and has lower polymer density, resulting in a lower elasticity.

The aging of the 3.9% w/w suspension continues up to $t_w = 30000$ s, whereas the 8% w/w suspension ages only up to $t_w \simeq 6000$ s (from the shift in figure 5(b)). This ending of the aging at shorter t_w for the harder particles can be understood as a total arrest of the particle dynamics by the neighboring par-

ticles. The harder particles are less deformable therefore they hardly provide any space for particle rearrangements.

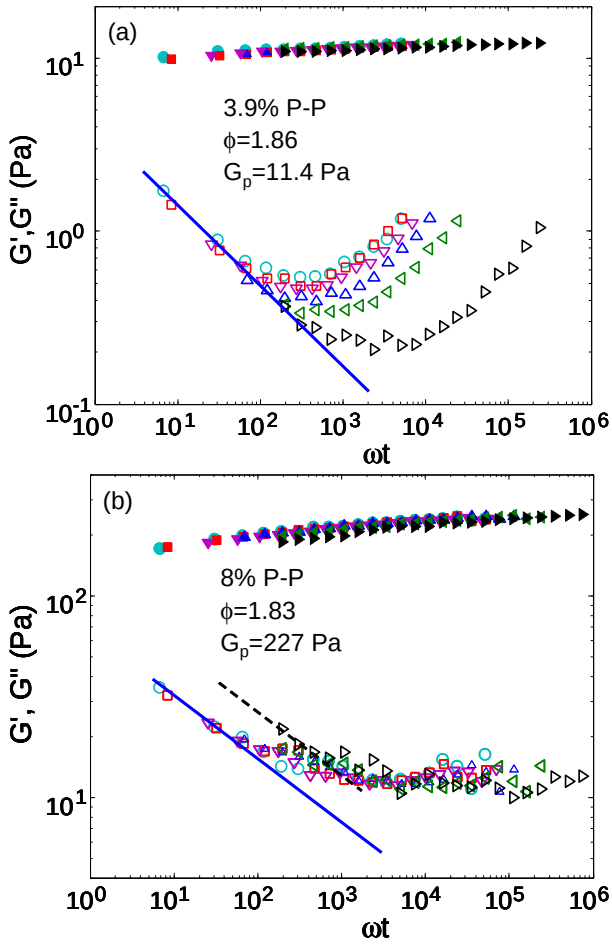

Figure 5. G' (filled symbols) and G''(open symbols) of core-shell suspension at volume fraction of around 1.8 obtained from 3.9% w/w and T=20 ^{o}C (a) and 8% w/w and T=35^{o}C (b). Different symbols show different waiting times (3s(◯), 30s(□), 300s(▽), 3000s(△),and 30000s(▷)), the line is drawn to indicate the master curve and the dashed line shows the shifting of G'' at t_w=30000 s from the master curve.

In conclusion, we show that using a core-shell thermosensitive system we can tune the degree of glassiness by controlling the temperature. The system is in the glassy state ($G' > G''$) at low temperature and behaves like a liquid ($G' < G''$) at high temperature. In the glassy state, the viscoelastic moduli show aging whereas in the liquid state, they are age-independent.

The glass transition depends both on volume fraction and particle softness. The volume fraction and the particle softness can be tuned independently by controlling the temperature and the mass concentration. The transition volume fraction approaches the hard sphere limit ($\phi^{HS}_{\rm trans} \sim 0.58$) as the particles become more elastic. We also find an indication that aging stops after a certain time if we approach the hard sphere limit with our particle softness.

Appendix

To estimate the accuracy of the values obtained for the fitting parameters x and G_p we calculate the χ^2 value of the fit to the experimental results as a function of the parameters x and G_p, where χ^2 is defined by:

$$\chi^2 = \frac{1}{N+M}\left(\sum_{n=1}^{N}\left[\log(G'_{\rm exp})-\log(G'_{\rm calc})\right]^2_n + \sum_{m=1}^{M}\left[\log(G''_{\rm exp})-\log(G''_{\rm calc})\right]^2_m\right)$$

Here N (M) is the number of experimental data points on the G' (G'') curve.

By considering $\log(G')$ and $\log(G'')$ in stead of G' and G'', we calculate χ^2 based on the relative differences between the calculated and the measured values. This follows from the observation that:

$$\begin{aligned}\log(G'_{\rm exp}) - \log(G'_{\rm calc}) &= \log(G'_{\rm exp}/G'_{\rm calc}) \\ &= \log(1 + (G'_{\rm exp} - G'_{\rm calc})/G'_{\rm calc}) \\ &\simeq (G'_{\rm exp} - G'_{\rm calc})/G'_{\rm calc}\end{aligned}$$

Last step is valid because $(G'_{\rm exp} - G'_{\rm calc}) << G'_{\rm calc}$. Using the relative errors results in more or less equal weights for the G' and the G'' curves in the fitting procedure. Around the optimal values for x and G_p , indicated as $\langle x\rangle$ and $\langle G_p\rangle$, respectively, the dependence of χ^2 on x and G_p can be approximated by a quadratic relation, because the first derivatives vanish in the optimum:

$$\begin{aligned}\chi^2(x, G_p) &= \\ &\chi^2_0\left(1 + \tfrac{(x-\langle x\rangle)^2}{\delta x^2} + \tfrac{(G_p-\langle G_p\rangle)^2}{\delta G_p^2} + \beta\tfrac{(x-\langle x\rangle)}{\delta x}\tfrac{(G_p-\langle G_p\rangle)}{\delta G_p} + ...\right)\end{aligned}$$

Here χ^2_0 is the least chi-square value and δx, δG_p and β are, still undertermined constants. Due to this quadratic relation the shape of $\chi^{-2}(x, \langle G_p\rangle)$ and $\chi^{-2}(\langle x\rangle, G_p)$ will be a Lorentzian. Assuming the model correctly describes the physical phenomenon, the half width at half maximum, i.e. δx and δG_p, can be considered as an estimate of the accuracy of $\langle x\rangle$ and $\langle G_p\rangle$, respectively, as explained for instance in chapter 14 of [22].

In figure A1 we plot χ^2 and its reciprocal, of the fits on the viscoelastic data of a 7 %w/w polyNipam-polyNipmam suspension at $T = 35°$C. The

experimental data and the best fit for this case have been presented in figure 2a. For $\chi^2(x, \langle G_p \rangle)$ and $\chi^2(\langle x \rangle, G_p)$ we observe a shallow parabolic minimum of χ^2. However, if we plot $\chi^{-2}(x, \langle G_p \rangle)$ or $\chi^{-2}(\langle x \rangle, G_p)$ a pronounced peak appears. This peak is compared with the best fitting Lorentzian. Although in the tails of the Lorentzian the agreement is less, around the peak the obtained χ^{-2} values fit very well, as expected from the quadratic approximation of χ^2 around the optimum for the considered fit parameter. From the peak position and the half width at half maximum we obtain $\langle x \rangle \pm \delta x = 0.67 \pm 0.03$ and $\langle G_p \rangle \pm \delta G_p = 43 \pm 3$ Pa. All values reported in this thesis for the fitting parameters and their accuracies are determined as described in this appendix.

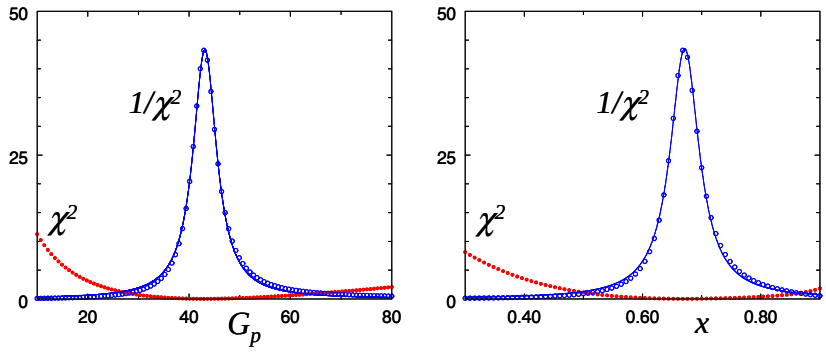

Figure A1. The calculated χ^2 and $1/\chi^2$ as a function of G_p for $x = 0.67$ (left graph) and as a function of x for $G_p = 43$ Pa (right graph). The sample in this case is a 7 %w/w polyNipam-polyNipmam suspension at $T = 35$°C. From the peak position and the half width at half maximum of both curves we obtain the optimal values for the fitting parameters: $G_p = 43 \pm 3$ Pa and $x = 0.67 \pm 0.03$.

References

[1] M. Cloitre *et al.*, Phys. Rev. Lett. **85,** 4819 (2000)

[2] R.E. Courtland and E.R. Weeks, J. Phys. Condens. Matter **15,** S359 (2003)

[3] C. Derec *et al.*, Phys. Chem. **1**, 1115 (2000)

[4] C. Derec *et al.*, Phys. Rev. E. **67,** 061403 (2003)

[5] V. Viasnoff and F. Lequeux, Phys. Rev. Lett. **89,** 065701 (2002)

[6] D. Bonn *et al.,* Europhys. Lett. **59,** 786 (2002)

[7] E.H. Purnomo *et al.,* Europhys. Lett. **76,** 74 (2006)

[8] E.H. Purnomo *et al.,* Phys. Rev. E. **76,** 021404 (2007)

[9] L. Bécu *et al.*, Phys. Rev. Lett. **96**, 138302 (2006)

[10] S. Cohen-Addad *et al.*, Phys. Rev. E **57,** 6897 (1998)

[11] P. Bursac *et al.*, Nature mater. **4,** 557 (2005)

[12] L. Cipelletti and L. Ramos, J. Phys. Condens. Matter **17,** R253 (2005)

[13] J.J. Crassous *et al.*, J. Chem. Phys. **125**, 204906 (2006)

[14] M. Kapnistos *et al.,* Phys. Rev. Lett. **85**, 4072 (2000)

[15] P. Sollich *et al.*, Phys. Rev. Lett. **78,** 2020 (1997)

[16] P. Sollich, Phys. Rev. E. **58,** 738 (1998)

[17] S.M. Fielding *et al.*, J. Rheol. **44**, 323 (2000)

[18] J.J. Crassous *et al.*, pre-print (2007)

[19] I. Berndt *et al.*, Langmuir **22**, 459 (2006)

[20] I. Berndt *et al.*, J. Am. Chem. Soc. **127**, 9372 (2005)

[21] I. Berndt and W. Richtering, Macromolecules **36**, 8780 (2003)

[22] W.H. Press *et al.*, *Numerical recipes, the art of scientific computing* (New York, 1986)

Chapter 6

Rheology and particle tracking on thermosensitive core-shell particle suspensions

Abstract By using both macro-rheology and particle tracking measurements, we show the liquid behavior of thermosensitive suspension at high temperature (low volume fraction) and the glassy behavior at low temperature (high volume fraction). In the glassy state, both bulk viscoelastic moduli (G' and G'') and the ensemble averaged mean squared displacement (MSD) depend on the age which strongly indicates that the system ages. We also extract the viscoelastic moduli (G' and G'') from the MSD using Mason's approximation of the generalized Stokes-Einstein relation and compare them to the bulk G' and G''. The particle tracking technique measures the viscoelastic moduli at a lower frequency range to determine the relaxation time (τ) that is inaccessible with macro-rheology measurements. We find that the relaxation time increases almost linearly with the age of the sample. Further investigation into the distribution of the particle displacement reveals that the short time particle dynamics are heterogeneous in the glassy state.

6.1 Introduction

Liquid-solid transitions [1], aging [2-4], dynamical heterogeneity [5], and slow relaxation processes [6] are topics of interest in the study of soft glassy mate-

rials. These topics are often studied using colloidal systems due to their larger size which inherently provides longer time scale than atoms and molecules. Moreover, the chemical and physical properties of colloidal particles can be flexibly manipulated to suit our interest [7].

For a colloidal hard sphere system, a glass transition is normally achieved by increasing its volume fraction via the mass concentration of the hard colloidal particles. As the system approaches the glass transition, its structural length scale (cluster size) increases and this increase is responsible for slowing down of the dynamics [1]. This slowing down of the dynamics has been observed with light scattering experiments on colloidal hard sphere dispersions, since a second plateau in the intensity correlation occurs when the glass transition is approached. It is well described by the mode coupling theory [8]. The mode coupling theory has also been applied successfully to describe quantitatively the flow curve of thermosensitive microgel particle suspensions as they approach the glass transition [9] and the viscoelastic moduli of a dense hard-sphere suspension as function of the applied frequency and strain amplitude [10]. However, this mode coupling theory still lacks to account for the inherent effect of aging on the evolution of the rheological properties [11]. On the other hand, the phenomenological soft glassy rheology model predicts the rheological behavior as the system approaches the glass transition and also deep in the glassy state including the aging effect [12-14].

Although the glass transition in colloidal hard sphere suspensions has been widely studied, the dynamic behavior of soft colloidal systems around the glass transition has not been thoroughly investigated. Examples of model soft systems are star polymers [15] and polyelectrolyte microgels [16]. In this study we use thermosensitive chore-shell microgel particles, in which the core consists of thermosensitive poly-N-isopropyl acrylamide (PNIPAM) and the shell is poly-N-isopropyl methacrylamide (PNIPMAM) polymer [17-19]. The size of the particle can be controlled reversibly by tuning the temperature which provide a unique way to control the volume fraction. Compared to the usual thermosensitive PNIPAM system, the size of the core-shell particle varies more gradually with temperature resulting in a wide temperature range to tune the particle size [4].

In this study we investigate both the rheology and the microscopic dynamics of a thermosensitive system while the system undergoes a transition from the liquid to the glassy state. From the macro-rheology we conclude that at high temperatures the system is liquid like (i.e. the loss modulus is higher than the elastic modulus and the moduli measured at a certain frequency are age-independent). In contrast, at low temperature, when the particles are swollen, the elastic modulus is higher than the loss modulus indicating that the system is solid-like. We also find that both the elastic and the loss modulus depend

on the age of the system which is a signature of aging. A qualitatively similar behavior is observed from particle tracking experiments. The ensemble averaged mean squared displacement (MSD) of probe particles added to the system increases linearly with time $(t - t_w)$ at high temperatures. However, at low temperatures, the MSD is constant at short times $(t - t_w)$ and diffusive at long times. This indicates caging-escape behavior typical for glassy system [1,6]. The caging plateau of the MSD vanishes as we increase the temperature and the MSD becomes diffusive. We also observe aging in the glassy state (low temperature) as revealed by the shifting of the cross over time with the waiting time. By using Mason's approximation of the generalized Stokes-Einsteins relation, we calculate the elastic and loss modulus from the MSD. This microrheology technique measures the viscoelastic moduli at lower frequency range that is inaccessible with the macro-rheology. Further investigation of the distribution of the particle displacements indicates the dynamical heterogeneity in the glassy state at short $t - t_w$.

6.2 Methods

6.2.1 System preparation and characterization

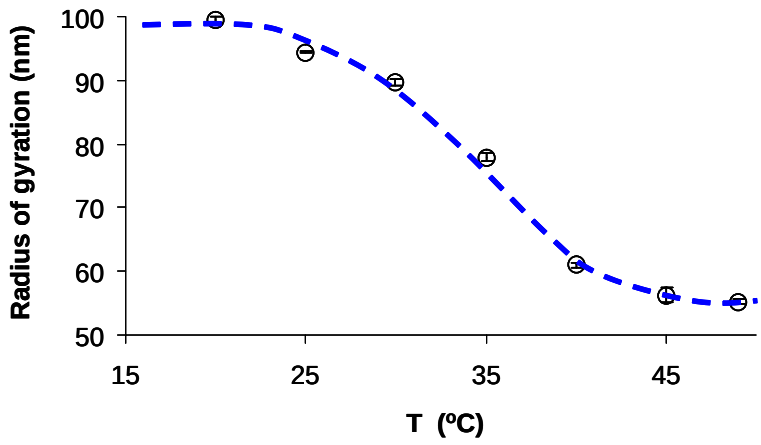

Figure 1. The radius of gyration of core-shell particle as function of temperature (T) measured using static light scattering. The line is drawn to guide the eye.

We used a thermosensitive core-shell system which has a PNIPAM core and a PNIPMAM shell [17-19]. The particle is swollen at low temperatures ($T < 30$ °C) and shrunken at high temperatures ($T > 45$ °C) with a gentle transition around 35 °C. The gyration radius varies by almost a factor of

2 as shown in figure 1. A 4% w/w suspension was prepared by adding solvent (bidistilled water) to freeze dried particles. Fluorescent labeled sulfate modified polystyrene particles with a radius of 113.5 nm were dispersed in the solvent with a concentration of 0.05% w/w. The mixture was stirred over night to mix the suspension homogeneously.

The volume fraction of the suspension was calculated based on the radius of gyration (R_g) of a very dilute suspension. First, we determined the volume fraction $\phi(T_0, c)$ at $T_0 = 24$ °C from the measured Einstein viscosity at known low mass concentrations c and we found that $\phi = 42 \times c$. For other temperatures ϕ was determined with $\phi\,(T, c) = \phi\,(T_0, c)\,(R_g(T)/R_g(T_0))^3$, where $R_g(T)$ was obtained from the static light scattering experiments (figure 1). The volume fraction could easily exceed unity due to the deformability of our soft microgel particles.

6.2.2 Macro-rheological measurements

We measured the elastic (G') and the loss (G'') modulus of the suspension (within a frequency range of $0.062 - 6.28$ rad/s) using a Haake RS600 rheometer with a cone and plate geometry (cone angle: 2°, diameter: 60 mm). A home built vapor lock was used to avoid evaporation. The temperature of the shielding was kept approximately 5 °C above the plate temperature to prevent condensation on it. This was sufficient to keep the concentration constant for more than a week as indicated by the reproducibility of the moduli. The suspension was introduced at ∼44 °C (shrunken state) and then the instrument was cooled down to the experimental temperature. Prior to any oscillatory measurement, the suspension was rejuvenated by a mechanical quench i.e. a stress well above the yield stress was applied for 60 s. The time $t = 0$ is defined at the end of the quench. The elastic modulus $G'(\omega)$ and the loss modulus $G''(\omega)$ were measured at several temperatures T and after different waiting times t_w. The age is defined as the total time since the end of the mechanical quench until the moment of data acquisition which includes the waiting time and the oscillation time [3,4].

6.2.3 Particle tracking experiments

In particle tracking experiments we measure particles displacements by taking images using a confocal scanning laser microscope (CSLM) at a rate ranging from 1 to 10 frames per second. The images are analyzed frame by frame to locate the particle positions. By comparing the frames, the particle trajectories have been constructed.

For this study we used a 4% w/w suspension. Two milliliter of the sample was put in a sample container together with a magnetic stirring bar. The

sample container was made by gluing a glass vial, from which its bottom was removed, on to a Delta T culture dish (Bioptechs, Butler, PA, USA) to control the sample temperature using the delta T heater from room temperature to 50°C with an accuracy of ±0.2°C. To prevent sample evaporation, 1 ml of mineral oil was added on top of the sample before tightly closing the vial.

Before we started to track the probe particle displacements, the sample temperature was stabilized for about 1 hour. The surrounding temperature was kept at the same temperature as the sample using an infrared lamp. To prepare a well defined initial state, the sample was stirred manually with the magnetic stirring bar. The age of the sample was measured from the moment the stirring was stopped.

The particle displacements were studied by recording 2500 images of the sample, using a 100× objective, with a rate of 1 image per second at two different waiting times $t_w = 300$ s and 3000 s and $T = 27$ °C. A higher recording rate (10 frame per second) was used for the higher temperatures.

The recorded images were analyzed using open source particle tracking routines written in IDL^{TM} to locate the position of the particles in every image [20]. Knowing the particle positions, we then constructed the particle trajectories and calculated the ensemble-averaged mean squared displacement (MSD) using routines developed in the course of this project that were written in "C" using the open source Lcc-win32 system. Since the sample was also still aging during recording, several waiting times can be considered by starting the analysis at a later recording time. For example, $t_w = 800$ s was obtained by calculating the MSD of the sample with $t_w = 300$ s but starting the analysis at 501^{th} image.

In order to minimize the contribution of the measurement time (t-t_w) to the age of the sample, for the analysis of the MSD in the aging glassy state (27 °C) we considered only the MSD for $0 < (t - t_w)/t_w \leqslant 0.4$.

The displacement probability at a certain time $t - t_w$ ($P(y, t_w)$) is determined by collecting the number of occurrence into a certain number of bins. The number of occurrence in a bin is normalized by the total number of particles times the bin width.

To determine the displacement resolution of the CSLM, the apparent displacement of probe particles glued on the culture dish were measured as function of time. The particles were glued to the dish by adding one drop of probe suspension (0.01% w/w) and drying the culture dish in an oven at 80 °C for about 4 hours. The position of the particles was tracked using the CSLM by taking 2600 images at a rate of 1 s^{-1}.

6.3 Viscoelastic moduli

Figures 2(a) and 2(b) show the elastic (G') and the loss (G'') modulus of the 4% w/w suspension at 32 and 27 °C, respectively, measured at different waiting times. From figure 2(a) we observe that at 32 °C (volume fraction of 1.19) the loss modulus is larger than the elastic modulus for most frequencies and only at frequencies higher than 3 rad/s the elastic modulus is larger than the loss modulus. We also observe that the moduli are age-independent at this temperature as indicated by the collapse of the moduli measured at different waiting times.

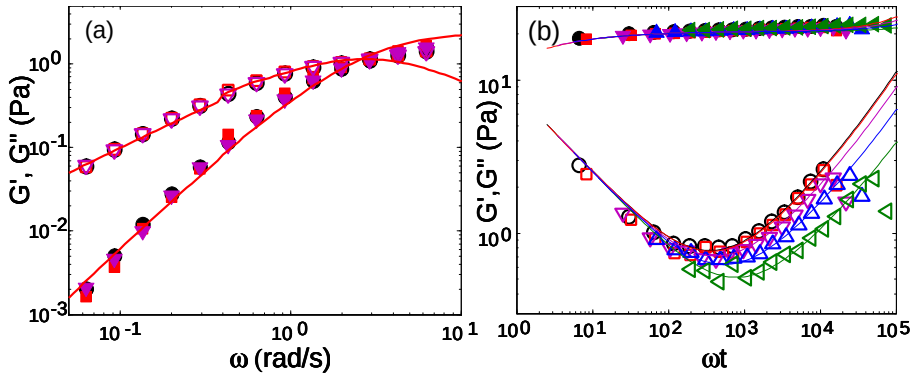

Figure 2. The elastic modulus (filled symbols) and the viscous modulus (empty symbols) of a 4% core-shell suspension measured at 32 °C (a) and 27 °C (b) which are related to $\phi = 1.19$ and $\phi = 1.53$ respectively. Different symbols show different waiting times (3 s (◯), 30 s (□), 300 s (▽) 1000 s (△), and 3000 s (◁)) and the lines are the predictions of the SGR model. The effective noise temperature x is >3 and the particle elasticity G_p is 2.4 Pa at 32 °C, whereas $x = 0.48 \pm 0.03$ and $G_p = 20.8 \pm 1.5$ Pa at 27 °C.

Figure 2(b) shows that at 27 °C (corresponding with a volume fraction of $\phi = 1.53$), the elastic modulus (G') is almost constant and larger than the loss modulus (G'') for all applied frequencies (ω). We also observe that the moduli measured at different ages depend on their age and form a master curve ($\omega t < 200$) when they are plotted as function of ωt where t is the age of the sample at the moment measuring that specific data point. The deviation of the scaling of $G''(\omega t)$ for $\omega t > 200$ is due to the dominance of local viscous and Brownian contributions, which are age independent [3,4].

The transition from a viscous dominated behavior at high temperature (figure 2(a)) to an elastic dominated behavior at low temperature (figure 2(b)) shows that the system undergoes a transition from liquid to glassy as we increase the volume fraction by decreasing the temperature. This unique way of

controlling the volume fraction to the glass transition is markedly different from controlling the volume fraction of a hard sphere suspension which is normally achieved by changing its concentration.

By quantitatively comparing the viscoelastic moduli with the predictions of the soft glassy rheology (SGR) model as indicated by the lines in figure 2 (see [12-14] for details) we found that the system at 32 °C is in the liquid state with an effective noise temperature $x > 3$. On the other hand, at 27 °C we obtain an effective noise temperature $x = 0.48 \pm 0.03$ which means that the system is in the glassy state and ages.

6.4 Mean squared displacement

Figure 3 shows the mean squared displacements (MSDs) of the probe particles embedded in a 4% w/w suspension measured at different temperatures. It also shows the displacement resolution of the CSLM which is ~ 6 nm (the lowest curve in figure 3). The MSDs were measured at a waiting time $t_w = 300$ s. The figure shows MSD curves which behave linearly at $T > 30$ °C, indicating the liquid like behavior of the suspension at these temperatures. For $T < 30$ °C the curves show a transition from liquid like to glassy, reflected by the onset of a plateau in the MSD curves. Moreover, all MSD curves shift downwards as the temperature decreases. We also observe that the MSDs measured at different temperatures are well above the displacement resolution.

At 32 °C, the MSD increases linearly with t as indicated by its slope which is ~ 1, whereas at lower temperature (30 and 31 °C) the slope is smaller than unity for $t - t_w < 2$ s and becomes unity at longer times $(t - t_w)$. A more interesting behavior is observed at 27 °C where the MSD curve shows a plateau at short time ($t - t_w \leq 10$ s) and increases linearly at long time. Although the behavior of the MSD at 27 °C is diffusive again at long $t - t_w$, its values are much smaller than those of the MSD at higher temperatures. A very similar behavior of the MSD has been found in molecular dynamic simulations of dense suspensions of star polymers. However, for star polymers the size of the particles increases as the temperature increases [21].

The linear increase of the MSD with time, observed at 32 °C (low volume fraction) over the entire observation range and for lower temperatures at long times, indicates that the probe particles behave purely diffusive which is typical for a liquid-like system. This result is qualitatively in agreement with macrorheolological data (figure 2(a)) where we found that the loss modulus is higher than the elastic modulus. The subdiffusive behavior, observed at intermediate temperatures at short time as indicated by the slope of the MSD, which is between 0 and 1, indicates the onset of elastic behavior [22].

At 27 °C, the slope of the MSD is zero at short time scales which in-

dicates that the particles are trapped within a cage formed by their neighboring particles and the systems behaves elastically. The relation between the elastic modulus (G') and the constant MSD ($\langle \Delta r^2 \rangle$) is shown by $G' \simeq (dk_BT/3\pi a) \times (1/\langle \Delta r^2 \rangle)$ where d is the dimension of the space in which the displacements have been measured (in our case $d = 2$). On the other hand, at long time the MSD grows linearly with time which indicates that the particles diffuse out of the cages. This diffusive behavior at long time scales is related to the energy dissipation and therefore the system is dominated by the viscous behavior ($\eta \simeq (dk_BT/3\pi a) \times ((t - t_w)/\langle \Delta r^2 \rangle)$). The same behavior is also observed in the macro-rheological measurements (figure 2(b)). For an aging glassy system, at very low frequencies beyond the measured frequency, the loss modulus is expected to be higher than the elastic modulus [13]. This indicates that the system is liquid-like at a very low frequency. At moderate and high frequencies, however, the elastic modulus is larger than the loss modulus showing that the system behaves elastically.

Figures 2 and 3 show that both the macro-rheological and particle tracking experiments reveal the transition from the liquid to the solid (glassy) state as we decrease the temperature of the thermosensitive suspensions. This transition is due to the increase of the volume fraction (particle size).

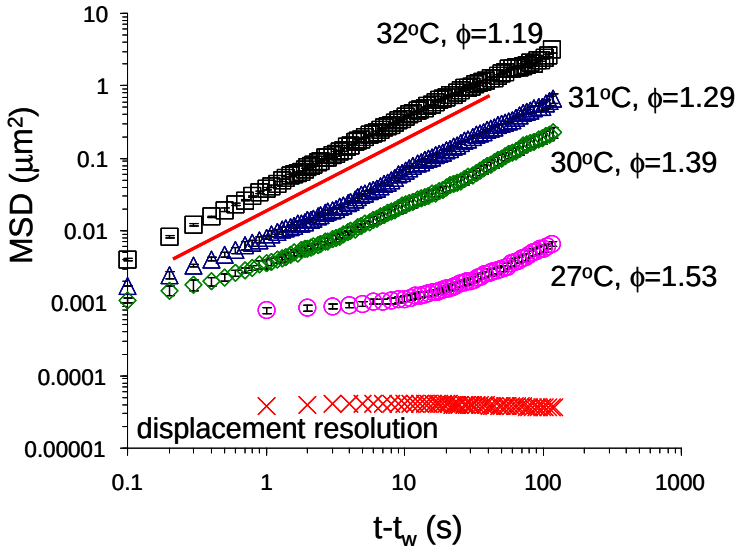

Figure 3. The mean squared displacement (MSD) of the probe particles embedded in a 4% core-shell suspension measured at different temperatures and t_w=300 s. The line indicates a slope of unity.

To investigate the gradual transition of the suspension from the liquid to the glassy state, we consider the MSDs at 31 and 30^{o}C both measured at two

different waiting times ($t_w = 300$ s and 3000 s) as shown in figure 4. Once in the glassy state, the system is expected to show aging behavior. We observe that the MSD measured at both temperatures is very similar. At 31 °C, the MSD measured at waiting time of 300 s is not significantly different from the one that is measured at $t_w = 3000$ s. However, figure 4 shows clearly that at 30 °C the MSD depends on the waiting time. This dependence becomes more pronounced as the volume fraction of the system increases (at lower temperatures).

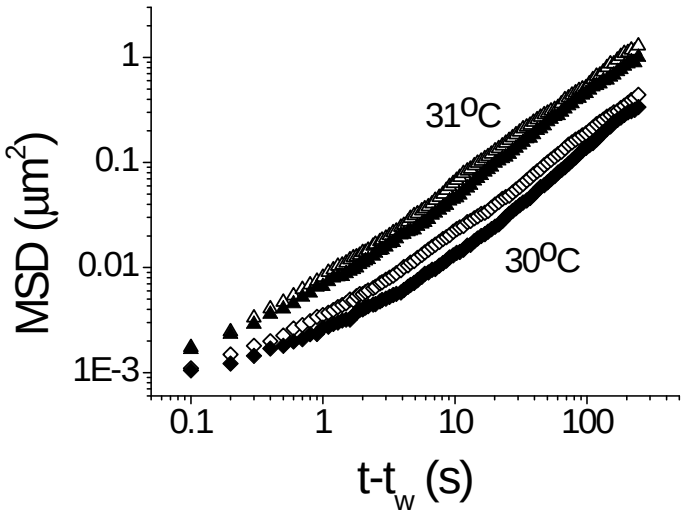

Figure 4. The MSD of a 4% core-shell suspension at 30 and 31°C measured at $t_w = 300$ s (open symbols) and $t_w = 3000$ s (closed symbols).

Further investigating the aging of the system in its glassy state, figure 5(a) shows the ensemble averaged MSD of the system at 27 °C. This figure shows clearly the evolution of the MSD as the waiting time (t_w) increases. The value of the MSD at short t_w is slightly higher than at longer t_w. We also observe that the upturn of the MSD curves shift toward longer times ($t - t_w$) as the waiting time (t_w) increases. This result strongly indicates the aging of the system.

Figure 5(b) shows that the normalized MSD measured at different waiting times form a master curve when they are plotted as function of $(t-t_w)/\tau$. The MSD is normalized with its corresponding MSD_0 which is the plateau value of the MSD at short $t - t_w$. The relaxation time (τ), used to normalize $t - t_w$, is determined from the transition from the plateau to the diffusive part of the MSD.

Figure 5(c) shows an almost linear increase of the relaxation time (τ) with the waiting time (t_w) which is indicated by the slope of 1.1 ± 0.06. This result is

qualitatively in agreement with the aging in the bulk rheological measurements where we can form a master curve from the moduli measured at different waiting times when we plot them as function of ωt (figure 2(b)). This ωt scaling indicates that the relaxation times depend linearly on the age (t). However, a sublinear increase of τ is found when it is determined by accelerating the relaxation processes using the strain rate frequency superposition technique (see the appendix).

When the particles are caged by their neighboring particles they behave elastically which is reflected by the plateau value of the MSD. Figure 5(d) shows the relation between the plateau value of MSD_0 and the corresponding elastic modulus (G'_∞) calculated using equation 6.2. The MSD_0 is expected to be inversely proportional to G'_∞ as indicated by the curve in figure 5(d).

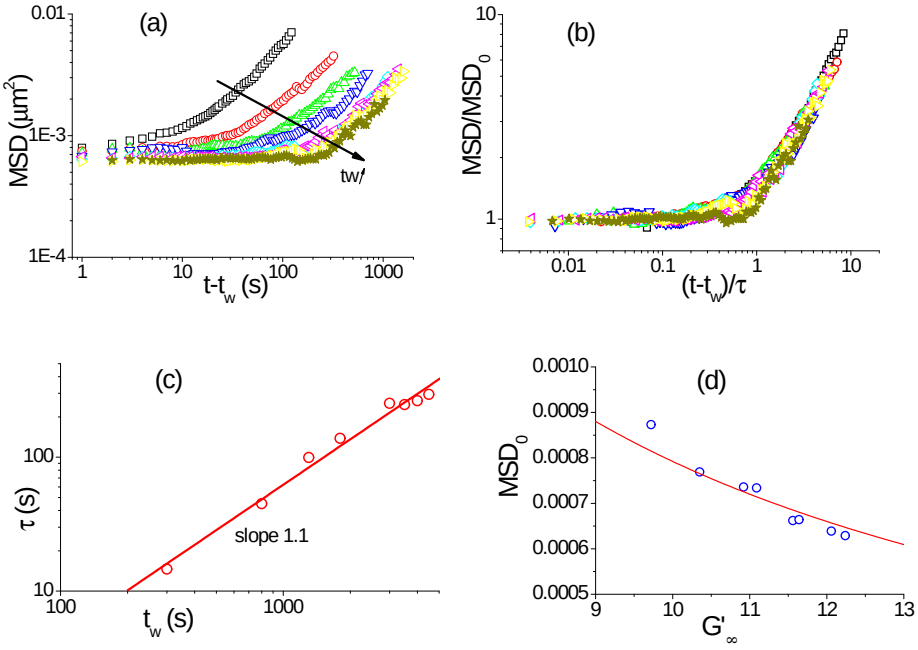

Figure 5. (a) The MSD of a 4% core-hell suspension ($T = 27\ ^{\circ}\mathrm{C}$) measured at different waiting times (300 s (□), 800 s (◯), 1300 s (△), 1800 s (▽), 3000 s (◇), 3500 s (◁), 4000 s (▷), 4500 s (★)). (b) The same data but the MSD and $t - t_w$ has been normalized with MSD_0 and τ respectively. (c) The relation between the relaxation time (τ) and the waiting time (t_w). (d) The relation between MSD_0 and G'_∞.

Since the motion of the probe particle contains information on the viscoelastic properties of the system, we can calculate the elastic and loss modulus (G'

and G'') from the mean squared displacement (micro-rheology) using Mason's approximation of the Generalized Stokes-Einstein Relation [22] (see also chapter 2):

$$G^*(\omega) = \frac{4k_BT}{6\pi a \left\langle \Delta r^2(1/\omega) \right\rangle} \frac{\exp\left(\frac{i\pi}{2}\alpha(\omega)\right)}{\Gamma[1+\alpha(\omega)]} \tag{6.1}$$

where

$$\alpha(\omega) = \left[\frac{d \ln \left\langle \Delta r^2(t-t_w) \right\rangle}{d \ln(t-t_w)} \right]_{t-t_w=1/\omega},$$

k_B is the Boltzmann constant, T is the thermodynamic temperature, a is the radius of the probe particles and Γ is the so called gamma function that is for $1 \leqslant z \leqslant 2$ well estimated by: $\Gamma[z] \approx 0.457(z)^2 - 1.36(z) + 1.90$. The elastic and the loss modulus, which are the real and the imaginary part of $G^*(\omega)$ respectively, are given by:

$$G'(\omega) = \frac{4k_BT}{6\pi a \left\langle \Delta r^2(1/\omega) \right\rangle} \frac{\cos(\pi\alpha(\omega)/2)}{\Gamma[1+\alpha(\omega)]} \tag{6.2}$$

$$G''(\omega) = \frac{4k_BT}{6\pi a \left\langle \Delta r^2(1/\omega) \right\rangle} \frac{\sin(\pi\alpha(\omega)/2)}{\Gamma[1+\alpha(\omega)]}. \tag{6.3}$$

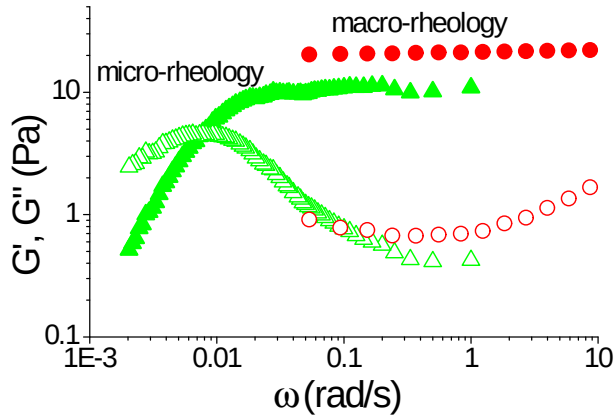

Figure 6. The G' (filled symbols) and the G'' (empty symbols) of a 4% core-shell suspension (T=27 °C) at $t_w = 1300$ s obtained from macro-rheology (◯) and micro-rheology (△).

Figure 6 shows the G' and G'' of a 4% core-shell suspension at 27 °C and $t_w = 1300$ s. With Mason's approach, one "measures" the moduli in the frequency range between $\omega_{\min} = 1/\Delta t_{\max}$ and $\omega_{\max} = 1/\Delta t_{\min}$ where $\Delta t = t - t_w$. In this range the crossing of G' and G'' is observed. This crossing is normally inaccessible using macro-rheological measurements.

In figure 6 also the viscoelastic moduli measured with our rheometer have been plotted. The G' obtained from macro-rheology is a factor of 2 larger than the G' from micro-rheology. More over, the slope of both G'' in the overlapping frequency does not match. These differences may come from the fact that the micro-rheology probe the local properties whereas the macro-rheology measure the bulk properties of the system. We can eliminate the possibility that the probe particles measure only the very local properties inside the microgels because the size of the probe particle is bigger than the size of the microgel particles.

The lower moduli measured using particle tracking may be due to an effective temperature [23], which is around 2 times the thermodynamic temperature, is necessary to match the bulk and the local moduli (see equation 6.1). In this case, the macro-rheology measurement is considered as the response of the system to an external force (equivalent with probing mobility) and the micro-rheology is obtained from the displacements of the probe particles embedded in the system (probing diffusivity).

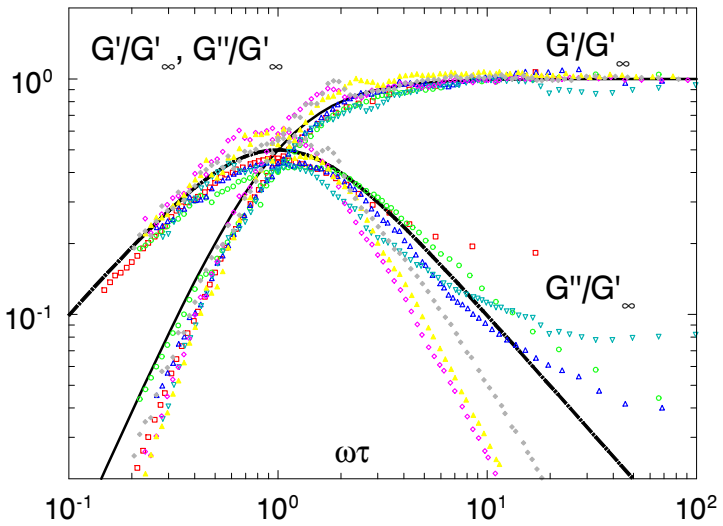

Figure 7. The normalized G' and the G'' of a 4% core-shell suspension (T = 27 °C) at different waiting times (300 s (□), 800 s (◯), 1300 s (△), 1800 s (▽), 3000 s (◇), 3500 s (▲), 4000 s (◆)) calculated using Mason's approximation of the Generalized Stokes-Einstein Relation (GSER). The line and the dashed line are the G' and the G'' of a Maxwell model.

By calculating the moduli from the MSD at different ages, we can determine the evolution of the relaxation time (τ), which is the inverse of the frequency

at which the moduli cross each other, as the system ages. Figure 7 shows the normalized moduli measured at different ages and plotted as function of $\omega\tau$ where τ is almost linearly proportional to t_w (figure 5(c)). The moduli as function of frequency at different ages collapse onto a master curve.

This is again in agreement with the bulk measurements where we observe that the moduli depend both on the frequency and the age of the system and they form a master curve when plotted as function of ωt (figure 2(b)). Therefore both the micro- and the macro- rheology show the aging of the microgel suspensions in the glassy state. The relaxation time increases linearly with the age of the glassy system.

From figure 7 we observe that the moduli behave like those of a Maxwell fluid with one dominant relaxation time. The elastic modulus (G') increases with a slope of 2 as ω increases before finally flattens at high frequency. Whereas the loss modulus (G'') increases linearly with ω (slope of 1) and then decreases with a slope of -1 after crosses with the elastic modulus. More over, the amplitude of the moduli when they cross each other is $\sim 0.5 \times G'_\infty$. The inverse of the frequency at which the crossing occurs is the relaxation time of the system.

The G'' at frequencies higher than the crossing frequency decreases faster than those obtained from macro-rheology. We also observe that the G'' of an older system decreases faster than the G'' of the younger system. This faster decrease of G'' is related the very small slope of the MSD at short times (figure 5(a)). The short time MSD at $t_w = 4500$ s has a slope of ~ 0 which results in $G'' \sim 0$ according to equation 6.3. This faster decrease of G'' at longer waiting times seems to indicate that the influence of short relaxation times at short waiting times disappears for longer waiting times.

6.5 Displacement probability

Not only $\langle \Delta x^2(\Delta t) \rangle$ and $\langle \Delta y^2(\Delta t) \rangle$ were obtained from the ensemble of particle trajectories but also the distributions $P(\Delta x(\Delta t))$ and $P(\Delta y(\Delta t))$. These distributions are considered at different temperatures and ages of the suspension. Figure 8(a) shows the ensemble averaged displacement distribution of the probe particles $P(\Delta y(\Delta t))$, taken at Δt=t-t$_w$=10s, when the system is in the liquid state (31 and 32^{o}C). The figure shows that at these temperatures, the distributions are Gaussian i.e. $P(\Delta y) \sim \exp(-\Delta y^2/2\sigma^2)$ with $\sigma^2 = \langle \Delta y^2 \rangle$.

The displacement distribution at 32 ^{o}C is broader than the one at 31 ^{o}C. This broader distribution at 32^{o}C indicates a higher diffusivity of the probe particles in the suspension as also shown in figure 3. This is due to the lower viscosity of the liquid. The viscosities at 32 and 31 ^{o}C, calculated using Stokes-Einstein relation:

$$\eta = \frac{4k_BT}{6\pi a}\frac{(t-t_w)}{\langle \Delta r^2(t-t_w)\rangle}$$

are 0.2 Pas and 1.2 Pas respectively.

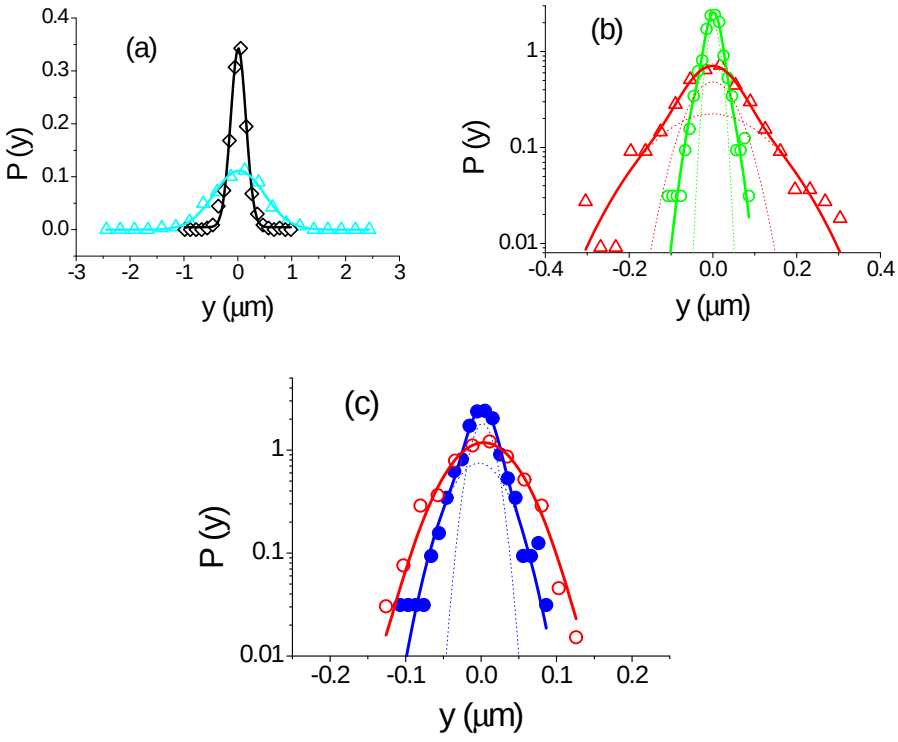

Figure 8. (a) The displacement probability ($P(y)$) of the core-shell system at 31 ($\diamond$) and 32 °C (Δ) taken at $t_w = 300$ s and $t - t_w = 10$ s and compared to Gaussian fits (lines). (b) $P(y)$ at 27 ($\bigcirc$) and 30 °C (Δ) taken at $t_w = 300$ s and $t - t_w = 10$ s and compared to a double Gaussian (lines). The dotted lines indicate the mobile and immobile populations. (c) ($P(y)$) at 27 °C taken at t_w=300 s and $t - t_w = 10$ s (closed symbol) and t-t_w=100 s (open symbol). At $t - t_w = 10$ s, $P(y)$ is well described with a double Gaussian while at $t - t_w = 100$ s can be described with one Gaussian.

The displacement distributions presented in figure 8(a) are averaged over all the probe particles. Every probe particle explores randomly its local environment resulting in a Gaussian displacement distribution. Averaging over all the particles will reveal the homogeneity of the sample. If there is a spatial inhomogeneity in the sample, the ensemble averaged displacement probability is non-Gaussian. On the other hand, a Gaussian displacement probability

shows that the sample is homogeneous, at least within a length scale of the observation window.

Figure 8(b) shows the displacement distribution of the probe particles when the suspension is in the glassy state at 30 °C which is just below the glass transition and at 27 °C which is deeper in the glassy state. The distribution at 30 °C is broader than the one at 27 °C where the system is more arrested and the probe particles have less freedom to move. In contrast to the distributions in the liquid state, the distributions in the glassy state are non-Gaussian. The non-Gaussian behavior is sufficiently described using a double Gaussian as shown by the solid line in the figure. A double Gaussian is the sum of two Gaussian distributions as indicated by the dashed lines in figure 8(b).

The non Gaussian behavior observed in the glassy state indicates dynamic heterogeneity as we perform ensemble averaging only [1,5]. From the double Gaussian observed in figure 8(b), we argue that there are two populations of particles dynamics in the glassy state. The broader Gaussian distribution represents the mobile population. Whereas the immobile population that shows smaller displacements is represented by the narrower Gaussian distribution.

Figure 8(c) describes the evolution of the displacement distribution of probe particles in a system at 27 °C. The displacement distributions are taken at $t - t_w = 10$ s and $t - t_w = 100$ s. At $t - t_w = 10$ s the particles are caged by the neighboring particles as indicated by the constant MSD shown in figure 3. Whereas at $t - t_w = 100$ s, the particles behavior is diffusive. The distribution is broader at longer $t - t_w$ as also indicated by the increase of its MSD shown in figure 3. The displacement in the caged part ($t - t_w = 10$ s) can be well described using a double Gaussian whereas we need only single Gaussian to describe the distribution at $t - t_w = 100$ s.

This evolution of displacement probability from non Gaussian at short times to Gaussian at long times is not in agreement with a recent theory developed based on a single Brownian particle moving in a periodic effective field [24]. The periodic effective field is used to describe the effect of caging and subsequent cage escape. This theory correctly predicts that the displacement distribution is Gaussian in the diffusive region of the MSD curve. However, it predicts that the distribution is also Gaussian at plateau region of the MSD which we do not observe in our experimental results. This disagreement may comes from the model's assumption that there is no dynamical heterogeneity in the system whereas in our system we observe it.

The fact that the distribution evolves from a non-Gaussian to a Gaussian does not only mean that the probe particles behave diffusively in the system but also indicates that at the corresponding time scale, the probe particles have explored a representative amount of sample. This may sound counter intuitive as the average displacement of the probe particle is only circa 75 nm.

This average displacement is comparable to the radius of a deformed microgel particle ($R \sim 70$ nm) at 27 ^{o}C and 4% w/w mass concentration. However, the relaxation time of the system at $t_w = 300$ s is ~ 15 s (see figure 5(c)). This relaxation time is related to life time of a cage [25]. Therefore, even though a probe particle displaces only in the order of the particles radius, it has probed ~ 7 different cages within 100 s. Since the number of probe particle in the observation window is ~ 400, in total we have probed 2800 different positions to have a representative amount of sample.

To investigate how this distribution of the displacement evolves as function of $t - t_w$, we quantify how far the distribution deviates from Gaussian by calculating the non Gaussian parameter [1]:

$$\alpha_2 = \frac{\langle \Delta r^4 (t - t_w) \rangle}{3 \langle \Delta r^2 (t - t_w) \rangle^2} - 1$$

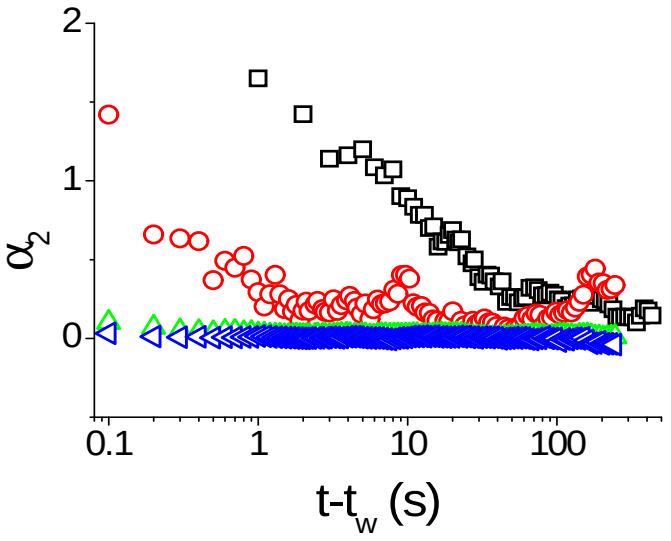

Figure 9. The non Gaussian parameter (α_2) of the 4% w/w core-shell suspension (t_w=300 s) at different temperatures (27 ^{o}C (□), 30 ^{o}C (◯), 31 ^{o}C (△), and 32 ^{o}C (◁)).

Figure 9 shows the α_2 of the microgel system at different temperatures. The analysis is done for the systems at $t_w = 300$ s. At high temperature (31 and 32 ^{o}C), the α_2 is zero over the entire observed time scales. However, at low temperatures (27 and 30 ^{o}C), the non Gaussian parameter is bigger than zero at short time scales and decreases to zero at longer time scales. We also

observe that the non Gaussian parameter approaches zero within relatively short time ($t - t_w \sim 1$ s) for the system at 30 °C while at 27 °C, it takes ~ 50 s to approaches zero.

Figure 9 indicates that α_2 is zero when the particles diffuse out of the cage and non zero when the particles are caged. This result is in contrast to the recent theory [24] which predict that α_2 peaks at the transition from the caged to the diffusive behavior. This theory specifically predicts that α_2 is zero when the particles are caged.

6.6 Conclusion

By combining the macro-rheology and particle tracking technique we show that using our thermosensitive system we can tune the system from the liquid to the glassy state reversibly by changing the temperature. The volume fraction of the system increases as we decrease the temperature due to the swelling of the core-shell particles. The viscoelastic moduli obtained from macro-rheology evolve from a viscous behavior to an elastic behavior as we decrease the temperature. Mean while, the mean squared displacement obtained from the particle tracking experiments evolves from diffusive behavior at high temperature to caging-diffusive behavior at low temperature.

We also find that the system in the glassy state (low temperature) shows aging behavior as indicated by the age-dependent behavior of the viscoelastic moduli obtained from macro-rheology and the MSD obtained from the particle tracking. The relaxation time extracted from the particle tracking measurements increases almost linearly with the waiting time and qualitatively in agreement with the macro-rheological results where the moduli measured at different ages form a master curve when plotted as function of ωt.

By using the Mason's approximation of the generalized Stoke-Einstein relation, we calculate the viscoelastic moduli from the MSD. The particle tracking experiments measure the moduli at lower frequency range that yield an access to the relaxation time of the aging glassy system.

Further investigation into the distribution of the particle displacement indicates that in the glassy state, the particle dynamic is non Gaussian at short $t - t_w$ but becomes Gaussian at longer times. The non Gaussian behavior indicates that the particle displacement is spatially inhomogeneous. We identify mobile and immobile particles in the glassy state at short $t - t_w$.

Appendix

Due to the slow relaxation processes of a system in the glassy state, its average relaxation time τ is not accessible using a linear rheological procedure. The

frequency at which the G' crosses the G'' curve is lower than the experimentally accessible frequency. In this chapter we have shown that the lower frequency range is accessible with particle tracking micro-rheology. In this appendix we report another method to determine the average relaxation time using the non linear strain rate frequency superposition (SRFS) technique [26].

In a linear frequency sweep experiment, a constant strain amplitude γ_0 is applied as the frequency ω increases. In the SRFS technique, however, the G' and G'' are measured at a constant strain rate amplitudes $\dot{\gamma}_0$. It is achieved by progressively decreasing the strain amplitude γ_0 as the frequency ω increases (inset of figure A1(a)).

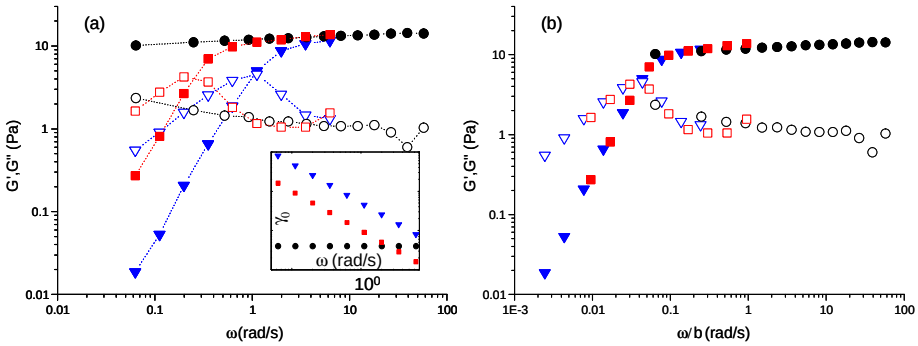

Figure A1. (a) The G' (filled symbols) and the G'' (empty symbols) of a 7% w/w suspension at 35° C measured in the linear regime (◯) and non linear regime using the SRFS technique at $\dot{\gamma}_0 = 0.01$ 1/s (□) and $\dot{\gamma}_0 = 0.05$ 1/s (▽). The age of the suspension (t) is 130 s. The inset shows the experimental protocols corresponding to the main figure. (b) The same data but plotted as a function of the scaled frequency ω/b to collapse the non linear measurements ($b = 6.6$ for $\dot{\gamma}_0 = 0.01$ 1/s and 25.6 for $\dot{\gamma}_0 = 0.05$ 1/s) to the linear measurement.

Figure A1(a) shows the moduli measured in the linear regime and the ones measured using the non linear SRFS technique. The linear G' decreases slightly as ω decreases whereas the G'' increases as ω decreases. Extrapolation of the moduli toward lower frequencies suggests the existence of a cross over of G' and G'' at $\omega_{cr.}$. The non linear moduli measured at a constant $\dot{\gamma}_0$ show this crossing between G' and G''. The crossing occurs at higher ω as $\dot{\gamma}_0$ increases.

The non-linear moduli measured at a constant $\dot{\gamma}_0$ can be mapped to the linear ones by scaling the frequency with some reference value $b(\dot{\gamma}_0)$ as shown in figure A1(b). The figure shows that at low frequencies the $G' \sim \omega^2$ and the $G'' \sim \omega$. The G'' reaches its maximum when G'' crosses G'. At higher frequencies, the G' flattens and the G'' decreases and then flattens. A qualitatively similar behavior is also observed from the micro-rheology as shown in figure

6. The frequency at which the moduli cross each other marks the average relaxation time $\tau = 1/\omega_{cr.}$ of the sample at the corresponding age of the linear data.

The possible explanation for the dependence of the relaxation process on $\dot{\gamma}_0$ is that it is accelerated when a larger strain rate amplitude $\dot{\gamma}_0 = \gamma_0\omega$ is applied. The dependence of the average relaxation time on the strain rate amplitude is described as [26]

$$\frac{1}{\tau\left(\dot{\gamma}_0\right)} \approx \frac{1}{\tau_0} + K\left(\dot{\gamma}_0\right)^v \tag{A1}$$

where τ_0 is the average relaxation time at $\dot{\gamma}_0 \simeq 0$ (linear regime), K and v are constants.

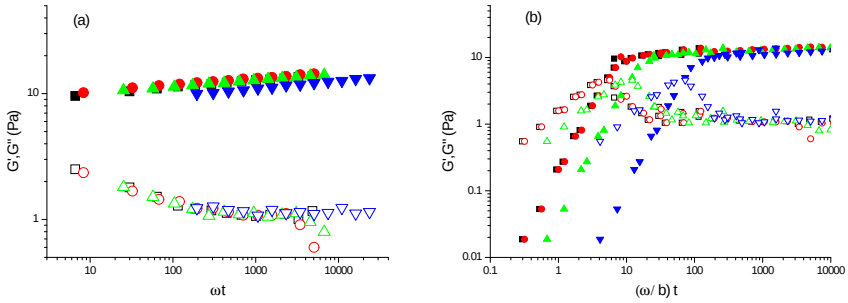

Figure A2. (a) The linear G' (filled symbols) and G'' (empty symbols) of 7% w/w suspension at 35° C measured at t=103 s (□), 130 s (◯), 400 s (△), and 3100 s (▽) plotted as function of ωt. (b) The linear and non linear G' (filled symbols) and G'' (empty symbols) of the suspension at 35° C measured at t=103 s (□), 130 s (◯), 1400 s (△), and 3100 s (▽) plotted as function of ωt. The ωt scaling is lost when the linear moduli is combined with the non linear moduli.

Aging is one of the unique properties of a system in the glassy state. Due to aging, the linear viscoelastic moduli of a system in the glassy state depend not only on the frequency ω but also on the age t. Figure A2(a) shows that the moduli measured at different ages, form a master curve when plotted as function of ωt. However, the moduli measured at constant $\dot{\gamma}_0$ are independent of the age. This is in line with the assumption, see equation A1, that for larger $\dot{\gamma}_0$ the relaxation processes are controlled by $\dot{\gamma}_0$. Therefore the ωt scaling is lost when we combine the linear and non linear measurements as shown in figure A2(b). This SRFS results suggest that the relaxation time does not increase linearly with the age of the sample. In contrast, our results from particle tracking micro-rheology (figure 7) show that the moduli measured at different ages form a master curve when plotted as function of $\omega\tau$ where $\tau \sim t^{1.1\pm0.06}$.

To extract the evolution of τ, we map the age-independent non linear data onto the age-dependent linear reference curves at different ages. The open symbols in figure A3 show the result of this procedure for three different thermodynamic temperatures, 2°C, 12°C and 22°C below the glass transition (T_g=37 °C), respectively. In all cases, τ is found to increase with increasing sample age. The samples turn out to age faster, the deeper they are in the glassy state. The aging rate is found to be controlled by the effective noise temperature (x) rather than the thermodynamic temperature (T), as evidenced by the data for the two lowest temperatures that display the same aging rate despite the rather big difference in T. As the glass transition is approached, the rate of aging decreases in line with the qualitative expectations and probably ultimately vanishes for $x \simeq 1$. The solid lines in figure A(3) indicate the predicted algebraic evolution of $\left\langle \tau^{-1} \right\rangle^{-1} = \langle Y \rangle^{-1} \sim t^{1-x}$ of the SGR model [14] using the effective noise temperatures extracted from the linear rheological data. $\langle Y \rangle$ is the average yielding rate of the elements trapped by the neighboring elements.

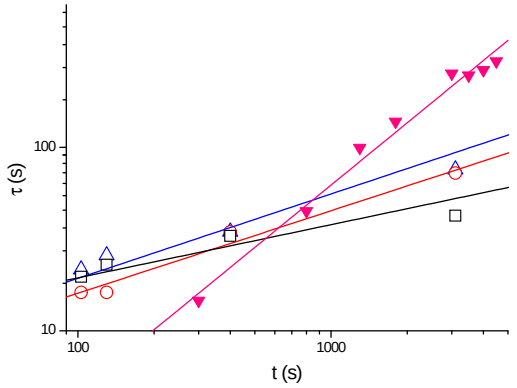

Figure A3. The increase of structural relaxation time of 7% w/w suspensions at different effective noise temperatures: T = 15 °C (△, $x = 0.54 \pm 0.04$), 25 °C (◯, $x = 0.55 \pm 0.02$) and 35 °C (□, $x = 0.71 \pm 0.04$). The lines are the inverse of the average yielding rate $\langle Y \rangle^{-1} \sim t^{1-x}$. The filled symbol is τ of a 4% w/w suspension at 27 °C ($x = 0.48 \pm 0.03$) measured using the particle tracking method shown also in figure 5(c).

In figure A3 we also plot the relaxation time of a 4% suspension ($x = 0.48 \pm 0.03$) measured using the particle tracking technique (filled symbol). The relaxation time increases almost linearly with the age, which is in agreement with the ωt scaling of the linear moduli and the SGR prediction ($\langle \tau \rangle \sim t$).

From these results we conclude that the average relaxation time of a glassy system increases almost linearly with the age when determined within the linear

regime, which is in agreement with the SGR prediction that $\langle\tau\rangle \sim t$. Measuring the relaxation time by accelerating the relaxation process via increasing $\dot{\gamma}_0$ results in $x-$dependent aging rate. The aging rate is in agreement with the SGR prediction that $\left\langle\tau^{-1}\right\rangle^{-1} = \langle Y\rangle^{-1} \sim t^{1-x}$. However, we still do not understand why the two methods indicate different behavior of relaxation as the suspension ages.

References

[1] E.R. Weeks *et al.,* Science **287**, 627 (2000)

[2] R.E. Courtland and E.R. Weeks, J. Phys. Condens. Matter**15**, S359 (2003)

[3] E.H. Purnomo *et al.,* Europhys. Lett. **76,** 74 (2006)

[4] E.H. Purnomo *et al.,* Phys. Rev. E. **76,** 021404 (2007)

[5] Y. Gao and M.L. Kilfoil, Phys. Rev. Lett. **99**, 078301 (2007)

[6] L. Cipelletti and L. Ramos, J. Phys. Condens. Matter **17,** R253 (2005)

[7] F. Sciortino and P. Tartaglia, Advances in Physics **54**, 471 (2005)

[8] W. van Megen and S.M. Underwood, Phys. Rev. Lett. **70**, 2766 (1993)

[9] J. J. Crassous *et al.,* J. Chem. Phys. **125**, 204906 (2006)

[10] K. Miyazaki *et al.*, Europhys. Lett. **75**, 915 (2006)

[11] J. M. Brader *et al.,* Phys. Rev. Lett. **98**, 058301 (2007)

[12] P. Sollich *et al.,* Phys. Rev. Lett. **78,** 2020 (1997)

[13] P. Sollich, Phys. Rev. E. **58**, 738 (1998)

[14] S.M. Fielding *et al.,* J. Rheol. **44**, 323 (2000)

[15] W.M. Holmes *et al.*, J. Rheol. **48**, 1085 (2004)

[16] M. Cloitre, R. Borrega and L. Leibler, Phys. Rev. Lett. **85**, 4819 (2000)

[17] I. Berndt *et al.*, Langmuir **22**, 459 (2006)

[18] I. Berndt *et al.*, J. Am. Chem. Soc. **127**, 9372 (2005)

[19] I. Berndt and W. Richtering, Macromolecules **36**, 8780 (2003)

[20] J.C. Crocker and D.G. Grier, J. Colloid Interface Sci. **179,** 298 (1996)

[21] A.N. Rissanou, D. Vlassopoulos, and I.A. Bitsanis, Phys. Rev. E. **71**, 011402 (2005)

[22] T.G. Mason, Rheol. Acta **39**, 371 (2000)

[23] B. Abou *et al.,* Phys. A. **387,** 3410 (2008)

[24] B. Vorselaars *et al.*, Phys. Rev. E. **75**, 011504 (2007)

[25] E.R. Weeks and D.A. Weitz, Phys. Rev. Lett. **89**, 095704-1 (2002)

[26] H.M. Wyss *et al.*, Phys. Rev. Lett. **98**, 238303 (2007)

Chapter 7

Conclusion and outlook

7.1 Conclusion

To study the glass transition (and aging in the glassy regime) of soft materials we use a suspension of thermosensitive PNIPAM and PNIPAM-PNIPMAM microgel particles. Their size depends strongly on the temperature. This thermosensitive property of the soft microgel particles provides a unique way to control the volume fraction *in situ*. A volume fraction bigger than unity is easily achieved due to the softness and the compressibility of the microgel particles.

We use rheology and particle tracking to study aging, the glass transition, relaxation processes, and dynamic heterogeneity of the model systems. Both the rheological and particle tracking techniques reveal that the soft colloidal system can be tuned reversibly from liquid at high temperature to glassy state at low temperature. The viscoelastic moduli obtained from macro-rheology evolve from viscous behavior ($G'(\omega) < G''(\omega)$) to elastic behavior ($G'(\omega) > G''(\omega)$) as we decrease the temperature. Mean while, the mean squared displacement (MSD) measured using the particle tracking technique evolves from diffusive behavior at high temperature to caging-diffusive behavior at low temperature.

In the glassy state, the systems show aging as indicated by the dependence of viscoelastic moduli ($G'(\omega, t)$ and $G''(\omega, t)$), creep compliance ($J(t-t_w, t_w)$), and the mean squared displacement (MSD $(t - t_w, t_w)$) on their age. In the liquid state, however, the viscoelastic moduli and the MSD show that the systems do not age.

Since a system in the glassy state shows aging behavior we have to start an experiment from a well defined initial state. The initial state is achieved by rejuvenating the sample and define age is zero (t=t_w=0) as the end of the

rejuvenation. The rejuvenation is done by either applying a stress that is higher than the yield stress to flow the sample or heating the sample above its transition temperature to shrink the particles and therefore decrease the volume fraction. However, the mechanical and the thermal rejuvenation do not result in the same initial state as indicated by the difference in the amplitude of $G'(\omega)$.

The mechanical rejuvenation can be stopped either abruptly (step stress rejuvenation) of gradually (fading stress rejuvenation). A step stress rejuvenation produces a strained system at the end of the rejuvenation, whereas a fading stress rejuvenation produces a strain and stress free system. For the oscillatory experiments, both the step stress and the fading stress rejuvenation result in almost the same behavior of $G'(\omega)$ and $G''(\omega)$. However, in the creep experiments, the fading stress rejuvenation results in a continuous increase of strain. On the other hand, for the step stress rejuvenation the strain increases only for short time $t - t_w < t_w$ and recovers for $t - t_w > t_w$.

We use soft glassy rheology (SGR) model to describe quantitatively the inherent effect of aging on the rheological properties. We also find that the SGR model describes quantitatively the behavior of the system in the liquid state. From the quantitative comparison with the model, we extract an effective noise temperature (x) and a particle elasticity G_p. The effective noise temperature x is a measure of glassiness. A system is in the aging glassy state for $x \leqslant 1$ and it is in the liquid state for $x > 1$.

Exploiting further the model systems by varying both the mass concentration and the temperature we can control the volume fraction and the softness of the particles independently. We find that the glass transition depends both on the volume fraction and the softness of the particle. The volume fraction at which the glass transition occurs (ϕ_{trans}) approaches the one of hard sphere particles ($\phi_{\text{trans}} = 0.58$) as the particles get harder. More over, from an aging study of two systems with an identical volume fraction but different mass concentration, we find that the aging stops after a certain time if we approach the hard sphere limit with our particle softness.

Aging of soft glassy materials is forever as their relaxation time increases linearly with the age of the samples. However, the structural relaxation time is inaccessible using macro-rheological technique. We show that using particle tracking techniques (micro-rheology), the relaxation time of an aging system can be determined experimentally. We find that the relaxation time increases linearly with the age of the system. The viscoelastic moduli of the system show an almost Maxwellian behavior with one dominant relaxation time. The influence of short relaxation times at short waiting times seems to disappears for longer waiting times.

From the particle tracking we find that in the glassy state, the distribution of the particle dynamics is non Gaussian at short $t - t_w$ but becomes Gaussian

at longer times. The non Gaussian behavior indicates that the particle displacement is spatially inhomogeneous. We identify mobile and immobile particles in the glassy state at short $t - t_w$.

7.2 Outlook

Even though the SGR model has been shown to describe quantitatively most of the rheological properties of aging suspensions. This model fails to describe the linear step stress experiment at $t - t_w > t_w$ due to its assumption that the system is stress and strain free directly after the rejuvenation. Incorporating the fact that there are strain recovery that stems from the quench will improve the model.

From the quantitative comparison between the experimental data and the SGR model we extract the effective noise temperature (x). However, the effective noise temperature is relative to the average energy barrier $\langle E \rangle$ and its absolute value is still unknown. One way to measure the absolute value of the effective noise temperature is to use the generalized Einstein relation developed by Pottier and co-workers [23 of chapter 6] by simultaneously measuring the response function to an external force and the position fluctuations of micrometric beads embedded in the system.

The SGR model assumes that the effective noise temperature x is independent of the age of the sample. However, this assumption may be violated because the particles are trapped in progressively increasing energy barrier which consequently decreases the effective noise temperature as the sample ages. Therefore it would be interesting to verify this assumption. The possibly good effective noise temperature to test this idea is for $x \sim 1$ where the sample is still transient and the evolution of the mechanical properties not too slow.

From the particle tracking experiments at $x = 0.48$, we find that the relaxation time increases linearly with the age of the system. However, it is also very interesting to study its evolution at other x values (different temperatures) and find out whether the aging rate depends on x or not. More over, the increase of the relaxation time is believed to be related to the decrease of the intermittent yielding of the caged particles. Therefore visualization and quantification of such an intermittent yielding will be an interesting topic to address in the future.

Using confocal scanning laser microscopy we only are able to probe a time scale $0.1 < t - t_w < 1000$ s due to the acquisition limit of the camera and the movement of the probe particle in vertical, out of plane, direction. Diffusive wave spectroscopy can be used to probe the particle displacement at shorter time scales whereas 3D particle tracking can be used to extent the observation

to longer time scales. Obtaining the particle displacements over a wide range of time intervals, and combined with the ability to tune the degree of glassiness, will provide useful information on the dynamics of glassy systems such as the evolution of the relaxation time and its length scale as the sample ages at different degree of glassiness.

Summary

Soft glassy materials are widely used in our daily life. Macroscopically, soft glassy materials behave like a solid but they have an amorphous structure just like a liquid. Due to their metastability and arrested structure, this class of materials often exhibits aging where their mechanical properties evolve continuously with time. We study this glassy behavior using model systems which contain colloidal thermosensitive soft particles (PNIPAM particles and core-shell PNIPAM-PNIPMAM particles). We use rheology and particle tracking to study aging the glass transition, relaxation processes, and dynamic heterogeneity of the model systems. Using standard rheometry we measured bulk viscoelastic properties of the systems, and with particle tracking we followed the displacements of probe particles embedded in the suspensions.

We start the study by characterizing our instruments (Haake RS600 rheometer and confocal scanning laser microscope(CSLM)) and our thermosensitive microgel systems. For the rheometer, we find that the temperature distribution inside a plate-plate geometry is within 0.2^oC, the maximum torque fluctuation at its lower limit (0.5 μNm) is 9% which is related to shear stress fluctuation of 0.8 mPa for the cone and plate geometry. For the CSLM, we find that the position accuracy of the set up is 6 nm at short times and rises to 9 nm at long times. For the thermosensitive systems, we find that they are swollen at low temperature, shrunken at high temperature and stable for up to 3 years. We also determine the relation between mass concentration and volume fraction of a suspension using Einstein's relation. The volume fraction at other temperatures can be calculated from the dependence of the radius of gyration ($R_g(T)$) on the temperature. The radius of gyration is determined using static light scattering.

As a system in the glassy state shows an aging behavior we have to start an experiment from a well defined initial state. This initial state is achieved by rejuvenating the sample and defining age zero ($t = t_w = 0$) as the end of the rejuvenation. The rejuvenation can be done either by applying a stress that is larger than its yield stress to flow the sample or by heating the sample above its transition temperature to shrink the particles (decrease its volume

fraction). We show that both ways of rejuvenation have the same effect on the behavior of the suspensions and for simplicity we use the stress rejuvenation for preparing the sample throughout this study.

Aging in soft glassy materials inherently affects their rheological properties and also affects the displacements of probe particles embedded in the system. Using a Haake RS600 rheometer we measure the elastic and the loss modulus $G'(\omega, t)$ and $G"(\omega, t)$ as function of the frequency ω at different waiting times t_w. We find that the moduli depend both on the frequency and the waiting time. They can be collapsed on a master curve by plotting them as function of ωt. Here, age t is defined as the total time since the end of the mechanical rejuvenation until the moment of data acquisition which includes both the waiting times and the oscillation times. More over, we also measure the creep compliance ($J(t - t_w, t_w)$) of the aging systems at different waiting times. We also find that $J(t - t_w, t_w)$ depends on the waiting time and can be collapsed on to a master curve when they are plotted as function of $(t - t_w)/t_w$ for $(t - t_w) < t_w$.

We use the soft glassy rheology (SGR) model developed by Sollich and coworkers to describe the rheological data. We find that the model describes quantitatively the experimental results obtained both from the oscillatory and the creep experiments. From the quantitative comparison between the experimental data and the predictions of the model we extract an effective noise temperature x and a particle elasticity G_p. The effective noise temperature obtained from both the oscillatory and the creep experiments is indeed less than 1 in agreement with the definition of aging. Moreover, the elasticity of the compressed particles G_p increases with increased compression, i.e. the degree of hindrance and consequently also the bulk elasticity (G' or $1/J$) increases with the degree of compression.

From the particle tracking experiments, we find that in the glassy state, the ensemble averaged mean squared displacement (MSD) of the probe particles depends on the waiting time t_w which indicates once more that the system ages. Remarkably, the MSDs at different waiting times form a master curve when plotted as a function of $(t - t_w)/t_w$ showing the linear dependence of the relaxation time. Further investigation of the distribution of the particle displacement reveals that the particle dynamics are inhomogeneous in the glassy state.

The glass transition is studied in more detail using a core-shell thermosensitive PNIPAM-PNIPMAM system since it has a more gradual decrease of size as we increase the temperature than a pure PNIPAM particle. Using both rheology and particle tracking techniques, we show that this soft colloidal system can be tuned continuously and reversibly between the glass at low temperatures and the liquid state at high temperatures. From the viscoelastic moduli

and their comparison with the SGR model, the glass transition is characterized by the effective noise temperature which evolve from 0.5 to above 3.0 as we increase the temperature. Whereas from the particle tracking, the glass transition is shown by the evolution of the mean squared displacement (MSD). At low temperatures, the MSD shows a transition from caging behavior at short times $(t-t_w)$ to diffusive behavior at long $t-t_w$. The caging behavior vanishes as we increase the temperature because the suspensions is in the liquid state. More over, by varying both the temperature and the mass concentration, we find that both the volume fraction and the softness of the particles determine the glass transition. The volume fraction at which the glass transition occur, ϕ_{trans}, approaches the one of hard sphere particles ($\phi_{\text{trans}} = 0.58$) as the particles get harder (i.e. more elastic). We also find that aging stops after a certain time if we approach the hard sphere limit with our particle softness.

Thus by varying in situ the volume fraction of our microgel suspensions, by tuning the temperature, we are able to control the state of the suspensions (liquid or glass). More over by analyzing the mechanical relaxation behavior, using both macro- and micro-rheology, the aging of the suspensions is characterized.

Samenvatting

Zachte glasachtige materialen gebruiken we dagelijks: we poetsen onze tanden met tandpasta, smeren gel in ons haar of margarine en chocoladepasta op ons brood. We kunnen dat doen omdat deze materialen zich als een vaste stof willen gedragen, maar onder invloed van kleine krachten al gaan stromen, omdat hun inwendige structuur, net als bij vloeistoffen, amorf is. Echter, de microscopische deeltjes waaruit een zacht glas is opgebouwd, vertonen een sterke wrijvingswisselwerking waardoor de structuur niet in evenwicht is maar nagenoeg vastgevroren in een metastabiele toestand. Daardoor vertonen zachte glazen een merkwaardig verouderingsgedrag. Hun mechanische eigenschappen evolueren in de tijd omdat de interne relaxatieprocessen met het verouderen van het materiaal steeds langzamer verlopen. In het onderzoek, dat in dit proefschrift wordt beschreven, bestuderen we de invloed van de interne structuur van zachte glazen op hun verouderings gedrag, met name in de buurt van de overgang van de vloeistof- naar de glasfase. Hiertoe worden modelsuspensies gebruikt, welke colloïdale microgel deeltjes bevatten. Deze deeltjes bestaan uit een kluwen van onderling verbonden polyNipam molekulen welke onder invloed van temperatuursveranderingen sterk in hun oplosmiddel kunnen zwellen, als de temperatuur afneemt, of juist krimpen, als de temperatuur toeneemt. In het tweede deel van ons onderzoek hebben we, om de grootte van het deeltje gevoeliger in te kunnen stellen, gebruik gemaakt van deeltjes met een polyNipam kern en daaromheen een polyNipmam schil. De diameter van deze zachte bolvormige deeltjes is in gezwollen toestand typisch 400 tot 500 nm. Om de glasovergang, de veroudering in de glasfase, en het relaxatie gedrag van deze modelsuspensies te onderzoeken, gebruiken we conventionele reometrie en deeltjespadenanalyse (particle tracking). Met een reometer meten we de viscoelastische bulkeigenschappen van het materiaal, via deeltjespadenanalyse leggen we de verplaatsingen van testdeeltjes vast, welke aan de suspensie zijn toegevoegd. Dit doen we met behulp van confocale laser microscopie (CSLM). De grootte van deze verplaatsingen bevat informatie over de locale viscoelastische eigenschappen.

Vooraf zijn de karakteristieke kenmerken van de experimentele methoden

en van de modelsuspensies vastgelegd. Omdat de suspensies zo temperatuurgevoelig zijn, is de temperatuurverdeling binnen de monsterhouder van de reometer (Haake RS600) nauwkeurig gemeten. Deze blijkt binnen 0.2 °C constant te zijn hetgeen voldoende voor ons onderzoek is. Vervolgens is ook de meetgevoeligheid vastgelegd: de fluctuaties in het opgelegde koppel zijn maximaal bij minimaal koppel (0.5 μNm) en bedragen dan ongeveer 9 %. Dit komt voor de gebruikte plaat-kegel-geometrie overeen met een variatie in de schuifspanning van 0.8 mPa. Om de nauwkeurigheid van de deeltjespaden te kunnen bepalen is de positie van een gefixeerd testdeeltje als functie van de tijd gemeten. Hieruit kon geconcludeerd worden dat de korte tijd nauwkeurigheid 6 nm bedraagt; voor tijden groter dan 500 s loopt dit op naar 9 nm. Uit de karakterisering van de microgel deeltjes, via statische lichtverstrooing, blijkt dat de gyratiestraal in gezwollen toestand ruwweg 2 keer zo groot is als in gekrompen toestand. De omslagtemperatuur varieert een beetje van systeem tot systeem, maar ligt rond de 32 °C. Gebleken is dat de supensies in ieder geval gedurende 3 jaar stabiel zijn. Ook is de volumefractie van de gebruikte suspensies vastgelegd. Bij een temperatuur beneden de omslag temperatuur is de viscositeit als functie van de massa concentratie gemeten. Daarbij was de concentratie zodanig laag gekozen, dat de volumefractie uit de Einstein uitdrukking voor de viscositeit afgeleid kon worden. Aangezien de gyratiestraal als functie van de temperatuur bekend is, kan nu ook de volumefractie voor ander temperaturen berekend worden.

Omdat de leeftijd van het systeem een belangrijke rol speelt, moet deze precies vastgesteld (of liever nog: ingesteld) worden. Dit gebeurt door het monster dat onderzocht wordt te "verjongen". Dit kan op twee manieren. Ofwel wordt gedurende een korte periode een schuifspanning, ruim boven de zwichtspanning van het monster, opgelegd, ofwel wordt gedurende een korte periode de temperatuur van het monster ruim boven de omslagtemperatuur gebracht. In het eerste geval wordt de inwendige spaning tussen de microgeldeeltjes zo hoog dat ze ten opzichte van elkaar gaan schuiven en zo de oorspronkelijke microstructuur geheel teniet doen. In het tweede geval wordt het monster kortstondig in de vloeistof fase gebracht en verliest het ook zijn oorspronkelijke microstructuur. De leeftijd wordt gemeten vanaf het eind van de schuifspanning- of temperatuurpuls. Beide manieren van verjongen hebben hetzelfde effect op het gedrag van zachte glazen. In de rest van het onderzoek gebruiken we de schuifspanningspuls om de leefttijd van de monsters te definiëren.

Na deze inleidende experimenten is als eerste het viscoelastisch gedrag van de suspensie bij een vaste concentratie en temperatuur bepaald. De opslagmodulus $G'(\omega, t)$ en de verliesmodulus $G''(\omega, t)$ zijn met de RS600 gemeten als functie van de frequentie ω en de leeftijd t. In de glastoestand hangen de waarden van de moduli zowel van de frequentie als van de leeftijd af, en wel op een

bijzonder manier: Als we de moduli uit zetten tegen het product ωt blijken de curves welke gemeten zijn op verschillende tijden, samen te vallen en een zogeheten mastercurve te vormen. Ook de gemeten kruipcompliantie $J(t-t_w, t_w)$ blijkt van de wachttijd t_w af te hangen. Nu ontstaat er een mastercurve wanneer we de compliantie uitzetten tegen $(t-t_w)/t_w$. Deze resultaten tonen aan dat de relaxatie- en retardatietijden van de suspensie in de glastoestand lineair toenemen met de leeftijd van het monster. In de vloeistoffase wordt deze afhankelijkheid van de leeftijd niet waargenomen.

Om de verkregen resultaten meer kwantitatief te begrijpen, vergelijken we ze met de uitkomsten van modelberekeningen. Hiertoe gebruiken we het SGR (soft glassy rheology) model van Sollich en collega's. Dit model beschrijft onze bevindingen goed. Het geeft ons tevens waarden voor de effectieve ruis temperatuur x van het monster en de elasticiteit G_p van de microgel deeltjes. Als het monster in de vloeistof fase is moet de ruistemperatuur $x > 1$ zijn, in de glasfase $x < 1$. Dit wordt experimenteel inderdaad waargenomen. De elasticiteit van de microgel deeltjes neemt toe met de mate waarin ze elkaar samendrukken. Als gevolg hiervan neemt ook de bulk elasticteit, G' en J^{-1}, toe naarmate de deeltjes meer gecomprimeerd worden.

De experimenteel waargenomen deeltjes paden lieten zien dat in de glastoestand de gemiddelde kwadratische verplaatsing (MSD, mean square displacement) van een ensemble van testdeeltjes afhankelijk is van de leeftijd (of de wachttijd t_w na de schuifspaningspuls) van het monster, wederom een teken dat het monster verouderd. Ook in dit geval kunnen we $MSD(t-t_w)$ metingen bij verschillende wachttijden met elkaar vergelijken door de MSD waarden niet tegen het tijdsinterval $(t-t_w)$ uit te zetten maar tegen $(t-t_w)/t_w$. Alle curves vallen weer netjes op elkaar. Door ook de verdelingsfunctie van de deeltjesverplaatsingen te bepalen, vinden we in de glastoestand voor korte tijdsintervallen een niet Gaussische verdeling. Dit duidt op heterogeniteit in de suspensie.

We hebben de glasovergang uitgebreider in kaart gebracht met de polyNipampolyNipmam deeltjes, omdat met dit systeem de deeltjesstraal nauwkeuriger ingesteld kan worden. Wederom zijn reometrie en deeltjespaden metingen gedaan. Door de temperatuur te variëren kan de suspensie reversibel en reproduceerbaar van de vloeistof- in de glasfase gebracht worden. De temperatuur waarop de overgang plaats vindt, hangt van de massaconcentratie van de deeltjes af: naarmate de massa concentratie hoger is, zal de overgang bij een hogere temperatuur plaats vinden. Ook de elasticiteit van de microgel deeltjes neemt, bij gelijkblijvende temperatuur, toe met de massaconcentratie. Dit kan verklaard worden door het beschikbare volume voor een enkel deeltje te beschouwen: dat volume is omgekeerd evenredig met de massaconcentratie. Hierdoor neemt de locale polymeerdichtheid in een deeltje toe met de massaconcentratie en daarmee ook de elasticiteit (of hardheid).van het microgel

deeltje in de suspensie. Door de reometrieresultaten weer met het SGR model te vergelijken, kunnen we de ruis temperatuur x bepalen als functie van de thermodynamische temperatuur T en de massaconcentratie c: $x(T, c)$. Deze blijkt te varieren tussen $x = 3$ in de vloeistoffase en $x = 0.5$ diep in de glasfase. Omdat de volumefractie ϕ als functie van T ook bepaald is bij de inleidende metingen, kunnen we nu ook de volumefractie $\phi_{\text{trans}}(c)$ bij de glasovergang ($x = 1$) vaststellen: ϕ_{trans} neemt af met toenemende concentratie c. Dit is ook te verwachten aangezien de deeltjes harder zijn naarmate c hoger is; voor een harde bollen suspensie wordt gevonden: $\phi^{\text{HS}}_{\text{trans}} \simeq 0.58$.

Ook uit de gemeten $MSD(t - t_w)$ curves kunnen we de vloeistof-glas overgang bepalen. In de vloeistoffase neemt de MSD nagenoeg lineair toe met toenemend tijdsinterval en de $MSD(t - t_w)$ curves zijn onafhankelijk van de wachttijd. Als de temperatuur verlaagd wordt (de microgel deeltjes zwellen dan op en de suspensie wordt in de glasfase gebracht) vlakt de helling voor korte tijdsintervallen af en ontstaat er een plateau. De testdeeltjes raken opgesloten in een kooi gevormd door de microgel deeltjes. Voor langere tijdsintervallen kunnen de testdeeltjes aan deze kooi ontsnappen en zal de MSD weer toenemen met de tijd. Het tijdsinterval waarbij de overgang van plateau naar lineaire groei plaats vindt, is gelijk aan de karakteristieke relaxatie tijd van het monster. Doordat in de glasfase ook nu weer de MSD curves alleen van $(t - t_w)/t_w$ afhangen, neemt de karakteristieke relaxatie tijd lineair toe met de leefttijd t_w: het systeem veroudert. Met de beschikbare $MSD(t - t_w)$ curves kan men de locale viscoelastische moduli $G'_{\text{loc}}(\omega)$ en $G''_{\text{loc}}(\omega)$ berekenen door de gegeneraliseerde Stokes-Einstein relatie toe te passen. Deze vertonen kwalitatief hetzelfde gedrag als de macroscopische moduli. In detail verschillen ze echter wel; de locale elasticiteit blijkt bij de gebruikte grootte van testdeeltjes een factor 2 kleiner te zijn dan de macroscopische terwijl de dominante relaxatietijd een factor 5 kleiner is. De oorsprong van deze verschillen is nog niet begrepen. Verder laten de locale moduli zien dat in jonge monsters ook zwakke relaxatieprocessen optreden met karakteristieke tijden korter dan de dominante tijd. Bij veroudering verdwijnen deze en het materiaal vertoont dan een nagenoeg perfect Maxwelliaans gedrag.

Tot slot hebben we sterke aanwijzingen gevonden dat voor glazen met een voldoende hoge elasticiteit van de microgel deeltjes de veroudering naar verloop van tijd stopt. Voor een polyNipam-polyNipmam glas met een massaconcentratie van 8 %w/w bleek bij een temperatuur van 24 °C de veroudering na 6000 s te stoppen. Soortgelijk gedrag is ook door andere onderzoekers waargenomen.

Acknowledgement

It is always difficult to list all the people who have been very supportive and helpful during my work. To honor the people that I could not mention one by one, my first acknowledgement goes to them.

I would like to thank my supervisor Dr. Dirk van den Ende who has been very kind and helpful. Without his encouragement and his thrust I would not be able to finish this work. He was extremely helpful and patient through out my research and especially during my first months in the former Rheology group. Together with Prof Mellema, they have been able to convince me to continue my work in this project. I also thank him for translating the summary of the thesis into the "samenvatting" during his holiday.

The next acknowledgement goes to Prof Frieder Mugele who often trigger new ideas during my research. Your questions during the biweekly meeting encouraged me to produce more meaningful output. My acknowledgement also goes to Prof. Jorrit Mellema who always care about my life and my family. Special thanks to Dr. Michel Duits from whom I learned about goal oriented working.

Thanks to the members of my doctoral committee (Prof. Peter Sollich, Prof. Walter Richtering, Prof. Wim Briels, Prof. Stefan Luding, Dr. Peter Schall, and Prof. Matthias Ballauff) for accepting to be part of the committee, reading my thesis, and giving comments and suggestions.

I would like to thank the Foundation for Fundamental Research on Matter (FOM) for funding this research. I also like to thank the Department of Food Science and Technology, IPB to allow me to pursue my Ph.D..

I also enjoyed fruitful discussions with Siva and from him I have learned how to "listen". For Nicki, my great thanks to her for editing my English although she was very busy with Amia and Ishan.

Thanks for my office mates and former office mates (Hao, Jane, Renske, Rina, and Manu) who gave me a lot of fun. My appreciation also goes to members and former members of the Physics of Complex Fluids Group (Gerrit, Ryan, Diana, Violeta, Niki, Helmut, Adrian, Tamara, Cock, Mariska, Fahong, Arun, Florent, Siva, Sissi, Dileep, Annelies, Gor, Dieter and Telli). My spe-

cial thanks to Butje and Susan who gave me an Indonesian flavor in a dutch environment.

To all my Indonesian friends in PPI and IMEA, I would like to say; *terima kasih atas persahabatan dan persaudaran kita selama ini. Buat Bu Nung, terima kasih atas nasihat, perhatian, undangan makan-makan, dan pizza di hari pertama kami pindahan. Tak lupa saya ucapkan terima kasih pula untuk mba Yati dan tante Hadi yang telah bersedia menerima saya sebagai anak kostnya. Untuk Pak Purwiyatno, terima kasih atas bimbingannya selama ini dan juga atas kunjungannya ke Enschede.*

Last but not least, to my family I would like to thank my wife and my lovely "Princess Renata". I will always remember how difficult my life was without them. I would also love to welcome to my son Reindra who was born at the time I had to finish off this thesis. In here I also want to pray for my father who passed away before I could do something for him. For my mum, my brothers, my sister, my parents in law, and my brothers in law: thank you very much for your pray and care.